5-2007

Innovative Methods of Biomedical Molecular Analysis: Capillary Electrophoretic Study of Amyloid Beta Conformations and Magnetically Assisted Transport Evanescent Field Fluoro-assays

Amber D. Wellman
University of Tennessee - Knoxville

To the Graduate Council:

I am submitting herewith a dissertation written by Amber D. Wellman entitled "Innovative Methods of Biomedical Molecular Analysis: Capillary Electrophoretic Study of Amyloid Beta Conformations and Magnetically Assisted Transport Evanescent Field Fluoro-assays." I have examined the final electronic copy of this dissertation for form and content and recommend that it be accepted in partial fulfillment of the requirements for the degree of Doctor of Philosophy, with a major in Chemistry.

Michael J. Sepaniak, Major Professor

We have read this dissertation and recommend its acceptance:

S. Douglass Gilman, Mark Dadmun, Youngmi Lee, Robert Hettich

Accepted for the Council:

Carolyn R. Hodges

Vice Provost and Dean of the Graduate School

(Original signatures are on file with official student records.)

To the Graduate Council:

I am submitting herewith a dissertation written by Amber D. Wellman entitled "Innovative Methods of Biomedical Molecular Analysis: Capillary Electrophoretic Study of Amyloid Beta Conformations and Magnetically Assisted Transport Evanescent Field Fluoro-assays." I have examined the final electronic copy of this dissertation for form and content and recommend that it be accepted in partial fulfillment of the requirements for the degree of Doctor of Philosophy, with a major in Chemistry.

Michael J. Sepaniak
Major Professor

We have read this dissertation
and recommend its acceptance:

S. Douglass Gilman

Mark Dadmun

Youngmi Lee

Robert Hettich

Accepted for the Council:

Carolyn Hodges

Vice Provost and Dean of the
Graduate School

(Original signatures are on file with official student records.)

Innovative Methods of Biomedical Molecular Analysis: Capillary Electrophoretic Study of Amyloid Beta Conformations and Magnetically Assisted Transport Evanescent Field Fluoro-assays

A Dissertation
Presented for the
Doctor of Philosophy Degree
University of Tennessee, Knoxville

Amber D. Wellman
May 2007

DEDICATION

To my exceptional parents,

Jack and Trina Wellman

For your unwavering faith,
your example,
your sacrifices,
and your gifts (most of which money could never buy);
I am eternally grateful

ACKNOWLEDGEMENTS

The past few years feel like forever and the blink of an eye, all at the same time. There are many people that I would like to thank for making this dream come true. I thank God for blessing me with life and surrounding me with wonderful people who inspire and uplift me daily. I especially thank my family, without whom I would be lost. I thank Mammaw and Pappaw for their love and support, and for all of the "gas money", which meant more than you will ever know. I thank my sister, Ashley, for being my first best friend…I am comforted knowing that you will always be there for me. I hope that, together with Tyson and Sami, our memories have just begun. I thank my parents, who have been my foundation. You taught me that I was capable of achieving every dream and never doubted me along the way, even when the self-doubt started to creep in. I strive to live up to your example and hope that I make you proud.

To the members of my graduate school family; Libby, Lance, Matt, Nahla, Pampa, and all of my current and former labmates, I thank you for your friendship and for making me a more well-rounded scientist and human being. I especially thank Kasey, Maggie, Jenny and Pete for being the people that I looked forward to seeing every day and for making the day (and lunch) pass by so much faster. Sometimes a little non-scientific conversation (or celebrity gossip) was just what I needed. I could not have made it through the first year of graduate school if not for Yohannes, whose patience and personality are second to none. He truly is a "prince". I thank Cara for being the person that I could grumble with about the trials of graduate school, and life in general. I am so thankful for having Courtney as a labmate and roommate (not to mention a friend for

life), to keep me sane and to keep me company. I also thank Kevin and Roushan for the parties, barbecues and poker games.

I thank Al Tuinman and Liguo Song for guidance in all things mass spec, and Tim Free for his technical skills in constructing many experimental set-ups. I thank Dr. Gilman and Indu for their guidance, ideas and support during my first three years of graduate school. I particularly thank Dr. Sepaniak for his direction, patience, intelligence, focus and professionalism, which are examples to everyone he mentors. For him to have believed in me enough to allow me to join his group in the middle of my career was more of an inspiration than he will ever know. Thank you.

Last, but certainly not least, I want to thank Sami Chanaa. Meeting you initiated a turning point in my life. I truly believe that we were meant to find each other and hate to think of what my path would've been had we not. You are my heart and the one that I lean on….I'm sorry if sometimes the load gets heavy. I want you to know that you brighten every day and I love you more than words can ever say.

ABSTRACT

Though the study of the human proteome (proteomics) is far more complicated than that of the genome, it may prove to be the next step toward gaining insight into the operation of biological systems. Understanding the role proteins and peptides play in disease, whether that be by their structure, expression or function, could lead to the identification of disease biomarkers for diagnosis or engender possibilities for treatment. To this end, the work discussed herein delves into the capillary electrophoretic (CE) analysis of amyloid beta conformations involved in abnormal aggregation and the creation and optimization of a novel bioassay method. By rapidly analyzing the conformations of Aβ present in heterogeneous mixtures, valuable insight may be provided into the mechanism of abnormal protein aggregation. Further, the novel bioassay described herein may supply a simplified method for analyzing and quantifying many different biologically relevant interactions (i.e. DNA hybridization and immunoassays).

Capillary electrophoresis is used to study the aggregation pathway of the amyloid beta peptide (Aβ). Since little is known about the mechanism of Aβ fibril formation, this research sought to rapidly characterize different conformations of Aβ present in a heterogeneous mixture of species using changes in effective mobility and peak shape during CE separation. Electron microscopy and mass spectrometry were used to confirm the presence of Aβ in the mixtures and collected peak fractions. Additionally, the interaction between wild type Aβ and a mutated Aβ species resulting in increased protofibril formation was analyzed using CE.

A novel bioassay method was also developed and termed magnetically assisted transport evanescent field fluoro-assays (MATEFFs). MATEFFs employ magnetic beads as both a solid phase for analyte pre-concentration and delivery method to a localized evanescent field. Using this technique, the measurement of signal can be performed without call for wash steps and while avoiding matrix interferents present in bulk sample solution. While not limited by analyte diffusion, this method still allows for targeted delivery using simple magnetic control of analyte-labeled beads. This could impact the bioassay field, as much focus is currently directed toward miniaturization of bioassay formats.

PREFACE

The research presented in this dissertation spans my time in two research groups. Part I covers the research efforts under the supervision of Dr. S. Douglass Gilman in capillary electrophoretic analysis of amyloid beta peptides. Part II encompasses the work performed under the supervision of Dr. Michael J. Sepaniak in development and optimization of a novel bioassay method. I have attempted to combine the two individual projects under the general theme of biomedical methods of analysis.

TABLE OF CONTENTS

List of Tables

List of Figures

Part I .
CAPILLARY ELECTROPHORETIC SEPARATION OF DIFFERENT AMYLOID BETA CONFORMATIONS ALONG THE FIBRILLOGENESIS PATHWAY

CHAPTER 1.
INTRODUCTION TO CAPILLARY ELECTROPHORESIS AND PROTEIN AGGREGATION

Coupling the separation power of electrophoresis with chromatography instrumentation and ease of automation, capillary electrophoresis (CE) has become a versatile analytical tool capable of separating a wide variety of compounds. Owing to plug like flow and limited sources of dispersion, CE possesses the highest resolving power of any liquid separation method, while consuming only minute sample quantities and requiring minimal analysis time.[1] Often, a simple change of buffer solution in CE facilitates the analysis of a spectrum of relevant samples with various physicochemical properties, ranging from metal ions to proteins. Furthermore, capillary electrochromatographic (CEC) techniques, whereby CE capillaries are packed with high performance liquid chromatography (HPLC) packing and a voltage is applied for separation, are relatively new and offer both the differential partitioning of HPLC and the electrophoretic migration of CE with no back pressure and plug like flow characteristics. CEC techniques lead to uniquely selective separations and promise superior resolving power as compared to traditional HPLC. With increasing complexity in analytical samples, especially those biological in nature, CE and CEC will continue to be essential separation techniques due to consequent rapid analysis, high efficiency, and minimal sample consumption, even with the existence of some disadvantages such as low sample

load and difficult reproducibility. The work discussed in this section of the dissertation will focus on traditional capillary zone electrophoresis.

Capillary Electrophoresis Fundamentals

History and Theory

Electrophoresis is simply defined as the migration of charged species when influenced by an applied electric field, with separation of these charged species a result of differential migration times owing to disparity in charge, size and shape.[2] As ions move toward the electrode of opposite charge under the influence of an externally applied electric field, frictional drag balances the electric force and a steady-state is reached with ion velocity (ν_e,cm sec^{-1}) being directly proportional to the strength of the electric field (E):

$$\nu_e = \mu_e E \tag{1-1}$$

where μ_e is the electrophoretic mobility of the ion (cm^2 V^{-1} sec^{-1}) and

$$E = \frac{V}{L_T} \tag{1-2}$$

where V is the total applied voltage and L_T is the total length of the separation medium (cm). The physical parameters of the analyte affect mobility as evidenced by the following equation:

$$\mu_e = \frac{q}{6\pi\eta r} \tag{1-3}$$

where q is the ion charge, η is the buffer viscosity and r is the ion radius. It is then evident that small, highly charged species have high electrophoretic mobilities.[3]

First described by Tiselius in 1930, classic free solution electrophoresis suffered from such problems as long analysis times, poor efficiencies, difficult detection and automation, and joule heating arising from ionic current passing between electrodes.[4] Joule heating can increase zone broadening due to density and temperature gradients, as well as lead to solvent evaporation. Introducing a support medium to aid in heat dissipation, such as a gel, combatted the problem of Joule heating. However, the high surface area available for solute adsorption when using a support, as well as an increase in the possible routes of migration, increase zone broadening due to eddy diffusion. Furthermore, the addition of the support medium served to make free solution electrophoresis an even more labor intensive technique.[2, 5, 6]

Though early experimentation with free solution electrophoresis in capillaries dates back to 1967, capillary electrophoresis (CE) in its modern form was developed in the early 1980s by Jorgenson and Lukacs, thereby solving many problems of classic electrophoresis.[7] In CE, fused-silica tubes with inner diameters typically ranging from 20 to 200 μm and lengths between 10 and 100 cm are used as the migration channel. The use of these narrow bore capillaries meant a high surface-to-volume ratio and concomitant efficient heat dissipation even when applying large electric fields. Resultant improvement in separation efficiency and decreased analysis time coupled with minimized reagent requirements made CE a very attractive solution to analytical problems associated with other separation methods.[8]

Instrumentation

The instrumentation employed for capillary electrophoretic separations is relatively simple. As shown in Figure 1.1, the basic CE system contains a narrow-bore, fused silica capillary whose ends are immersed in electrolyte buffer reservoirs, with said buffer filling the inside of the capillary. Each buffer reservoir contains an electrode connected to a high voltage power supply, by which an external potential is applied across the capillary. As separations are typically performed from the anode to the cathode (normal polarity), the sample is loaded by removing the capillary from the buffer reservoir containing the anode and placing the end into the sample reservoir where an external pressure or electric field is applied. The sample reservoir is then replaced by the buffer reservoir and an electric field or external pressure is again applied in order to perform the separation. Detection can be performed online in capillary electrophoresis by simply removing the polyimide coating so that a window is formed on the end of the capillary opposite that of injection.[3]

Once injected into the capillary, analytes move under the influence of the applied electric field by two independent processes: electrophoresis and electroosmosis.[9] The net analyte movement is the vector sum of these two processes (Figure 1.2). Normal polarity conditions would result in migration of only the cationic species toward the cathode, with neutral species remaining stationary at the point of injection and anionic species being driven toward the anode and thus away from the detector. Only by the process of electroosmotic flow can all ionic species be driven through the capillary and thereby detected.

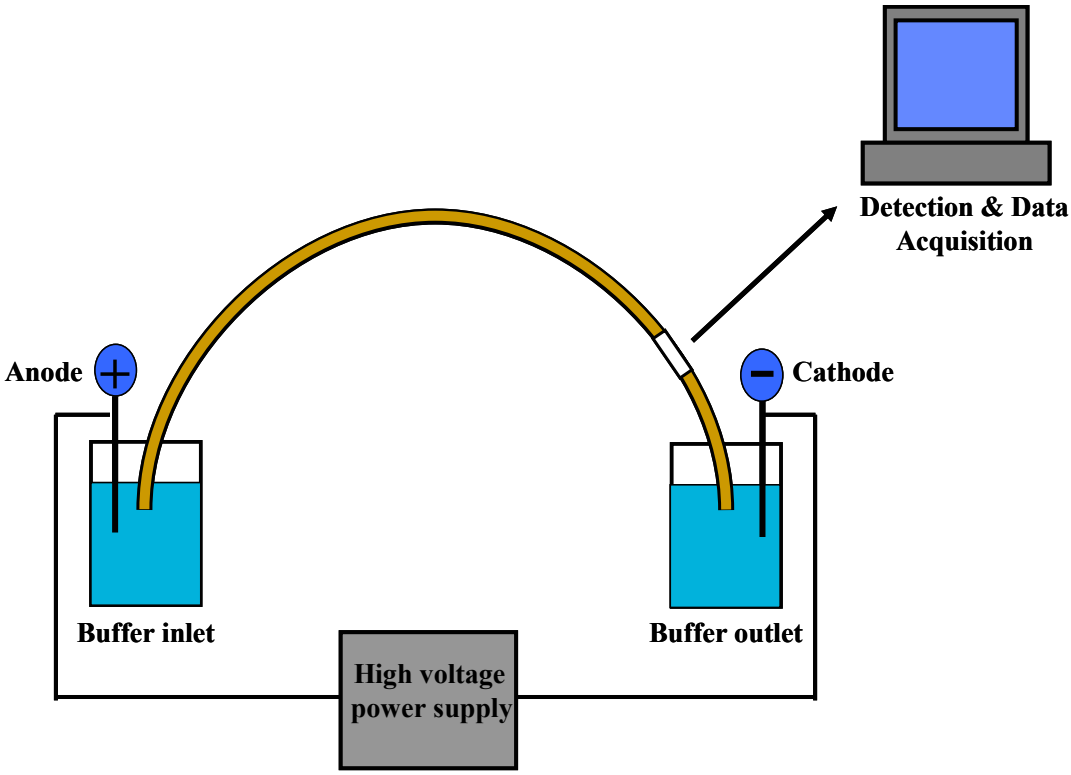

Figure 1.1 Capillary Electrophoresis Instrumentation Schematic

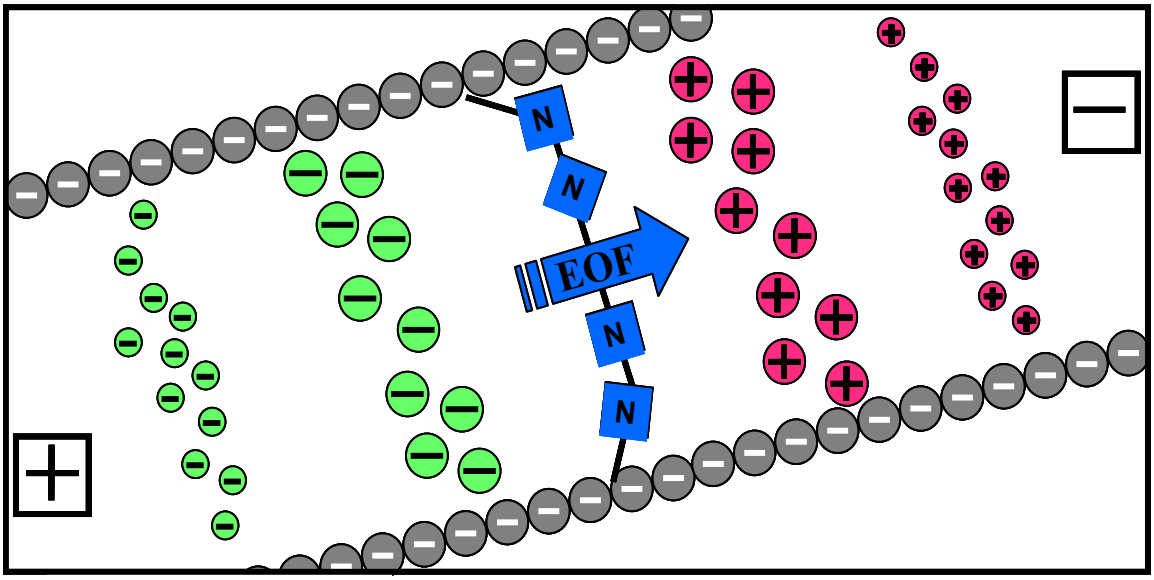

Figure 1.2 Illustration of net analyte movement in capillary electrophoresis as the vector sum of electrophoretic solute migration and electroosmotic flow.

Electroosmotic Flow (EOF)

Electroosmosis, playing a fundamental role in capillary electrophoretic separations, is solvent flow originating at the solid-liquid interface of the capillary wall due to the applied electric field. This flow is often referred to as the electroosmotic flow (EOF).[5] EOF occurs when exposed silanol groups (SiOH) along the inner surface of the capillary wall begin to ionize as SiO^- at buffer pH values above 2 due to the range of silanol pKa values. These anionic silanol groups interact electrostatically with buffer cations, forming a double layer comprised of both the stern layer (fixed and held tightly by the silanol groups) and the diffuse layer (mobile layer pulled toward the cathode once the electric field is applied). This double layer creates a potential difference, or zeta potential, along the capillary wall. When a potential is applied across the capillary under conditions of normal polarity, these solvated buffer cations drag the bulk solution toward the cathode and thus the detector (Figure 1.3).[10] The velocity of the bulk solution traveling through the capillary due to EOF (ν_{EOF}, cm sec^{-1}) is given by:

$$\nu_{EOF} = \mu_{EOF} \cdot \frac{V}{L} \tag{1-3}$$

where μ_{EOF} is the mobility of the EOF (cm^2 V^{-1} sec^{-1}), V is the voltage applied across the capillary and L is the total length of the capillary (cm).[7] The net migration velocity of an analyte traveling through the capillary (ν), then, is the sum of ν_e and ν_{EOF}:[5]

$$\nu = (\mu_e + \mu_{EOF}) \cdot \frac{V}{L} \tag{1-4}$$

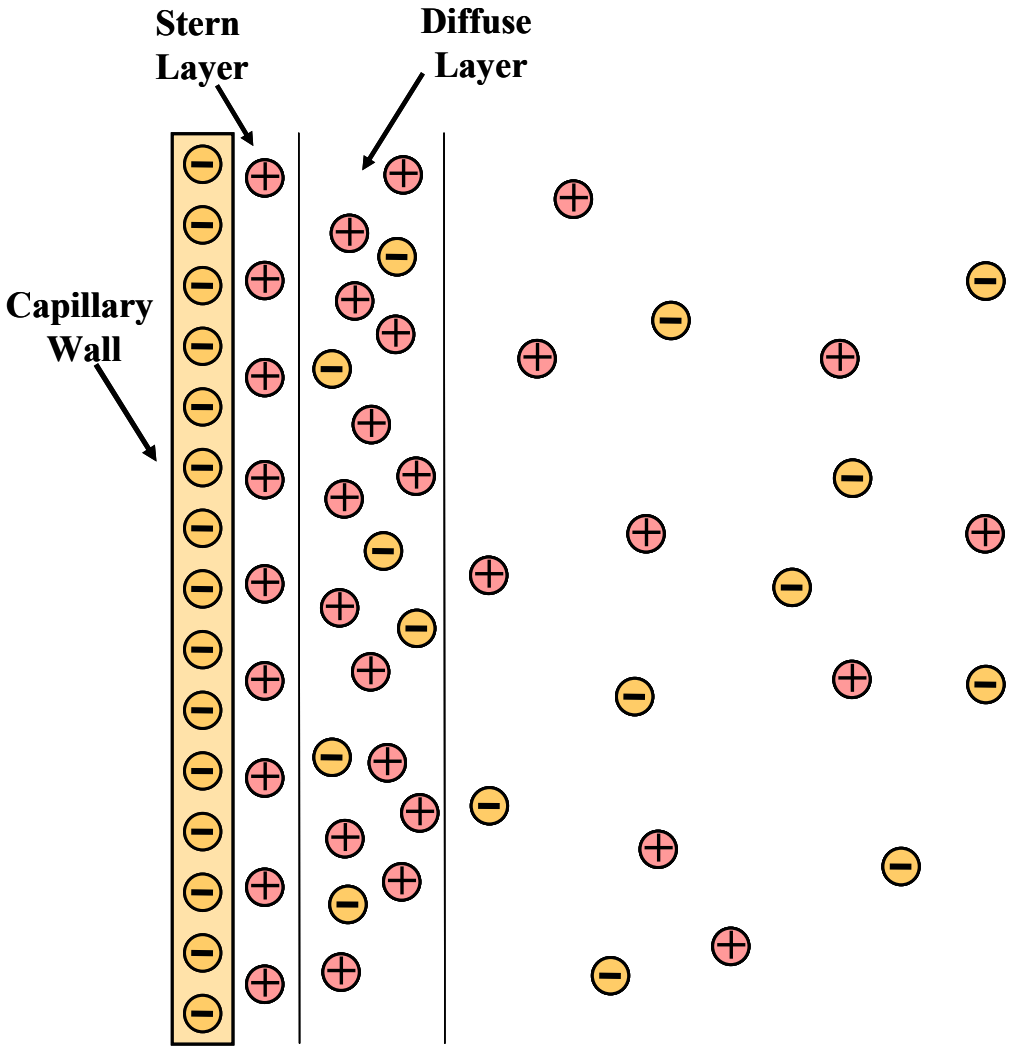

Figure 1.3 Representation of the double layer formed at the capillary surface upon application of an electric field.

Normally, the magnitude of the EOF is greater than the electrophoretic mobilities of the analytes present in a sample. This leads to the separation of cations, anions and neutrals (as a group) in a single run with the order of migration depicted in Figure 1.2.[3] It is important, though, to control EOF as slow EOF could result in zone broadening and increased analysis time. Several factors influence EOF including buffer pH and ionic strength, temperature, and electric field. Ultimately, anything that affects the inner capillary wall and, therefore, the zeta potential will impact EOF.

A very important additional benefit of EOF is the flat profile of the bulk flow due to the fact that the driving force of the flow arises at the capillary walls.[11] This flat profile leads to negligible zone broadening due to resistance to mass transfer in the mobile phase, in sharp contrast to the laminar or parabolic flow resulting from pressure-driven systems such as HPLC.[12] Laminar flow can result in significant zone broadening due to a velocity gradient, where the solvent velocity in the center is high and drops to zero along the walls.[13] While EOF aids in high resolution separations and, in theory, only axial molecular diffusion occurs in CE, several factors may result in dispersion by their affect on EOF or otherwise.[14]

Efficiency and Resolution

Ideally, the lone contributor to band broadening in CE is axial diffusion and the equation for efficiency (or theoretical plate number, N) is given below

$$N = \frac{\mu E l}{2D} \tag{1-5}$$

where μ is mobility ($cm^2V^{-1}sec^{-1}$), E is applied electric field (Vcm^{-1}), l is the capillary length to the detector, and D is the diffusion coefficient of the solute (cm^2sec^{-1}). It can

then be inferred that high voltages will increases theoretical plates and improve efficiency by minimizing the time for diffusion and that CE can be highly efficient for both large and small molecules due to the high mobility of small compounds and low diffusion coefficients of larger molecules.[15] Unfortunately, other dispersive factors can contribute to band broadening and loss of efficiency in CE.

Although the small dimensions of the capillaries employed for CE separations help to efficiently dissipate heat, with the tens of kilovolts separation voltages normally used for efficient separations, joule heating can contribute to band broadening due to changes in buffer viscosity.[6] Adsorption of molecules to the capillary surface, aside from changing the zeta potential and EOF, could result in distortion of peak shape. Peak fronting or tailing could also result from sample overload or from differences in conductivity between the running buffer and sample (electrodispersion).[12] Additionally, injection plug length and hydrostatic flow can play a role in band broadening. All of these dispersion factors can be avoided by a general attentiveness to experimental design including judicious choice of buffer concentration, sample ionic strength and concentration, and capillary coatings

High efficiency is the "claim to fame" of CE and is undoubtedly important; however, the ultimate goal in separation science is resolution. Under conditions such that axial diffusion is the sole source of band dispersion, the resolution (R) between two solutes in CE is defined as

$$R = 0.177\Delta\mu\sqrt{\frac{V}{D(\bar{\mu} + \mu_{eof})}} \tag{1-6}$$

where $\Delta\mu$ is the difference in mobility between the two solutes, $\overline{\mu}$ is the average mobility of the two solutes, μ_{eof} is the electroosmotic mobility, V is the applied voltage and D is the diffusion coefficient of the solute.[15] Factors that linearly increase efficiency, voltage for example, come under the square root sign and do not linearly affect resolution. The effects of joule heating limit the application of voltage increases to improve resolution. From equation (1-6), infinite resolution is attained when the average and electroosmotic mobility are equal and opposite. This is not possible, however, since it also results in infinite analysis time. The goal, then, is to balance resolution and time by manipulating EOF.

Detection Methods in Capillary Electrophoresis

Detectors used in CE must be highly sensitive, a consequence of the minute sample volumes injected and limited observation time for this technique. Unfortunately, a problem arises in that the most sensitive detectors are also the most selective.[4] A very sensitive, but also universal method of detection in CE would be very useful. The most common means of on-column detection are optical methods, such as ultraviolet (UV) absorbance and fluorescence. Optical methods of detection do face instrumental problems such as short optical path lengths defined by the inner diameter of the capillary and the cylindrical capillary's poor optical surface .[15] Laser-based detection can solve these problems since laser light sources can be focused to very near the diffraction limit of light and collection of emitted light at right angles to the excitation source can

eliminate stray light using spectral and spatial filters.[16] In addition to optical methods, electrochemical detection and mass spectrometry find application in CE.

UV Absorbance Detection

UV absorption is the most popular detection system for capillary electrophoresis due to its universal nature. On-column detection is achieved by removing a window of polyimide coating from the capillary near the end of the column. This window serves as the cell where UV detection is performed. Sensitivity in absorbance detection is limited by the path length, which is defined by capillary inner diameter. However, this method is attractive because a large number of analytes, especially proteins, absorb quite well in the UV range.[5] The limits of detection for UV absorbance are around 10^{-6} M, but can be optimized by choosing the wavelength for optimal molar absorptivity, using a buffer with minimal UV absorbance, as well as extending the pathlength of the capillary.[15] Multiwavelength or scanning UV detection systems can be used in order to detect analytes absorbing at different wavelengths in the same run or determine spectral information of an unknown.[13]

Laser-Induced Fluorescence (LIF) Detection

Fluorescence detection is attractive because sensitivity is not dependent upon the path-length. In LIF detection, a laser serves as the excitation source and is tightly focused on the window where the polyimide coating has been removed, with emitted light is usually collected at 90° relative to the incident laser beam. Employing lasers as the excitation source, much smaller capillaries can be utilized, as lasers can be focused to nearly the diffraction limit of light.[16] The detection limits for on-column LIF detection are the

lowest reported for CE, with routine LODs around 10^{-9} M.[17] However, with this high sensitivity comes increased selectivity. Commercial lasers are either a fixed wavelength or tunable over a small range, with a limited selection of available laser wavelengths. At each available laser wavelength, only select chemical species absorb with high emission quantum efficiency.[16] In addition, not all analytes of interest exhibit native fluorescence. This introduces an additional derivatization step so that non-fluorescent analytes can be detected.

Mass Spectrometric Detection

Coupling CE to mass spectrometry (MS) is attractive due to the combination of sensitivity and structural information provided by MS.[12] Though MS is one of the most expensive CE detectors, when dealing with complex, especially biological, samples it is necessary to identify the components based on something more reliable than migration time. For direct detection, electrospray has been the preferred ionization method, although continuous flow-fast atom bombardment, matrix assisted laser desorption ionization, and atmospheric pressure chemical ionization have been employed. Most major types of mass analyzers have been used with CE, including quadrupole, magnetic sector, time of flight; ion trap and Fourier transform ion cyclotron resonance. Detection limits for CE-MS have been reported in the attomole or zeptomole range and CE-MS continues to develop, both instrumentally and functionally.[8]

Electrochemical Detection

Electrochemical (EC) methods of detection in CE are attractive due to the possible high selectivity and sensitive detection of electroactive species without derivatization.

Detection limits are in the attomole range and not at all affected by the small dimensions of CE. Additionally, instrumentation is relatively inexpensive in comparison to other detection methods. The major dilemma in the use of EC detection with CE is the noise arising from high separation potentials native to CE separations. It becomes important to develop a method which isolates the EC signal.[18] Though conductivity, a non-selective and simple method of ionic species detection in solution, was the earliest form of EC detection with CE, current EC detection methods include amperometry, potentiometry and scanning electrochemistry.

Laser Light Scattering (LLS) Detection of Particles

Light scattering detection techniques have not been extensively used in CE. However, this method has some advantages over other detection methods. LLS detection is performed by focusing a laser beam on the detection window of the capillary and detecting the light scattered (usually at angles 15-180° from the incident beam) as the analyte passes through the window. This detection method is based on the concept that scattered light contains information, such as size and refractive index, about the scattering particle.[19] Mie scattering theory can be used to characterize light scattering distributions taking into account the effects of particle size, refractive index, detection angle and geometry.[20] LLS detection is attractive because it is capable of measuring the properties of individual particles passing through the laser beam one at a time (using the appropriate data collection rates and a tightly focused laser beam) and not the average properties of a population of analyte particles. This allows particles to be individually counted and the scattered light intensity of *each* particle to be related to its size. However, LLS is not a

selective technique, as any system contaminants or particulates, such as bubbles, large enough to scatter light will produce a background scattering signal. However, with a contaminant-free system, detection limits can be as low as 1000 particles/mL.[21] Lower size detection limits for LLS detection have not been fully explored, although reliable detection of particles as small as 110 nm has been reported.[22, 23] LLS is especially useful in mixtures of protein or other biological macromolecules because it is a non-invasive detection method that does not require tagging or dilution. Changes in particle numbers, density, length and diameter can be measured and these changes can provide important information about such things as aggregation pathways of proteins.[19]

Indirect Detection

With CE being an attractive method of separation for all kinds of compounds, a universal detection method is desirable. Indirect detection methods, whether UV absorbance, fluorescence or electrochemical, offer just that. When an analyte does not have any native UV absorbance or fluorescence, a component of the buffer is used to absorb light or fluoresce, producing a constant buffer signal in the absence of analyte. When analyte is present, it displaces some of the buffer ions and results in a negative peak proportional to amount of analyte present.[5] Indirect detection methods frequently suffers from .column overloading and band broadening, with detection limits related to buffer absorbance and stability of transmitted light.[18]

Modes of Capillary Electrophoresis

In attempt to expand the number of applications of CE, several modes of operation have been developed geared toward the separation of different types of compounds.[4]

Most of these methods are variations of electrophoresis that were adapted to the capillary format. The most common modes of capillary electrophoresis are capillary zone electrophoresis (CZE), micellar electrokinetic chromatography (MEKC) and related pseudo-phase techniques, size selective capillary electrophoresis (SSCE), capillary isoelectric focusing (CIEF), and capillary isotachophoresis (CITP).[18]

Capillary Zone Electrophoresis (CZE)

Being the simplest and most popular, CZE will be the method used in the research discussed herein. In CZE, essentially free solution electrophoresis, the buffer is the same in the reservoirs and the capillary. The analyte migrates in zones under the influence of the applied electric field depending upon the charge/size ratio.[2] It is important, in order to achieve a good separation with CZE, that the mobilities of each analyte in the injected sample differ from one another, that the buffer is homogeneous throughout the capillary, and that there is no interaction of the solute or matrix with the capillary wall. Separation of both cations and anions are possible, owing to EOF, while neutrals coelute with EOF.

Micellar Electrokinetic Chromatography (MEKC)

MEKC, introduced by Terabe in 1984, allows separation of neutral species. A surfactant above the critical micelle concentration is added to the running buffer and neutral solutes partition into the micelles. The retention factor determines the order of separation for the neutral species, making MEKC much like reverse-phase high performance liquid chromatography (RP-HPLC).[24] Sodium dodecyl sulfate (SDS) is the most common micellar phase used in MEKC. The micellar phase is referred to as pseudostationary since, in the case of anionic SDS, it moves slower than the mobile

phase. In addition to micelles, charged cyclodextrins, polymers, bile salts, and microemulsions have been employed as pseudostationary phases. The peak capacity for MEKC is limited by the elution range determined by the difference between the EOF (t_0) and the micelle migration time (t_m).[18]

Size Selective Capillary Electrophoresis (SSCE)

In order to permit size based separations, a sieving matrix can be formed within the capillary or pumped in under high pressure. This matrix can be in the form of a gel or an entangled polymer. Analyte migration is still driven by the electric field, but also affected by the required migration through the gel or polymer matrix. This results in analyte mobility inversely proportional to size under ideal conditions, as small molecules easily pass through pores while larger biomolecules may travel an arduous path.[15]

Capillary Isoelectric Focusing (CIEF)

CIEF separates proteins and peptides based on their isoelectric point (pI) using a pH gradient formed inside the capillary by a solution of ampholytes. Ampholytes are zwitterionic and have pI values than span a range of pH values (usually 3 to 9). The capillary is filled with an analyte containing solution of ampholytes and the gradient is formed by placing the cathode in basic solution and the anode in acidic solution followed by application of an electric field. The charged ampholytes and analytes will move under the influence of the electric field until they reach a region where they become uncharged (their pI). Once this focusing is complete, current no longer flows and the zones are passed by the detector either by a separate mobilization step in the absence of EOF,

simultaneous focusing and mobilization via careful control of EOF, or mobilization of the detector or capillary.[12]

Capillary Isotachophoresis (CITP)

Literally meaning moving at the same speed, CITP utilizes a leading and trailing buffer system to create separated analyte zones moving at the same velocity toward the detector. Used to detect *either* cations or anions, the leading buffer contains the highest mobility ion and the trailing buffer the lowest mobility ion. The analyte containing sample is injected between these two zones and the analytes separate in order of mobility. The highest mobility compounds have the lowest field strength and vice versa. Therefore, all the zones, once equilibrium is reached, will move at the same velocity (refer to equation (1-1)). With no carrier electrolyte, the zones will remain in contact with one another. A major advantage of CITP is the compression of low concentration analytes resulting in trace component enrichment.[2]

Capillary Electrophoretic Peptide Separations

An important application of CE is in the area of bioanalytical chemistry, more specifically the separation of peptides and proteins. In the post genomic era and with emerging proteomic technology, the ability to rapidly separate mixtures of peptides and proteins is of utmost importance. Proteome research will provide insight into the molecular basis of biological processes and aid in development of targeted drug therapies. With protein structure and function determined by their peptide fragments, now more than ever it is important to understand the peptide makeup of cells (the

peptidome).[25] CE has found utility in monitoring of enzymatic peptide digests, determining purity of peptide synthesis and in isolating individual peptides from complex mixtures.[26] Due to high efficiency and ability to resolve small differences in solute mobility, CE is capable of resolving peptides with the same charge, but differing in mass by one amino acid, as well as peptides that have the same mass but differ in charge by one. CE is non-denaturing, allowing separation of polypeptide molecules in their native states. In comparing CE to complementary techniques in chromatography, such as RP-HPLC, CE is faster and less labor-intensive.[27] Furthermore, the fact that polypeptides and proteins have small diffusion coefficients increases separation efficiency in CE, whereas these small diffusion coefficients lead to slow mass transfer between stationary and mobile phase, increased band broadening and reduced separation efficiency in chromatography.[6] However, a key limiting factor for CE, especially when applied to proteome research, is the limited sample loading capacity. This can be detrimental in terms of the dynamic range provided when interfacing CE with other analytical techniques, such as mass spectrometry.

Predictive models for peptide migration are necessary for analysis of large numbers of peptides contained in cells and tissues. There is a correlation between the electrophoretic mobility of peptides and their charge, size and shape. The best fit theoretical model for predicting peptide mobility, μ_p, is the Offord model which accounts for a shear factor related to peptide surface area.[28] This model proposes that

$$\mu_p = \frac{q}{M^{\frac{2}{3}}} \tag{1-7}$$

where q is the charge of the peptide molecule and M is the molecular weight. It can be difficult to predict the charge of a peptide, however, as a function of pH since pK_a values of amino acid groups in peptides may differ from that of amino acids in free solution.

A major application of CE is found in characterization of peptides and their consequent proteins. The monitoring of dynamic changes in peptide preparations, whether chemical modifications or physical alterations, can provide useful insight into denaturation, folding/unfolding and conformational states.[25] The separation, analysis and characterization of peptides by CE is attractive due to the advantages of high efficiency, small sample consumption, and ease of automation, but not without challenges.[5]

A continuing challenge in the analysis of peptides with CE is the suppression of adsorption to the capillary wall. Polypeptides have a high affinity to adsorb on the fused-silica capillary wall believed to be due to electrostatic interactions between positively charged residues and negatively charged silanol groups on the inner wall of the capillary. This issue, if not addressed, results in a loss of separation efficiency, poor reproducibility and low recovery.[29] In dealing with this problem, coatings can be used to shield the silanol groups and eliminate sites for adsorption. However, the coating procedure is laborious and has a limited lifetime. Buffer additives, such as cationic surfactants or polymers, are another option to reduce peptide-capillary interactions. In these cases, high ionic strengths are usually required, resulting in problems with Joule heating. Perhaps the simplest approach is to manipulate the pH of the buffer to a value well above the isoelectric point (pI) of the peptide, so that it is negatively charged and repulsed by the anionic charges on the capillary inner surface.[29] As with any CE separation method,

appropriate buffer conditions, electric field strength and capillary length, among other things, must be ascertained for successful peptide separations.

Capillary Electrophoretic Analysis of the Amyloid Beta Peptide

The amyloid-β peptide (Aβ) is comprised of 39-43 amino acid residues and is the proteolytic product of the amyloid precursor protein (APP). Aβ is the primary constituent of the extracellular amyloid fibril deposits found in the brains of Alzheimer's disease (AD) patients, in addition to being associated with more than 20 other amyloid diseases.[30] There are many lines of evidence suggesting that Aβ fibril formation plays a central role in the onset of AD. The overexpression of mutant APP by transgenic animals leads to the development of amyloid plaques made up of fibrillar Aβ. In addition, the mutations associated with early onset familial AD all lead to increased production and/or deposition of Aβ in the brain. Moreover, several mutations affecting the processing of APP result in increased levels of Aβ, particularly the more amyloidogenic Aβ42 (the 42 amino acid variant of Aβ peptide).[31, 32]

There is current debate as to the exact identity of the toxic agent in AD. It has been demonstrated that Aβ fibril formation proceeds via a complex multi-step polymerization mechanism involving nucleation and elongation steps (Figure 1.4).[31] Recent research suggests that the toxic form of Aβ may not be the insoluble fibril species, but rather the soluble oligomeric intermediate state in the mechanism. These intermediates are sometimes referred to as protofibrils. Recent evidence better correlates the protofibril content of Aβ in the brain with the severity of AD than the fibril content.[31-33] Exploration

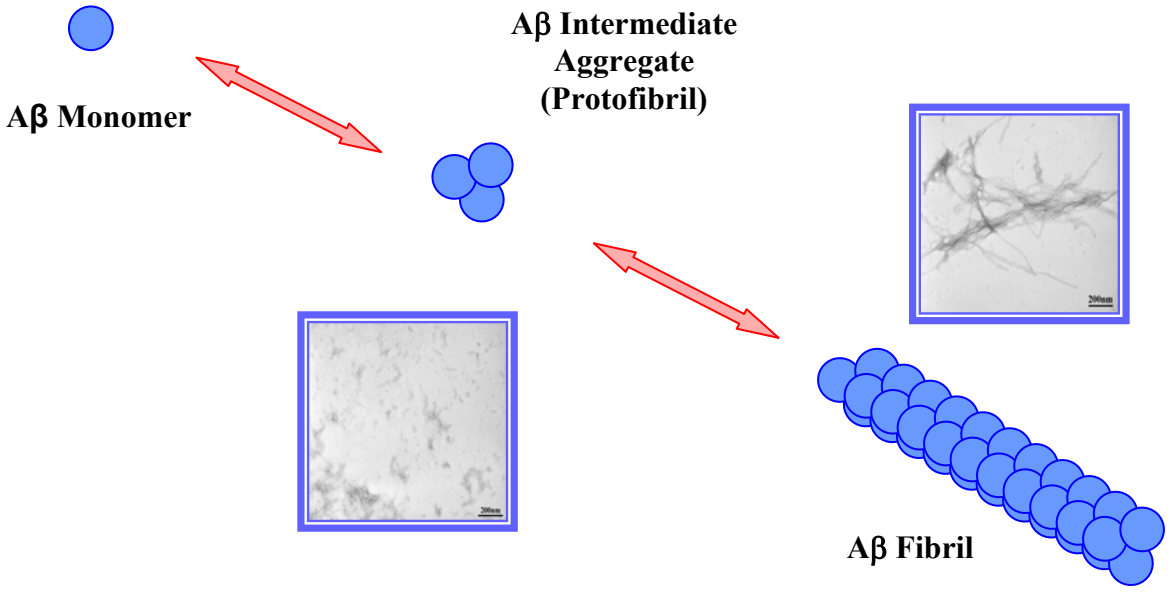

Figure 1.4 Aggregation scheme for amyloid beta (Aβ) peptide. Electron micrographs represent the protofibril and fibril species.

of the role of protofibrils in amyloid assembly could lead to a better understanding of AD and suggest a method for inhibiting amyloid pathogenesis.

There has been very little reported on the analysis of Aβ peptides by CE. Varesio et al. report the use of CE coupled to electrospray mass spectrometry to detect Aβ 1-40 peptide, but do not attempt to determine the conformational species present in the sample.[34] CE separations of different length Aβ fragments have also been reported.[35, 36]However, no attempts are made to identify the conformation of Aβ producing the observed peaks. Changes in peak shapes or peak mobilities are attributed to aggregation or different species along the aggregation pathway.

Motivation for Aβ Characterization by CE

Developing a method for elucidation of the components of a heterogeneous mixture containing Aβ species present during fibril formation would facilitate investigation of the fibrillogenesis process. CE provides an avenue to rapidly explore Aβ populations in real time under mild conditions while consuming minimal material. The efficiency of CE allows separation of oligomeric species that differ slightly in mass, charge or shape, which could result in discrimination between the different conformations of Aβ along the pathway to fibril formation, not possible using many other analytical techniques. Calibration can be performed using well characterized particles, such as polystyrene spheres, in order to better understand changes such as mobility and peak shape for the separation of more complex peptide and protein mixtures. The work described herein will seek to rapidly characterize Aβ species using CE, with confirmation of their identity by electron microscopy and mass spectrometry. A better understanding of Aβ

aggregation, and protein misfolding in general, would aid in diagnosis of amyloid related diseases as well as, and more importantly, the evaluation of possible therapies for their treatment and/or prevention.

CHAPTER 2.
ANALYSIS OF AMYLOID BETA CONFORMATIONS USING CAPILLARY ELECTROPHORESIS

Introduction

Protein aggregation normally represents the failure of a protein to reach the correct spatial arrangement, folded state, in order to function properly. If the proper fold is not attained, the protein acquires an abnormal conformation, misfolded state, or abnormally persists in an intermediate state which would normally be transiently visited along the folding pathway. In these misfolded states, unusually large non-polar areas of the protein are exposed and extremely sensitive to intermolecular hydrophobic interactions with other misfolded proteins, resulting in aggregation. [37]

The accumulation of these misfolded proteins is a common feature in several neurodegenerative disorders. Moreover, a class of late-onset, slow-progressing diseases seem to result from the gain in function of these misfolded aggregate states.[38] The extracellular deposition of aggregated protein is a hallmark of Alzheimer's disease (AD), while intracellular protein aggregation characterizes Parkinson's disease, amyotrophic lateral sclerosis and polyglutamine disorders.[39] The structure of these disease-related protein deposits is commonly referred to as the amyloid fibril. Amyloid fibrils are normally rigid and unbranched structures with a diameter of 5-13 nanometers and a length of up to several microns. Genetic evidence, as well as the correlation between fibril deposits and disease, suggest that fibril formation is pathogenic.[40] It is important to

gain a better understanding of the mechanism by which protein misfolding, and ultimately fibril formation, occurs in order to therapeutically battle the neurodegenerative diseases characterized by this phenomenon.

The amyloid β (Aβ) polypeptide family is the primary constituent of extracellular fibril deposits isolated from the brains of AD patients, in addition to being associated with more than 20 other amyloid diseases.[41] The Aβ monomer is a 39-43 amino acid residue peptide that is the proteolytic product of the amyloid precursor protein (APP). The predominant species generated by APP metabolism is the 40 amino acid residue peptide ($A\beta_{WT}$), although many other species can be produced including the more amyloidogenic 42 amino acid peptide, $A\beta_{1\text{-}42}$.[42] It has been demonstrated that Aβ fibril formation proceeds via a complex multi-step polymerization mechanism whereby monomer is converted to a soluble oligomeric intermediate, or protofibril, that disappears upon further aggregation into the fully formed fibril species.[31] There are many lines of evidence suggesting that Aβ fibril formation plays a central role in the onset of AD including the increase in Aβ production and/or deposition by the mutation associated with early onset AD and increased levels of Aβ created by mutations affecting APP processing.[31, 41]

There is current debate as to the exact identity of the toxic agent in AD, with recent research suggesting that the toxic form of Aβ may not be the insoluble fibril species, but rather the soluble protofibril.[32, 41] It has been discovered that protofibril content better correlates with AD severity than fibril content, and a mutation of the Aβ peptide associated with early onset familial AD called the Arctic mutation ($A\beta_{ARC}$), an

autosomal dominant mutation of the Aβ monomer at the 22nd amino acid residue (E22G), when compared to $A\beta_{WT}$, forms protofibrils more rapidly and to a greater extent. This suggests that early onset AD resulting from this mutation could be due to the toxic protofibril species.[41, 43] However, with protofibril formation being a normally transient process along the pathway to fibrillization, detailed characterization of protofibril structure is rendered difficult.

Williams and coworkers, using a screening assay for Aβ aggregation stimulators, found that calmidazolium chloride (CC) is particularly effective in stabilizing protofibrils.[44] When adding 100 μM CC to $A\beta_{WT}$ monomer, the monomer is rapidly converted to a pelletable aggregate or protofibril that persists for days. This stabilization will permit more detailed analysis of these intermediates and possible determination of their role in the aggregation process.

In the present work, capillary electrophoresis is used to separate samples of $A\beta_{WT}$ monomer, calmidazolium chloride stabilized protofibrillar aggregates (CC-$A\beta_{WT}$), and fully formed $A\beta_{WT}$ fibrils. Additionally, $A\beta_{ARC}$ is separated and compared to $A\beta_{WT}$ monomer. As previously mentioned, this mutation serves to promote the formation of stabilized protofibrils and speeds up fibrillogenesis when mixed with $A\beta_{WT}$ monomer. CE is attractive for these separations due to the advantages of high efficiency, small sample consumption, and ease of automation.[5] The presented work shows a clear distinction between the electrophoretic mobility and peak shape of monomer and fibril species. In addition, the stabilization of an intermediate aggregate by calmidazolium chloride allows for the interrogation of this otherwise transient species. The isolation of the different conformational species of Aβ along the aggregation pathway (i.e. monomer,

protofibril, and fibril) in the preparation steps reported herein, confirmed by electron microscopy, warrant the conclusive identification of the observed peaks resulting from each species. Collected peak fractions were analyzed using matrix assisted laser desorption ionization-time of flight mass spectrometry (MALDI-TOF MS) to confirm the presence of Aβ. Furthermore, fibrillogenesis was monitored over a period of several days using CE to separate a mixture of $A\beta_{WT}$ and $A\beta_{ARC}$ monomers. The observed data was in agreement with published reports indicating the acceleration of fibrillogenesis in mixed solutions of $A\beta_{WT}$ and $A\beta_{ARC}$. The separations herein provide a means for rapid species identification based on a difference in mobility as well as a simple avenue for monitoring aggregation and exploring the effect of aggregation inhibitors or accelerators.

Experimental

Materials and reagents

Tris-HCl (tris(hydroxymethyl)aminomethane hydrochloride) and calmidazolium chloride were purchased from Sigma (St. Louis, MO). TFA (trifluoroactetic acid) was purchased from Pierce (Rockford, IL). HFIP (1,1,1,3,3,3-hexafluoro-2-propanol) was purchased from Acros (Suwanee, GA). All buffer and stock solutions were prepared in deionized, distilled water from a Barnstead Epure System (18MΩ resistivity, Newton, MA) except for calmidazolium chloride, which was prepared at a concentration of 1 mM in DMSO (dimethyl sulfoxide).

Monomer, protofibril, and fibril preparation

Chemically synthesized $A\beta_{WT}$(1-40), amino acid sequence DAEFRHDSGY EVHHQKLVFF AEDVGSNKGA IIGLMVGGVV, and $A\beta_{ARC}$ (1-40 Arctic (E22G))

peptides were purchased from Keck Biotechnology Center (Yale University). These peptides were disaggregated in order to remove any preexisting aggregates by a TFA/HFIP protocol as previously described.[30] The disaggregated peptides were then lyophilized for one hr and dissolved stepwise in equal volumes of 2 mM NaOH and 2X PBS (pH 7.4), containing 0.1 % sodium azide, to a final peptide concentration of approximately 50 μM. The samples were then centrifuged to remove any remaining aggregates ($A\beta_{WT}$ overnight at 315000 g and $A\beta_{ARC}$ for 30 min at 13000 g). The supernatant concentration was checked using HPLC, and the monomer solutions were removed for CE analysis at this point. In order to form CC-Aβ aggregates, the $A\beta_{WT}$ monomer was combined with calmidazolium chloride to a final concentration of approximately 30 μM $A\beta_{WT}$ monomer and 100 μM calmidazolium chloride in 1X PBS containing 10 % DMSO from stock calmidazolium chloride solution. Fibril samples were prepared by incubation of the monomer in 1X PBS at 37 °C for approximately 7 days. Thioflavin T assay was used to monitor fibril growth.[45] For $A\beta_{WT}$ and $A\beta_{ARC}$ mixture samples, the monomer samples were combined in a 1:1 ratio.

Capillary Electrophoresis Separations

All CE separations were performed using a Beckman Coulter P/ACE™ MDQ CE System. The instrument was equipped with a UV source and wavelength selectable UV detector with which absorbance detection was performed at 214 nm. Fused silica capillaries (50 μm inner diameter, 358 μm outer diameter; 60 cm total length, 50 cm to detector) were placed in the capillary cartridge and thermostatted at 25 °C along with the sample holding chamber. At the beginning of every day, the capillary was flushed

sequentially at 20 psi with the following solutions: 1 M HCl for 10 min, Epure water for 2 min, methanol for 5 min, Epure water for 2 min, 1 M NaOH for 10 min, Epure water for 2 min, and 10 mM Tris-HCl, pH 7.8 running buffer for 5 min. Between runs, a 20 psi buffer flush was performed for 5 min.

A buffer exchange step was performed on all peptide solutions in order to replace the high salt PBS buffer with one more compatible with CE separations. Microcon® YM-3 centrifugal filter units (Fisher) were used as directed for buffer exchange procedures on $A\beta_{WT}$ monomer peptide samples. For CC- $A\beta_{WT}$ aggregates and $A\beta_{WT}$ fibril samples, a centrifugation step (30 min at 13000 g) was used to pellet out the peptide. The PBS buffer was then removed and the peptide was washed with 10 mM Tris-HCl. This wash step was repeated again before a final resuspension of peptide in 10 mM Tris-HCl. Pressure injections were used (5.0 s at 1.0 psi) and the applied separation potential was 12 kV, producing an electric field of 200 V/cm for all samples.

For $A\beta_{WT}$ and $A\beta_{ARC}$ mixture separations, PBS buffer was exchanged using Microcon® YM-3 centrifugal filter units, with the centrifugation step carried out in a refrigerated centrifuge to avoid aggregation. The monomer mixture was then resuspended in 2 mM Tris-HCl. Electrokinetic injections were used for these samples (5.0 s at 10 kV), with a separation potential of 12 kV, producing an electric field of 200 V/cm.

Data was acquired using 32 Karat™ Software Version 5.0 from Beckman Coulter. Peak fractions were collected using the Manual Fraction Collection feature and specifying appropriate peak elution times and peak widths. Thirty consecutive CE runs

were performed, with peaks collected, for each sample. All data was exported and analyzed using Microsoft Excel®.

Matrix Assisted Laser Desorption Ionization-Time of Flight Mass Spectrometry (MALDI-TOF MS)

Mass spectra of collected peak fractions (collected as described above) were acquired on an Applied Biosystems Voyager DE-PRO™ MALDI-TOF MS, equipped with a 20 Hz repetition rate nitrogen laser (337 nm). The instrument was controlled by Voyager Version 5.0 Software with Data Explorer™ and operated in the linear mode. CHCA (α-cyano-4-hydroxycinnamic acid) matrix was prepared in acetonitrile/H_2O (50:50, v/v) containing 1.0 % TFA to a final concentration of 10 mg/mL and combined with equal volumes of peptide sample from collected peak fractions. The samples were then spotted on a standard 100 well stainless steel MALDI sample plate. Laser power was adjusted for each sample spot, with 200 shots acquired per spectrum.

Electron Microscopy

$A\beta_{WT}$ samples in 10 mM Tris-HCl (fibrillar and protofibrillar) were adsorbed onto glow-discharged carbon-coated copper grids. Grids were then stained with freshly prepared 0.75 % uranyl formate. A Hitachi H-800 electron microscope operated at 100 kV was used to inspect the specimens, and images were taken at 50,000x nominal magnification.

Results and Discussion

Monomer

The monomeric form of amyloid beta peptide is normally present in human plasma and cerebrospinal fluid (CSF), with the 40 amino acid variant the most common.[36] However, upon pathogenesis, the peptide begins to aggregate into soluble oligomers and insoluble fibrils that are deposited in the brain. The 40 amino acid $A\beta_{WT}$ monomer samples used in this work were prepared according to the procedure outlined above to a final concentration of 38 μM. Analysis of the separation of the $A\beta_{WT}$ monomer species by CE reveals two peaks (Figure 2.1). The first peak was well-resolved, reproducible and attributed to $A\beta_{WT}$ monomer, while the second peak is believed to be a system peak as it was not consistently present from run to run. The baseline dip in Figure 2.1, which appears after the monomer peak, is the result of the fraction collection programming during which time the end of the separation capillary was transferred to another sample vial for peak collection. Approximately 30 CE fractions were collected and analyzed using MALDI-TOF MS. The inset of Figure 2.1 depicts the observed MS peak, which corresponds to the molecular ion, $[M+H]^+$, of $A\beta_{WT}$ (4330.5 Da). The weak MALDI MS signal could be the result of the low peptide concentrations from CE fraction collection or the inefficient MALDI ionization of the Aβ peptide due to limited basic amino acid residues. Based on its pI value of 5.2, $A\beta_{WT}$ monomer migrated under its anionic form, and the peak retention time was changed to electrophoretic mobility using a neutral marker.[46] An electrophoretic mobility of -1.22×10^{-4} $cm^2 V^{-1}sec^{-1}$ was observed for the monomer peak, with this mobility and peak shape remaining constant throughout

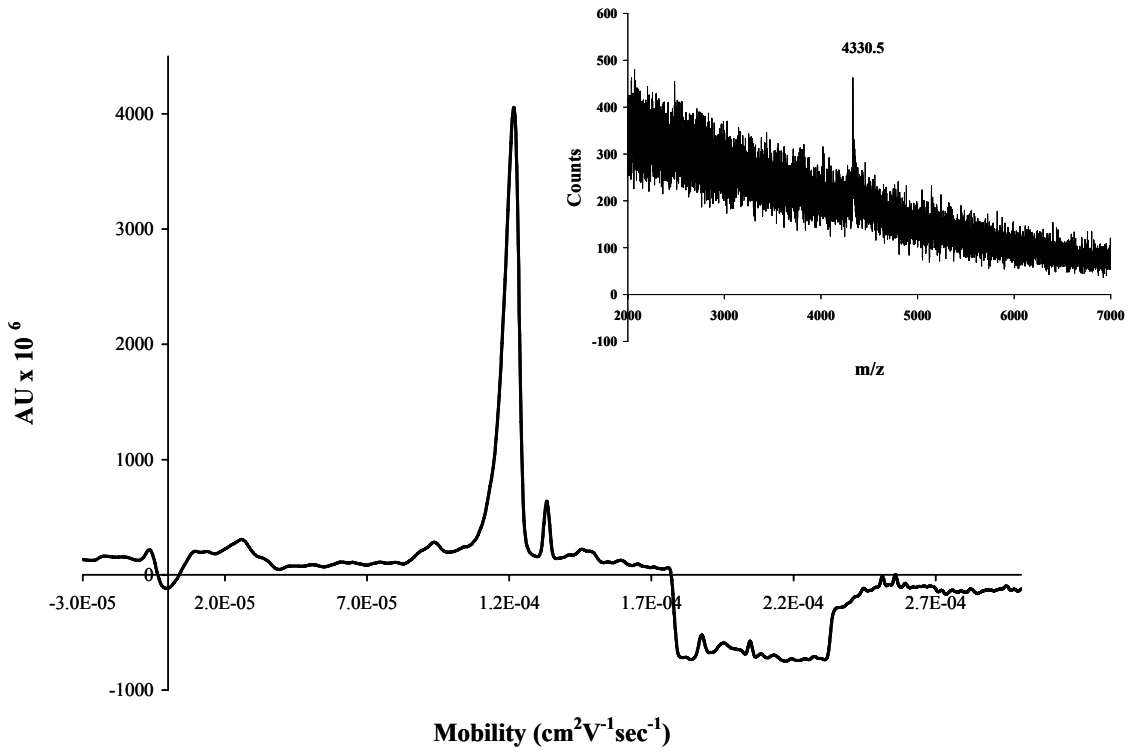

Figure 2.1 Electropherogram of 38 μM $A\beta_{WT}$ monomer sample injected for 5.0 s at 1.0 psi into a capillary filled with 10 mM Tris-HCl, pH 8.0. Manual fraction collection was used to collect monomer peak, and the inset depicts the collected MALDI-TOF mass spectrum from the monomer fraction.

multiple injections. Prior to CE separation, the monomer sample was spotted on a copper grid for EM analysis. As expected, there were no discernable shapes in the EM images due to the small monomer size and inadequate resolution of the electron microscope (Figure 2.2A). However, this did confirm that aggregate species were not present in the monomer sample, as they would be obvious in the EM images.

Aggregate

Studies suggest that the neurotoxic species in AD may be the soluble intermediate (protofibril).[47] However, because they are transient in the fibrillogenesis process and tend to dissociate in buffer solutions, they prove difficult to analyze using many biophysical techniques. Calmidazolium chloride (CC) was previously found to interact with soluble Aβ, resulting in a rapid conversion to a pelletable aggregate species. This interaction did not increase the signal from a Thioflavin T (ThT) fluorescence assay used to measure fibril formation, suggesting that the aggregate species induced by CC resemble a protofibril, and not mature fibril, species.[44] In the work reported herein, CC-$A\beta_{WT}$ aggregate samples were prepared according to the procedure outlined above to a final aggregate concentration of 29 μM. Analysis of the separation of the CC-$A\beta_{WT}$ aggregates by CE revealed a single, narrow peak with electrophoretic mobility of -1.55 x 10^{-4} cm^2 $V^{-1}sec^{-1}$ attributed to CC-$A\beta_{WT}$, as well as a peak representing mesityl oxide used as the neutral marker (Figure 2.3). The fact that CC-$A\beta_{WT}$ elutes after the monomer species is presumably a result of the greater negative charge of the aggregate species resulting in an increase in electrophoretic mobility. The presence of CC seems to lead to a clustering of individual protofibrils, possibly facilitated by CC binding. Because CC is

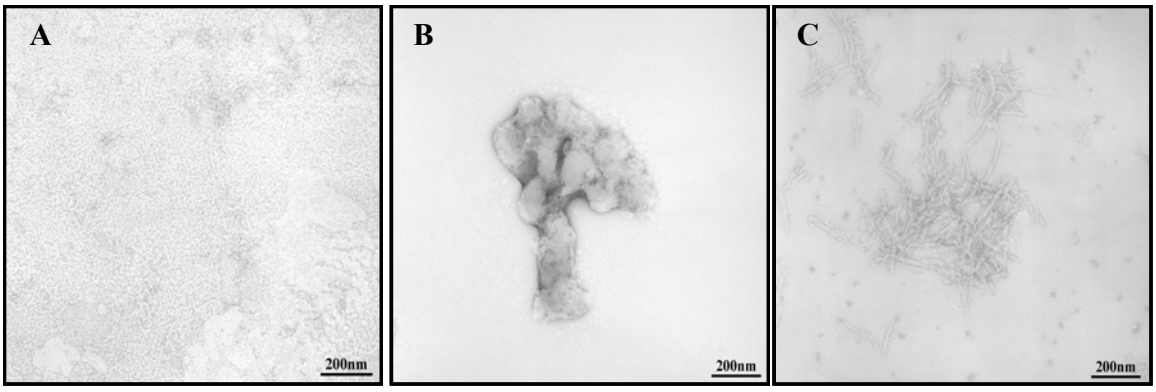

Figure 2.2 Electron micrographs of A) $A\beta_{WT}$ monomer; B) $A\beta_{WT}$ calmidazolium chloride stabilized aggregate; C) $A\beta_{WT}$ fibril species.

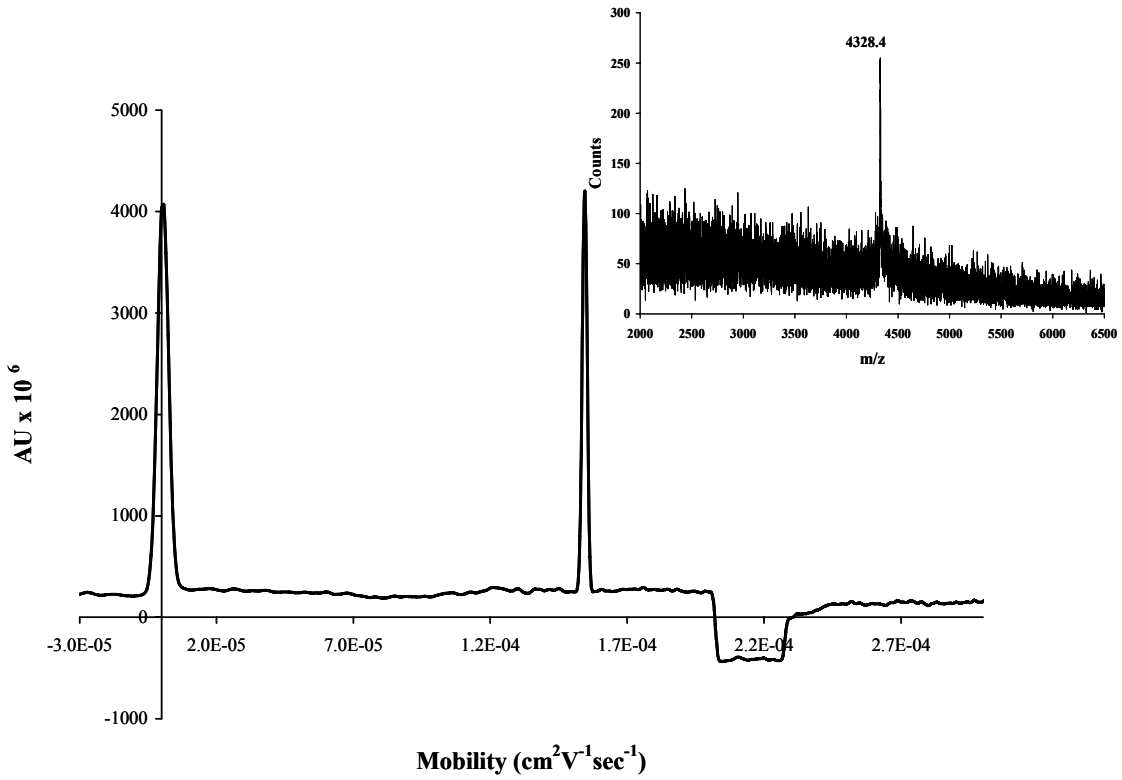

Figure 2.3 Electropherogram of 29 μM CC-$A\beta_{WT}$ aggregate sample injected for 5.0 s at 1.0 psi into a capillary filled with 10 mM Tris-HCl, pH 8.0. Manual fraction collection was used to collect the aggregate peak, and the inset depicts the collected MALDI-TOF mass spectrum from the aggregate fraction.

used to stabilize the protofibrillar intermediate aggregate, the normally transient species between the monomer and fully formed fibril can be analyzed using CE. The dip present in the electropherogram is, again, a result of the fraction collection method. The inset of Figure 2.3 illustrates the mass spectrum from the collected CC- $A\beta_{WT}$ fraction with a molecular ion peak at 4328.4 Da. The CC-$A\beta_{WT}$ sample, prior to CE separation, was spotted onto copper grids for EM analysis. The electron micrographs revealed large, fine-structured spheroids similar to previous reports of isolated protofibrils characterized by EM, but no fully formed, mature fibril species (Figure 2.2B).[31, 48]

Fibril

Deposition of insoluble, fully formed fibrils in the brains of AD patients is a hallmark of the disease. Fibrils are normally long unbranched filaments with widths of ~10 nm and varying lengths up to several microns. The $A\beta_{WT}$ fibrils used in the experiments reported herein were prepared according to the procedure outlined above to a final concentration of 51 μM. Analysis of $A\beta_{WT}$ fibril separation by CE revealed a broad collection of peaks with a range of electrophoretic mobilities from -1.98×10^{-4} to -2.88×10^{-4} $cm^2\ V^{-1}sec^{-1}$ (Figure 2.4). The range of peaks is a result of the heterogeneous nature of the fibril sample. Once again, the fact that the fibril peaks elute after the monomer and protofibril species under conditions of normal polarity presumably indicates that this $A\beta_{WT}$ species possesses a greater negative charge relative to the radius change, resulting in increased electrophoretic mobility. The peaks corresponding to the fibril species were again collected using manual fraction collection and analyzed using MALDI-TOF MS to confirm the presence of $A\beta_{WT}$. The peak corresponding to the molecular ion appears at

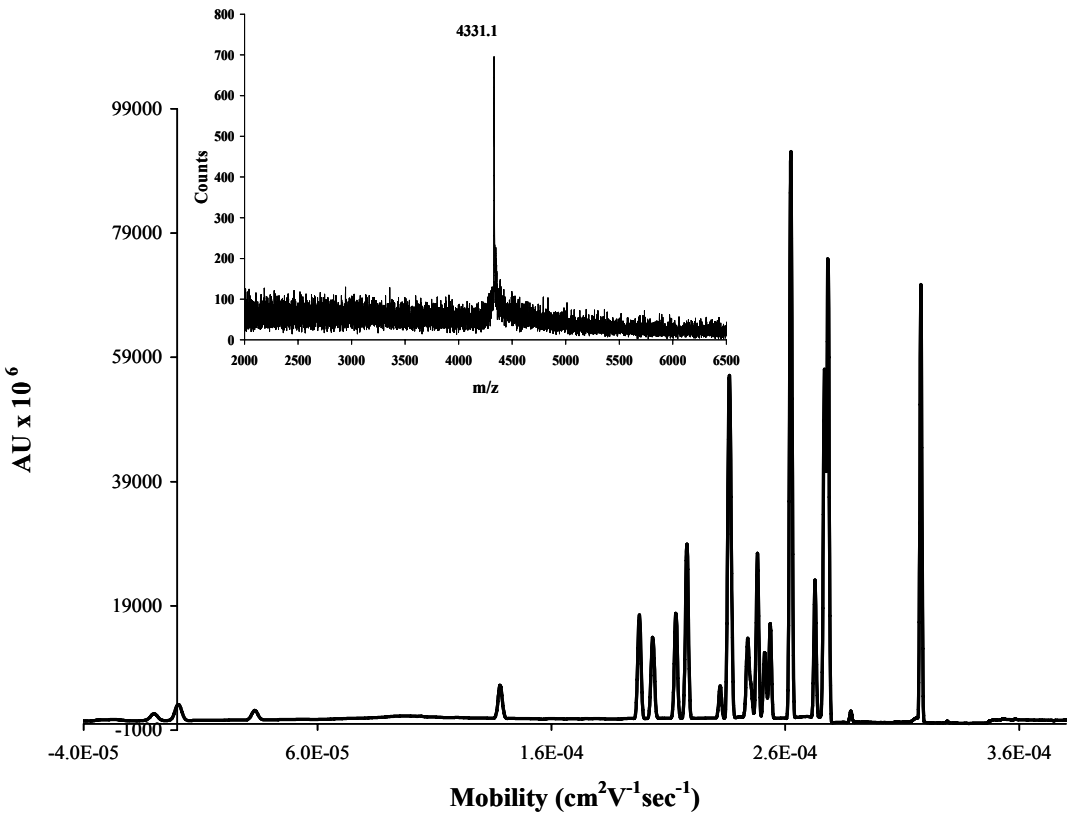

Figure 2.4 Electropherogram of 51 μM AβWT fibril injected for 5.0 s at 1.0 psi into a capillary filled with 10 mM Tris-HCl, pH 8.0. The separation potential was 20 kV. Manual fraction collection was used to collect the fibril peak, ,and the inset depicts the collected MALDI-TOF mass spectrum from the fibril fraction.

4330.1 Da, as shown in Figure 2.4. In addition, the EM images from this sample reveal the characteristic long, unbranched rod-like fibril structure (Figure 2.2C).

MALDI-TOF Analysis

Fractions of all CE separated $A\beta_{WT}$ samples were collected and analyzed using MALDI-TOF MS as discussed in the experimental section. Each collected fraction produced a single, representative peak in the mass spectra resulting from the $[M + H]^+$ ion of $A\beta_{WT}$ peptide, which has a molecular weight (MW) of 4328.9 Da (i.e. a molecular ion $[M + H]^+$ of 4329.9 Da). Although the peaks in each of the three mass spectra (monomer, aggregate, and fibril) are slightly different in mass, they are all within the mass accuracy of the instrument for the MW of $A\beta_{WT.}$ The MS results confirm that the peaks collected from each of the separations did indeed contain $A\beta_{WT}$ peptide. Since the peaks exhibited quite different electrophoretic mobilities, the only conclusion is that they represent different conformational species of $A\beta_{WT}$ along the pathway to fibrillogenesis.

AβWT and AβARC Mixture

A mutation of APP, where glutamic acid at the 22nd amino acid residue of the amyloid peptide is substituted for glycine (E22G), termed the Arctic mutation ($A\beta_{ARC}$), results in a decrease of $A\beta_{WT}$ in the plasma of carrier individuals, as well as an increase in protofibril formation *in vitro*. This suggests that the $A\beta_{ARC}$ mutation initiates an alternate pathogenic mechanism for AD manifestation, possibly implementing the protofibril as the primary neurotoxic species.[49] Since carriers of the Arctic mutation are heterozygotes and express both $A\beta_{ARC}$ and $A\beta_{WT}$, it is of interest to understand the *in vitro* behavior of mixed solutions. Previous studies showed that addition of $A\beta_{WT}$ to $A\beta_{ARC}$ samples

stabilized the protofibril species, with the protofibril primarily comprised of $A\beta_{ARC}$.[41] For studies reported herein, monomer samples of $A\beta_{WT}$ and $A\beta_{ARC}$ were prepared as outlined above to a final concentration of 21 μM and 18 μM, respectively. Initially, a monomer control sample for each Aβ species was separated using CE. Subsequently, $A\beta_{WT}$ and $A\beta_{ARC}$ samples (55 μM) were mixed together in a 1:1 ratio and incubated at room temperature in PBS for the duration of the experiment. Each day, a sample was removed from the mixture and the buffer exchanged for CE separation. The $A\beta_{ARC}$ and $A\beta_{WT}$ monomer species had different electrophoretic mobilities of -1.12×10^{-4} and -1.47×10^{-4} $cm^2\ V^{-1}sec^{-1}$, respectively (Figure 2.5). It is interesting to note the difference in the mobilities for these two Aβ species, as they differ only in one amino acid residue. However, the replacement of glutamic acid at position 22 by glycine results in a loss of charge for $A\beta_{ARC}$ as compared to $A\beta_{WT}$, resulting in a decrease in electrophoretic mobility. For the first separation after mixing of the two monomer solutions (day 0), the monomer peak is split because it results from a mixture of $A\beta_{ARC}$ and $A\beta_{WT}$ monomer species. The original separations seen in Figure 2.5 were before the use of a refrigerated centrifuge and a second peak in the $A\beta_{ARC}$ monomer and mixture separations can be seen. This peak is believed to be caused by aggregation accelerated by the centrifuge. A refrigerated centrifuge was used in all subsequent separations. Samples were extracted from the incubating monomer mixture each day and separated using CE. Figure 2.6 depicts the change in separation of the mixture throughout the experiment. An aggregate peak can be seen growing in at longer incubation times as the $A\beta_{ARC}$ peak begins to be

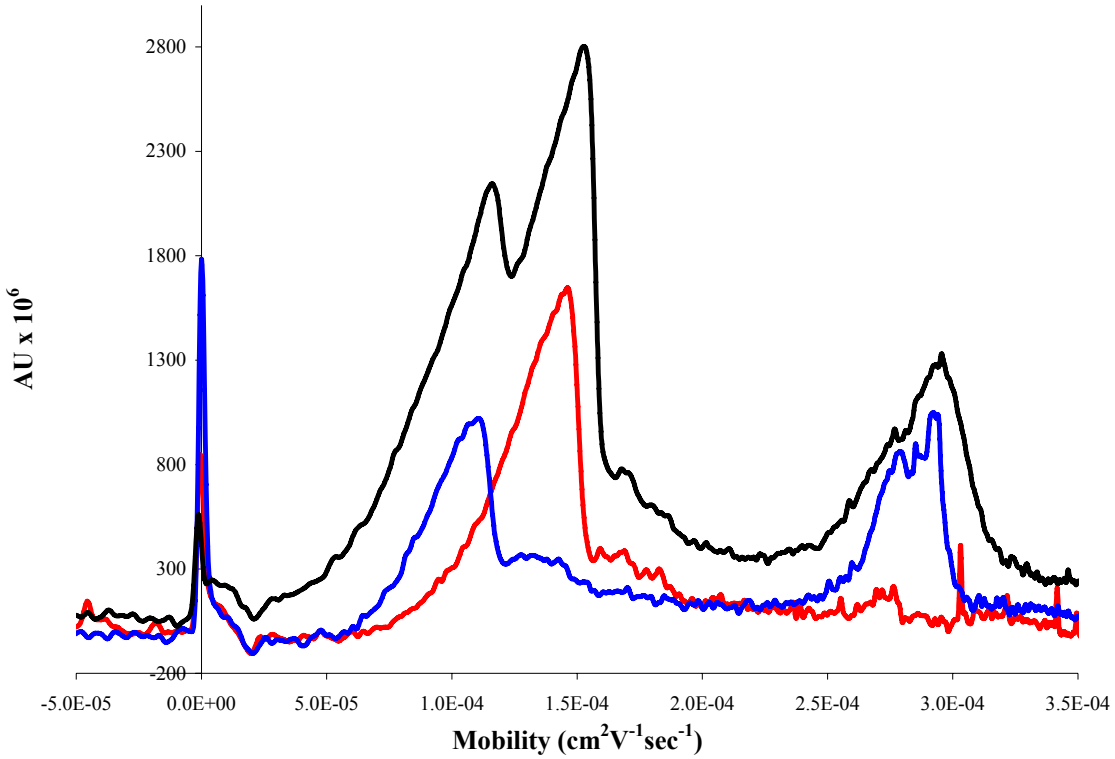

Figure 2.5 Electropherogram of 21 μM $A\beta_{WT}$ (red), 18 μM $A\beta_{ARC}$ (blue) and a 1:1 mixture (55 μM) of the two species (black). All samples were injected for 5.0 s at 10 kV into a capillary filled with 2 mM Tris-HCl, pH 8.49.

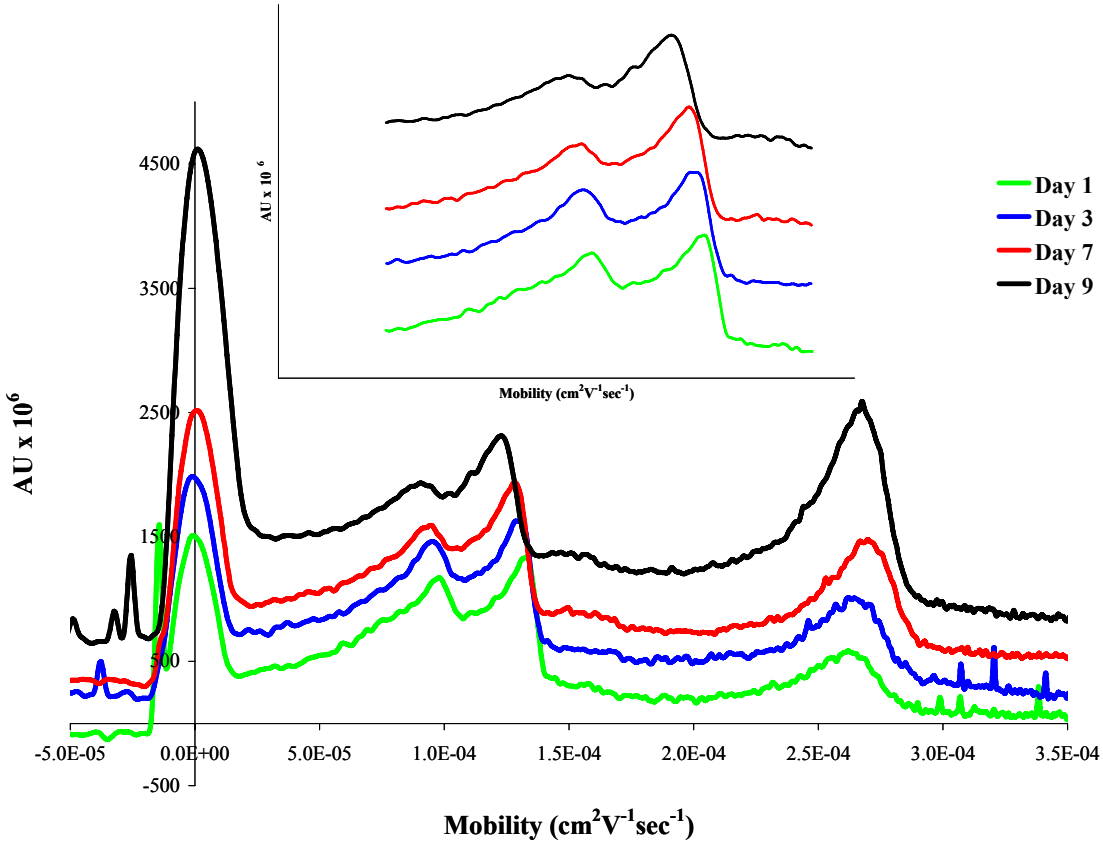

Figure 2.6 Electropherograms of 55 µM 1:1 $A\beta_{WT}$:$A\beta_{ARC}$ mixture from day 1-9 of the fibrillogenesis process. All samples were injected for 5.0 sec at 10 kV into a capillary filled with 2 mM Tris-HCl, pH 8.49. The inset highlights depletion of the $A\beta_{ARC}$ peak as fibrillogenesis proceeds.

depleted relative to the $A\beta_{WT}$ monomer peak (Figure 2.6 inset). This result supports earlier findings that $A\beta_{WT}$ monomer stabilizes protofibril intermediates formed by $A\beta_{ARC}$ monomers, but is preferentially excluded from the protofibril and fibril species.[41] This would cause the $A\beta_{ARC}$ peak to be diminished more quickly that the $A\beta_{WT}$ monomer.

Conclusions and Future Work

Part I of this dissertation highlights the decisive identification of three conformational species of Aβ along the aggregation pathway (monomer, aggregate and fibril). This is the first report of the separation and conclusive identification, using electron microscopy and mass spectrometry, of the aforementioned Aβ conformations. Clear distinctions are made in electrophoretic mobility and peak shape for each conformation of Aβ analyzed. The results reported herein would make possible rapid species identification and screening of aggregation accelerators or inhibitors. Moreover, the separations performed on the $A\beta_{ARC}$:$A\beta_{WT}$ mixture demonstrate the ability to monitor aggregation of Aβ peptides over time, possibly shedding light on the elusive mechanism of aggregate and fibril formation.[37, 38] Work on this project is ongoing and recent experiments support the findings reported herein. Additionally, continuing work established a detection limit of 4 μM for the monomer species of Aβ at a signal to noise ratio of 3.[50] ThT fluorescence studies of the Aβ fibrillization process correlated well with the results of CE separation and proved the importance of monomer sample preparation, as in vitro studies are extremely susceptible to experimental conditions used in sample preparation, and the presence of any aggregate species in a monomer sample will accelerate fibrillogenesis.

PART II .
DEVELOPMENT OF MAGNETICALLY ASSISTED TRANSPORT EVANESCENT FIELD FLUORO-ASSAYS

CHAPTER 3.
INTRODUCTION TO IMMUNOASSAYS AND EVANESCENT SENSING

Taking advantage of the specific affinity of an antibody for its target antigen, immunoassays have developed into one of the most fruitful contributions to medicine and life science of the last century. Dating back to 1900, the immunoassay concept originated with the blood typing research of Ehrlich and Landsteiner.[51] The modern immunoassay was detailed in the late 1950's with the investigation of diabetes by Berson and Yalow.[52] In their research, they experimented with radiolabeled and unlabeled insulin and described the first radioimmunoassay, winning the Nobel Prize in 1977. Today, immunological techniques are involved in over one billion clinical tests annually in the United States alone, ranging from drug tests to pregnancy tests. However, immunoassay utility has not been confined to the medical field, as they have found application in environmental, food, pharmaceutical, veterinary and forensic sciences.[53] In addition to the range of applications, there have been many novel and clever immunoassay designs introduced which sought to enhance sensitivity, simplify protocols, and/or increase throughput. The concept of Magnetically Assisted Transport Evanescent Field Fluoro-assays (MATEFFs) aims to reconcile the advantages of some current immunoassay strategies while implementing, for the first time, a localized evanescent sensing surface and magnetic delivery of a target analyte to the surface for detection.

Immunoassay Theory and Basics

The Antibody

It is serendipitous that nature provides the key element used in the study of so many biological processes. The antibody is a protein belonging to the immunoglobulin family, and is produced in humans and animals in response to some foreign substance, or antigen. The most common class of immunoglobulin and that which provides the majority of antibody based immunity is IgG, although there are also IgM, IgA, IgD, and IgE subclasses with different biological properties and response to antigen. The typical structure of IgG is illustrated in Figure 3.1. Each type of antibody is made up of a Y-shaped monomer unit comprised of four polypeptide chains: two identical heavy chains and two identical light chains connected by disulfide linkages. Each light chain has a molecular weight of about 25,000 Da and is composed of both a variable (V_L) and constant domain (C_L). The heavy chains, with a molecular weight of 50,000 Da (making the entire antibody structure ~150,000 Da), contain one variable domain (V_H) and three or four constant domains (C_{H1}, C_{H2}, C_{H3}) depending upon the subclass. The variable domains, at the two tips of the Y structure, differ in amino acid composition and determine the antibody specificity for a particular antigen. Antibodies can be proteolytically digested into Fab, $F(ab')_2$ and Fc fragments, depending upon the cleaving enzyme employed. Papain cleaves above the disulfide linkages which act as a hinge, forming two Fab fragments and the Fc portion, while pepsin cleaves below the hinge leaving one $F(ab')_2$ portion and the Fc portion. The Fab and $F(ab')_2$ fragments are responsible for antigen binding, with the Fc portion mediating the physiological effect upon antibody response.

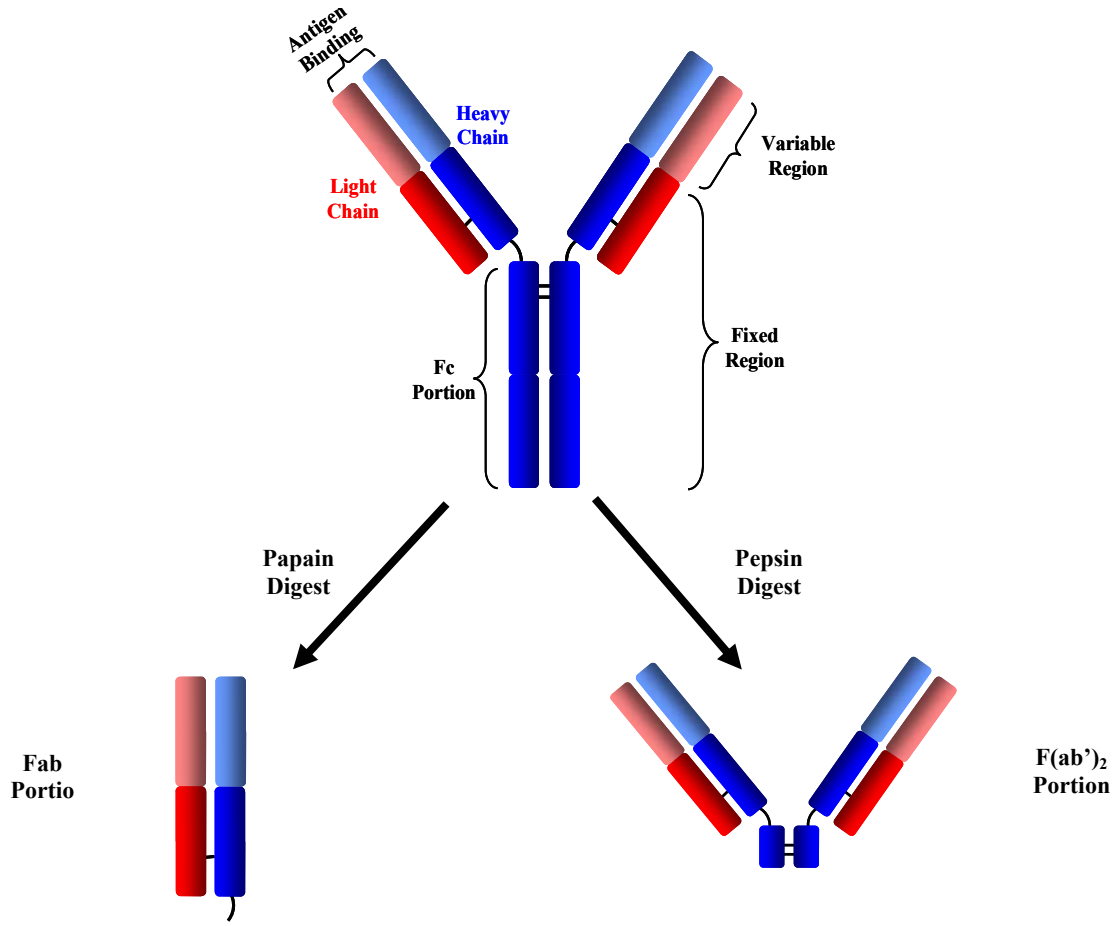

Figure 3.1 Basic IgG structure and the Fab and F(ab')$_2$ products produced by protease digestion.

Antibodies can be elicited against a large variety of compounds (antigens), both natural and man-made, as a result of the enormous number of possible amino acid sequence combinations within the binding site. Once obtained, the antibody is specific for its target antigen (more so than most other reagents), able to bind to diminutive concentrations of analyte in the presence of many similar substances. Small molecules that are not able to stimulate an immune response on their own, termed haptens, can be attached to a large carrier molecule (bovine serum albumin, for example) for antibody generation in response to the hapten-carrier adduct. One of the resulting antibodies may then be specific for the small molecule even in the absence of the carrier molecule, facilitating generation of an antibody for a molecule that would otherwise be unrecognizable to the immune system. Further, with the development of recombinant techniques allowing rapid cloning and DNA characterization, antibodies are now being engineered to produce specific functional properties for a desired application.[54]

The strength of binding between an antibody and its antigen is dependent upon the sum of these contributing non-covalent forces; electrostatic interactions, hydrogen bonding, Van der Waals forces, and hydrophobic interactions. Van der Waals and hydrophobic forces operate over short distances due to structurally similar surfaces, while electrostatic interactions and hydrogen bonding are a result of specific reactive groups shared by the antigen and antibody. Though antibody-antigen interactions are non-covalent, the affinity of an antibody for its antigen can be quite high. The affinity constant (K_a) measures the "tightness" of binding between one antibody binding site and the antigen epitope for which it is specific, and represents the ratio of bound to unbound analyte. At equilibrium

$$K_a = \frac{[Ag - Ab]}{[Ag][Ab]} \tag{3-1}$$

where [Ag] represents concentration of free antigen, [Ab] signifies free antibody concentration, and [Ag-Ab] corresponds to the concentration of antigen-antibody complex.[55] Typical affinity constants for IgG antibodies are 10^5-10^9 L/mole, but some antibodies can have affinity constants as high as 10^{13} L/mole.[56] Sometimes, a better measure of binding in a biological system is the antibody avidity, which represents the overall binding between an antibody and antigen This includes binding between multiple epitopes of an antigen and the different binding sites for the antibody (IgG has two possible binding sites).[57]

Antibodies can be either monoclonal or polyclonal, and both are useful depending upon the immunoassay application. Polyclonal antibodies (PAbs) are a result of classical immune response whereby an injected antigen stimulates production of many antibodies, recognizing several epitopes on the antigen. Because of the heterogeneity of PAbs, the effect of small changes in an antigen epitope is less likely to be significant. Additionally, PAbs are stable in a range of pH and salt concentrations, and less likely to be altered by covalent attachment of a fluorophore or other reporter molecule. Since PAbs are produced by a large number of B cells in response to the antigen and are therefore a combination of antibodies with unique specificities, they are generally more specific than monoclonal antibodies (MAbs).[57] MAbs, first developed by Kohler and Milstein some 30 years ago, are produced when single B-cells are fused with immortal myeloma cells to produce a hybridoma that can yield multiple copies of the exact same antibody.[58, 59] MAbs are homogenous and consistent, making them quite useful when evaluating

conformational changes or protein interactions. However, this homogeneity renders them much more susceptible to small changes in epitope structure. MAbs are constantly generated once a hybridoma is successfully created, making them a renewable resource. Furthermore, MAbs are generated at a higher concentration and purity for a given antibody than PAbs. The generation of MAbs is expensive, time consuming, and requires considerable technical skill as compared to PAbs. This is not an issue, however, if the antibodies are readily commercially available. The decision of whether to use PAbs or MAbs is, again, dependent upon the intended use. In summary, PAbs are generally more robust, can be generated by a variety of species, and are more tolerant of small conformational changes in the antigen. MAbs, on the other hand, are excellent primary antibodies because of their specificity and yield reproducible results due to their homogeneity.

Immunoassay Classification

Competitive vs. Non-competitive

Immunoassays can normally be categorized as either competitive (reagent limited) or non-competitive (reagent excess). Competitive assays normally require a fixed concentration of labeled antigen (or tracer) that competes with unlabeled antigen for a limited number of antibody binding sites. The signal from this form of competitive assay, as it is generated by the tracer antigen, is inversely proportional to the concentration of unlabeled antigen in the sample. An example is illustrated in Figure 3.2A. Alternatively, the antibody can be labeled and allowed to react with bound antigen in the presence of an antigen containing sample solution. After washing, the signal from

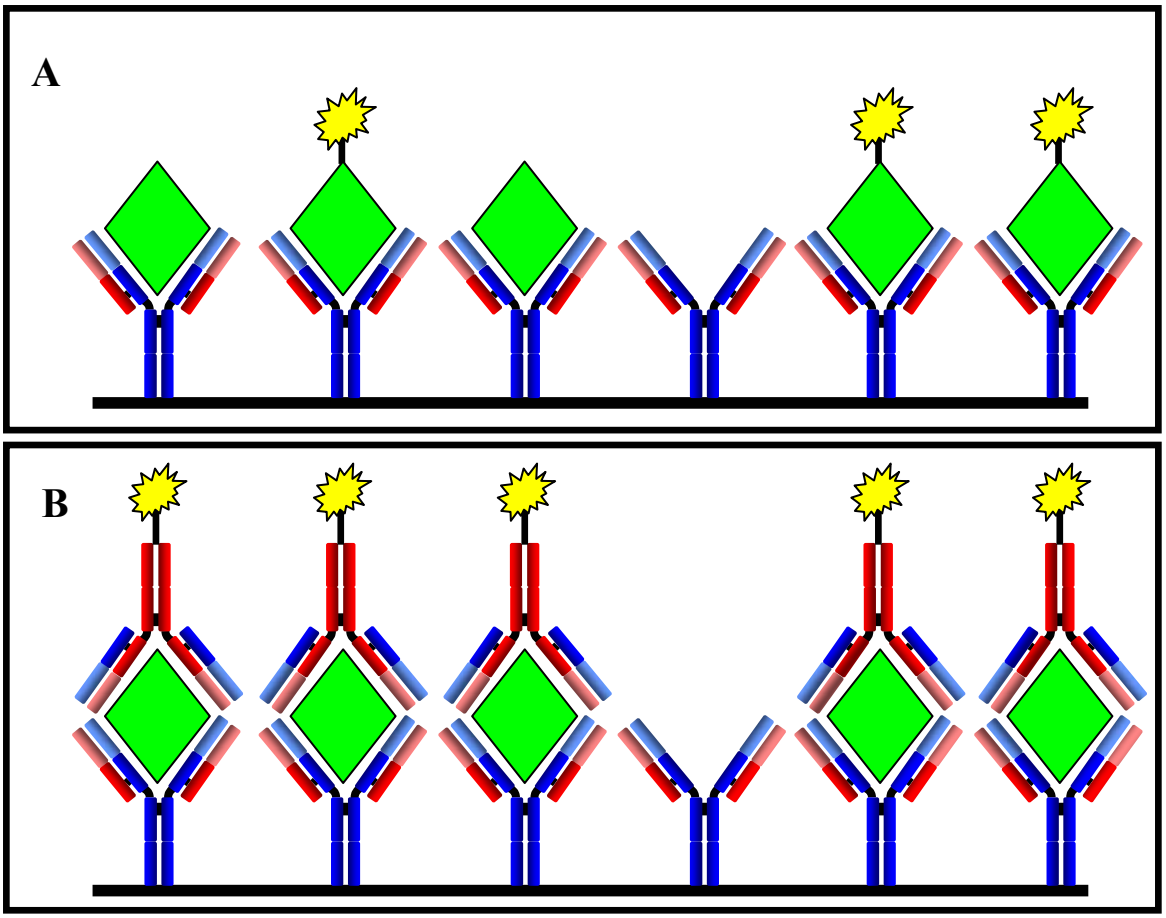

Figure 3.2 A) Competitive immunoassay illustration (solid phase separation). B) Non-competitive immunoassay illustration.

the labeled antibody bound to the surface is measured and is, again, inversely proportional to the sample antigen concentration.

In a non-competitive assay (sandwich) format, the antigen is normally bound by two antibodies; one that acts as the capture antibody and one that is labeled and acts as a reporter antibody. An example is shown in Figure 3.2B. In this case, the signal generated is directly proportional to the concentration of analyte. In order to carry out a sandwich assay, the antigen of interest must contain two separate epitopes, or antibody binding areas.[33, 58]

When choosing between non-competitive and competitive assay designs, several factors must be considered. Normally, small molecules are analyzed using a competitive immunoassay format since they offer only one site for antibody binding. Additionally, competitive assays are sometimes preferred when analyzing a broad range of analyte concentrations. Non-competitive assays, on the other hand, have many advantages over competitive assays. They are normally faster and easier to use on-site, have greater specificity for the target analyte, and boast lower limits of detection.[60-62] For these reasons, the sandwich assay design will be implemented in the work discussed in this dissertation.

Homogeneous vs. Heterogeneous

Immunoassays are also classified as either homogeneous or heterogeneous, depending upon whether or not a solid phase is employed. Homogeneous assays do not require the separation of bound and free analyte/antibodies before signal measurement. In these

cases, the act of binding between the antibody and antigen results in some modulation of signal that can be detected in the presence of free antigen and antibody (Figure 3.3A). The level of modulation is a factor in limiting sensitivity since there must be a clear differentiation between signal and background. Homogeneous immunoassay strategies involve turbidity measurement, fluorescence protection, fluorescence energy transfer, and fluorescence polarization, to name a few.[53, 63-65] The use of homogeneous assay techniques is obviously attractive as it simplifies the steps and decreases the time required for the immunoassay. In theory, the homogeneous assay should be more sensitive than its heterogeneous counterpart, as complicated and possibly denaturing wash steps are avoided. However, the sample matrix proves to be a formidable foe when attempting to decrease background signal. Furthermore, many homogeneous assays do not realize the full potential of decreased analysis time since the addition of several reagents is required prior to detection.

In heterogeneous assays, either the antigen or antibody is immobilized on a solid support surface. After allowing sufficient time for binding between the antigen and antibody, a wash step removes the free antigen or antibody before signal measurement takes place (Figure 3.3B). It is advantageous to remove the sample matrix, especially in those cases where the matrix is biological in nature with the presence of many possibly interfering species. Furthermore, solid-phase immunoassays facilitate concentration of the bound complex on a surface for detection, such as in the case of strip kit pregnancy and ovulation tests. However, heterogeneous assays are generally time and reagent consuming, as the antibody or antigen must diffuse to the solid surface for binding to take place and multiple wash steps diminish throughput and, sometimes, sensitivity.[66, 67]

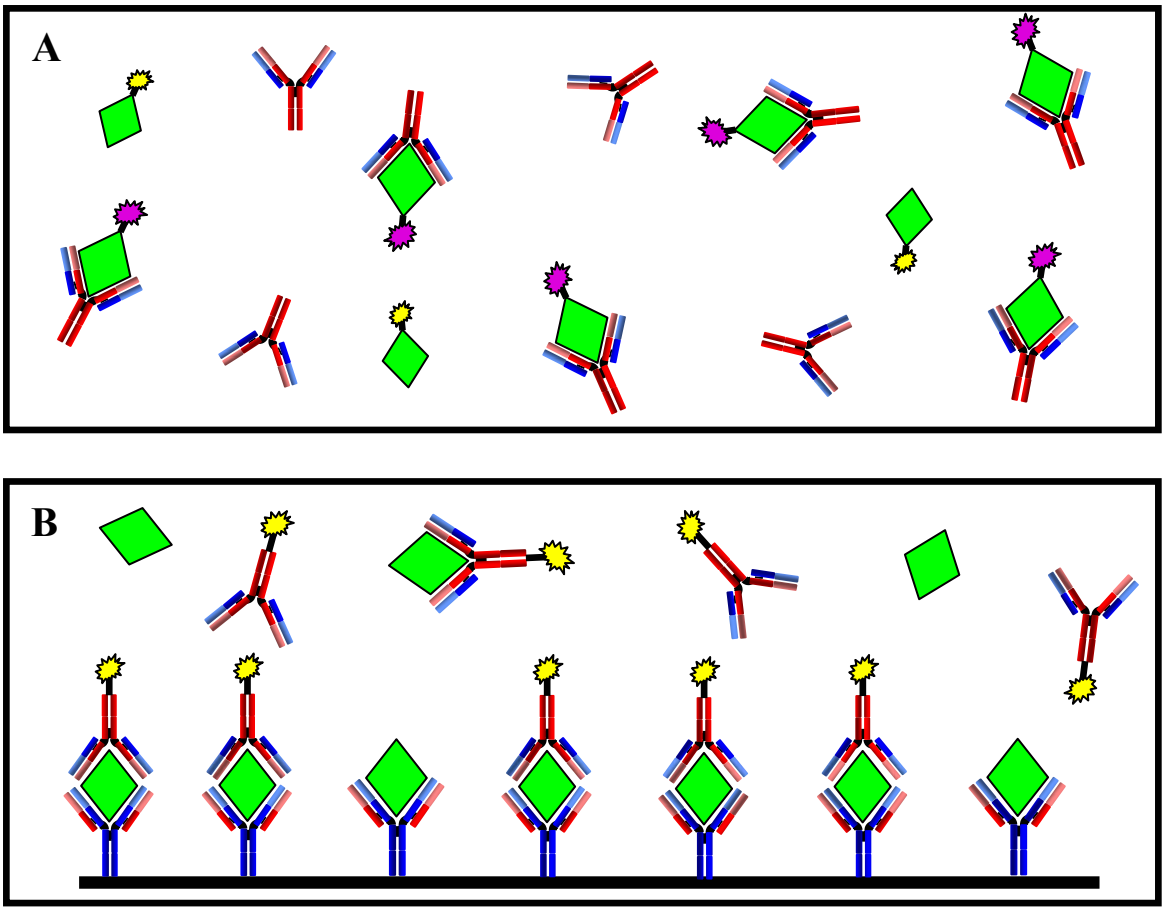

Figure 3.3 A) Example of homogeneous immunoassay. B) Example of heterogeneous immunoassay format (before wash steps).

Labels

Virtually all immunoassays rely on the use of a label for signal generation. There are a variety of labels currently employed in the immunoassay field including, but not limited to, radioisotopes, enzymes, fluorophores and particles.[68] Radioimmunoassays (RIAs), introduced in the 1950s, were very common in early immunoassay research. Radioisotopes are unstable atom variants that spontaneously emit energy in the form of particles or electromagnetic particles as they decay to a more stable state. The half-life, or time required for half of the radioisotope to decay, is specific to each isotope employed, with the most commonly used isotope being Iodine 125 (half life of 60 days).[53] Radioisotopes are easily detected with minimal interferences, but require a separation step, special detection equipment, and special precautions for disposal.[68]

Enzyme labels, introduced in the 1970s, are now the most widely used immunoassay label. Benefiting from the catalytic properties of enzymes to generate colored, fluorescent or luminescent compounds from neutral substrates, detection limits for enzymeimmunoassays (EIAs) can be quite low. However, signal generation in EIAs is susceptible to interferences from temperature, pH, and possible enzyme inhibitors. Consequently, special skill and experience is required in order to optimize not just the antibody-antigen interaction, but the production of signal.[69] The most commonly used enzymes for EIAs are horseradish peroxidase and alkaline phosphatase, with different substrates employed depending upon the signal source chosen.

Fluoroimmunoassays (FIAs) have gained in importance to the immunoassay field due to the inherent sensitivity of fluorescence spectrometry, commercial availability of a large

number of fluorophore labeled antibodies, and the increase in availability of cost-effective lasers for excitation. Fluorophores absorb light of a specific wavelength, and emit a photon of longer wavelength as they return to the ground state. This process can occur many times until some chemical damage or modification results in loss of the ability to fluoresce. FIAs suffer from high background, especially in biomedical analysis, as a result of scattering and autofluorescence from the sample matrix and are sensitive to temperature, pH and dissolved oxygen. The difference between excitation and emission wavelength (Stokes shift) should be maximized in order to minimize noise from incident light scatter, and the quantum efficiency, or proportion of absorbed energy that is re-emitted, should be as close to a value of 1 as possible. Fluorescein, rhodamine and their derivatives are most commonly employed in FIAs. More recently, quantum dots have become attractive fluorescent reporters with their high quantum yields, sharp emission spectras, chemical and photostability, tunability, and long shef-lives. These features make them quite attractive for multiplexing and ultrasensitive applications.[70] All immunoassay research in this dissertation made use of FIA techniques.[71]

Finally, particles ranging from dyed latex to colloidal gold to liposomes have been used as labels in immunoassay. Dyed latex labels are employed in some over-the-counter pregnancy tests in order to produce a visually recognizable response. Colloidal gold has been used as a label in order to aid in visualization by electron microscopy or to allow measurement of optical property changes upon binding and aggregation. Additionally, liposomes can be used in agglutination reactions upon immunocomplex formation or liposome lysis resulting in release of a trapped marker can be used for amplification.[53, 68]

Current Efforts in Immunoassay

The current push in immunoassay development, as in so many other areas of science, medicine, and technology, is toward miniaturization. The microarray immunoassay offers the ability to detect multiple analytes simultaneously in the same sample using spatially isolated individual immunoassays on a solid surface. Theoretically, these assay formats can be at least as sensitive as their macroscopic counterparts. It is imperative that antibody affinity and the number of active capture antibodies be maximized for microarray formats to be successful. This will require superior binding capacities on the solid surface and efficient binding strategies in order to retain maximum antibody activity. Since antibody microarrays depend heavily upon mass transport to the surface for binding, anything that improves the mass transport can potentially improve sensitivity.[62, 72, 73] The research efforts discussed in the following two chapters of this dissertation attempt to improve upon current bioassay methods and address the issues that will impact their success in the future.

Total Internal Reflection

Theory and Applications

When light travels across the boundary between two mediums possessing different refractive indices, the beam will normally be both refracted and reflected. However, under the special case where the light is traveling from a high index of refraction medium to one with a lower refractive index and the angle of incidence at the interface is greater than the critical angle, total internal reflection (TIR) will occur. The critical angle is the minimum incident angle at which TIR will occur, where the incident angle is measured

with respect to the normal at the boundary. Applying Snell's law, the fundamental law governing the refraction of light, where the angle of refraction is 90º, the critical angle, θ_c, is given by

$$\theta_c = \arcsin\frac{n_2}{n_1} \tag{3-2}$$

where n_2 is the refractive index of the less dense medium and n_1 is the refractive index of the more dense medium. At the precise critical angle, light will be reflected along the boundary between the two materials. At angles greater than θ_c, the light will be totally reflected except for an evanescent wave (EW) that penetrates into the lower refractive index medium (Figure 3.4). Evanescent means "tending to vanish", which is appropriate considering the EW decays exponentially as it penetrates into the lower refractive index medium with the penetration depth (*d*) given by [74, 75]

$$d = \frac{\lambda}{4\pi\sqrt{n_1^{\,2}\sin^2\theta - n_2^{\,2}}} \tag{3-3}$$

where λ is the wavelength of light and θ is the incident angle. The intensity of the evanescent wave at a distance *z* from the interface, *I(z)*, is given by

$$I(z) = I(0)e^{\frac{-z}{d}} \tag{3-4}$$

The most recognized application of TIR is in fiber optics, where this property of light is used to transmit focused light without significant loss and revolutionized the telecommunications industry. However, the localization of the evanescent field at the interface makes it attractive from a spectroscopic standpoint. System design changes

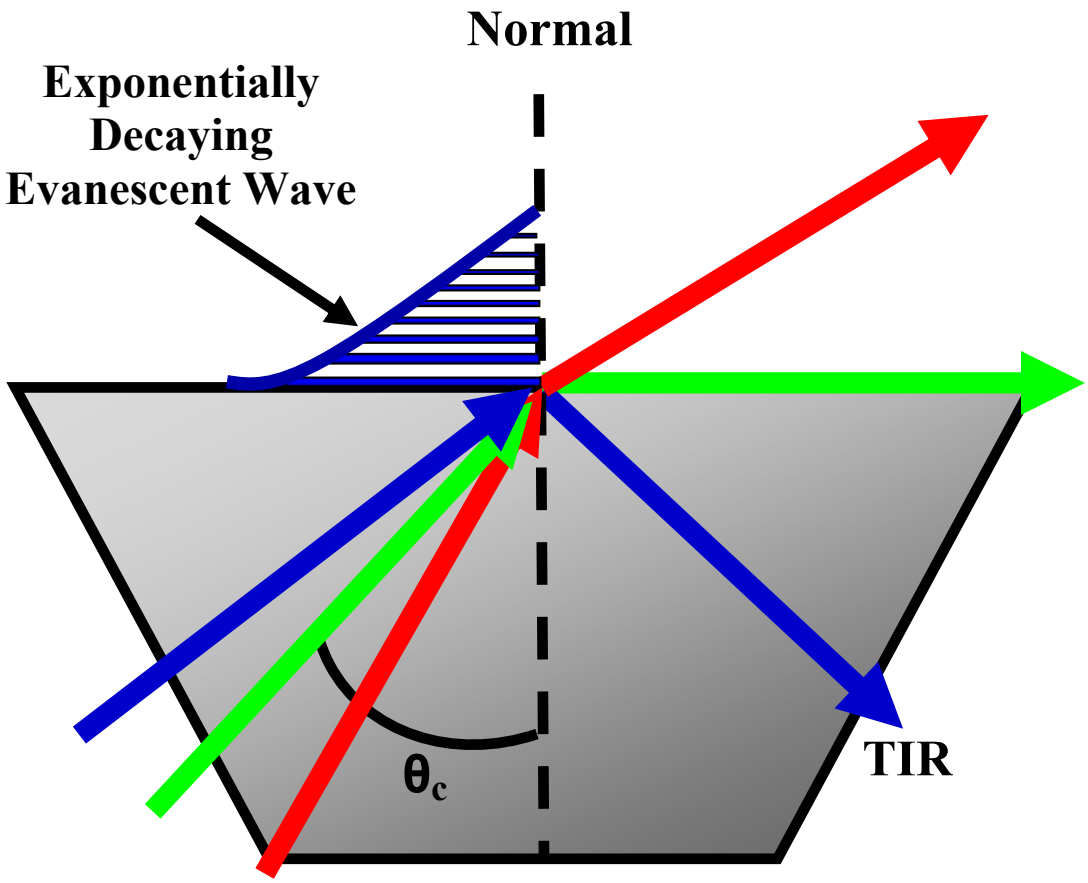

Figure 3.4 Total internal reflection in a prism with illustration of evanescent wave formation.

when the goal is not just to confine light within a TIR element, but to make use of the EW radiation for probing materials on the TIR element surface.

Currently, attenuated total reflectance (ATR) is used for absorbance measurements of samples (liquid or solid) directly in contact with an ATR crystal or prism. The shallow EW is advantageous when analyzing thin films or samples that are too optically dense for standard transmission techniques. Additionally, total internal reflectance fluorescence (TIRF) can be used to interrogate fluorescent molecules that are either tethered or in close proximity to a surface. With TIRF microscopy, developed in the early 80's by Axelrod, one can overcome the diffraction limit of light for excitation and illumination of molecules or specimens immediately adjacent to a glass/liquid boundary.[76] This has been invaluable in selective visualization of cell membranes, as well as cell-surface interactions, molecular dynamics of DNA and unfolding of immobilized proteins.[77-79] With the introduction of microarray technology, detection of bioanalytical system interactions (hybridization or antigen/antibody binding) using TIRF has appeal.[80, 81] Target molecules from within a sample medium can be examined, taking advantage of the high sensitivity provided by fluorescence spectroscopy, without significant interference from the bulk matrix. TIRF will be implemented in the research discussed in the following chapters of this dissertation.

Transducers

The reflection elements, or transducers, used for EW excitation can take several forms. The transducer refractive index will determine the range of incident angles that can be interrogated above the critical angle and, therefore, the possible range of penetration

depths, making high refractive index materials the most popular choice. The simplest structure is that of the prism, or single reflection element. Normally, a laser beam is used to illuminate one edge of a prism, with the EW created at the base of the prism if the incident angle is greater than the critical angle. The sample can be placed directly on the prism base for examination. Using a right angle prism, TIR will take place once at the prism base resulting in a single EW spot of uniform intensity with dimensions that depend upon the laser spot size and focusing optics. The simplicity of laser coupling and EW creation make this approach attractive for interface studies of cells, proteins and DNA. However, the single internal reflection element design does not lend itself to multiplexed applications.

Waveguides are structures that literally guide waves (electromagnetic radiation) by way of repeated TIR. The cylindrical fiber optic, as mentioned above, is the most common type of waveguide, but the discussion in this section will be limited to planar waveguides. Bulk planar waveguides, a type of multiple internal reflection element, are appealing because of their 2-dimensional surface which makes possible patterning of multiple arrays or attachment of microfluidic architecture. Bulk planar waveguide thickness is large in comparison to the wavelength of incident radiation. One example of a bulk planar waveguide is a simple microscope slide with a thickness of approximately 1 millimeter. In this arrangement, multiple modes of radiation are allowed at a given wavelength.[82] Coupling of radiation into a multi-mode waveguide is simple as it only requires direction of the incident beam onto the end face of the waveguide at an appropriate angle. The light will then be confined and guided by TIR within the waveguide. The relatively large face of a bulk planar waveguide allows for slight

changes in alignment without compromising efficient coupling. Further, bulk planar waveguides are commercially available and inexpensive. While the number of reflections within the waveguide (N_R) is a function of waveguide thickness (t), incident angle (θ) and length of the waveguide (L) as given below,

$$N_R = \frac{L}{2t\tan(\theta)} \tag{3-5}$$

the evanescent field on the waveguide surface can be made essentially uniform.[80] Cylindrical lenses focusht in only one axis, so that light focused by a cylindrical lens to a narrow slit on the edge of the bulk waveguide will be guided in an un-collimated manner through the waveguide with divergence of the beam in only the direction of propagation. This results in an area of uniform EW illumination after just a couple of reflections that will serve as a sensing field, as compared to several discrete EW spots without the use of a cylindrical lens (Figure 3.5).

Integrated optical waveguide (IOW) thickness is comparable to the wavelength of the propagating light. For this reason, there are approximately 10^3-10^4 reflections/cm of beam propagation when using IOWs.[83] This results in overlap of discrete reflections so that they become virtually indistinguishable, resulting in high light intensity and significant improvement in sensitivity over thicker bulk optical waveguides.[80] Figure 3.6 compares a bulk waveguide to an IOW. However, other criteria come into play when choosing the appropriate waveguide system. IOWs are typically able to support only one mode of radiation, making coupling an issue. Simple end coupling is no longer an option, and special prisms or grating are generally used in order to couple light into the

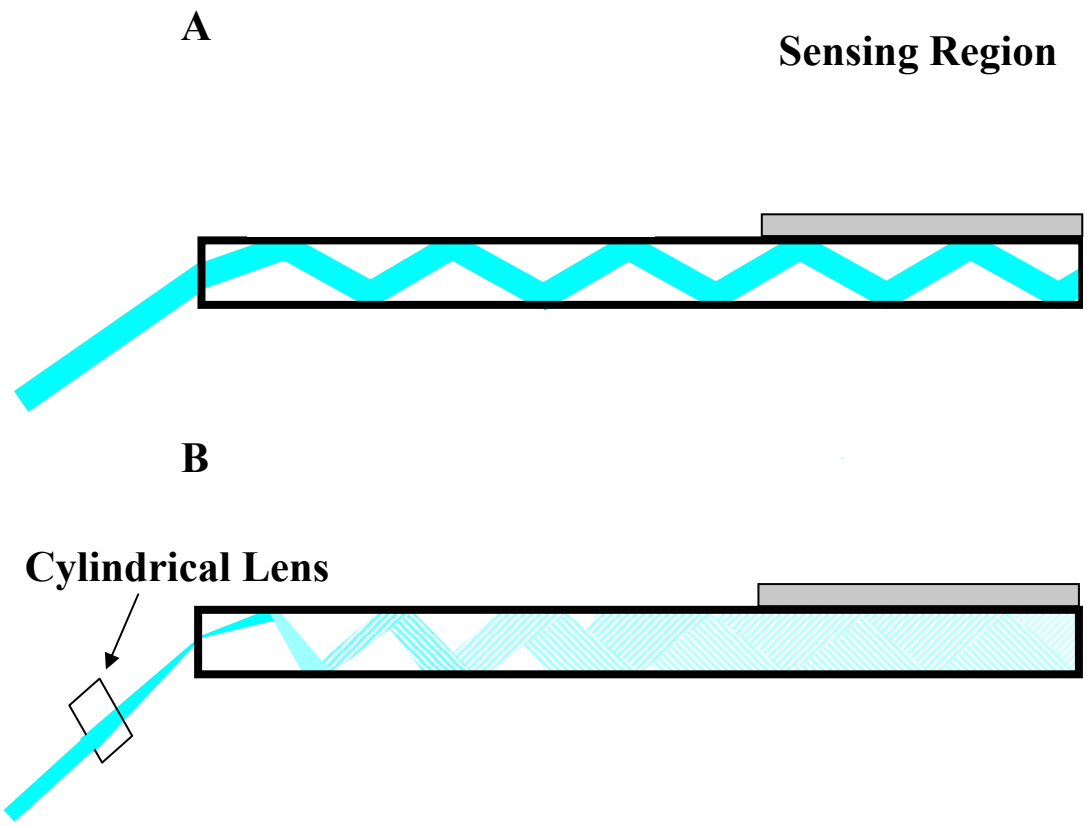

Figure 3.5 A) Propagation of light through a waveguide without focusing. B) Propagation of light through a waveguide with cylindrical lens focusing to create an area of uniform illumination.

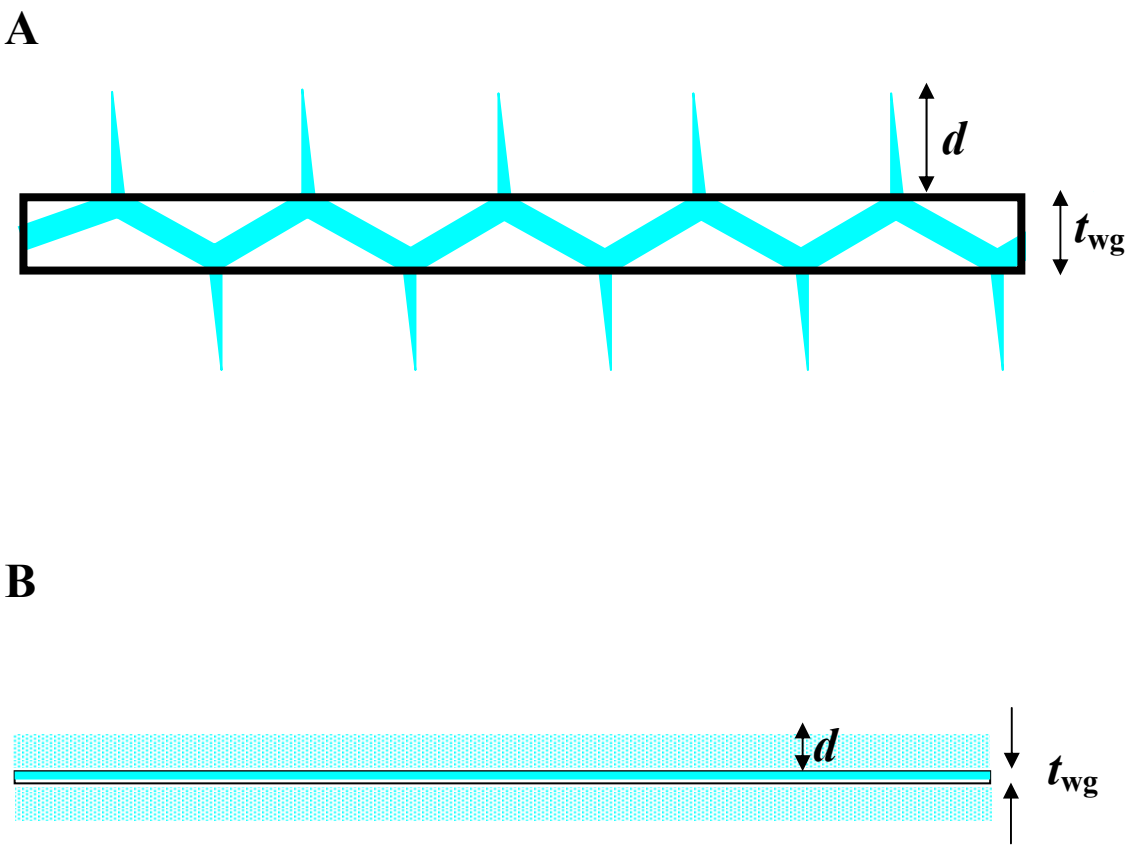

Figure 3.6 A) Bulk optical planar waveguide regime. B) Integrated optical waveguide regime. t_{wg} denotes the waveguide thickness, with d representing the depth of the evanescent wave.

waveguide. The angular alignment requirements are, therefore, very precise and complicate IOW use. Furthermore, the mere creation of IOWs is quite a task. The waveguide can be formed using solution phase techniques such as spin or dip coating, normally used for polymer materials. Deposition procedures can also be employed, creating sputtered or vapor deposited films. Ion exchange techniques can be used to produce graded index waveguides with a gradual transition from the substrate to waveguide refractive index. Additionally, sol-gel processing can be used to produce high quality metal-organic thin films from solution phase processes. All of these techniques require tolerances on the tens of nanometers scale and, as such, result in high cost of fabrication and complicated processing steps.[84]

EW Technology and Immunoassay

While the field of immunoassay, and bioaffinity sensor systems in general, have benefited from the use of evanescent wave excitation, there is a key drawback. Whether using optical fibers or planar waveguides, the biological system of interest (antibodies, proteins or DNA, for example) is immobilized on the waveguide surface using covalent immobilization, physical adsorption, or entrapment within polymer matrices. The result of this surface immobilization is limited mass transport. The assay is, then, diffusion limited and signal may take hours or even days to develop.[85]

Magnetic Particles

Besides the hot research area of microfluidics and other miniaturized systems, microparticles and nanoparticles are garnering much attention in the scientific

community. While functional microparticles or "beads" can serve as useful mobile substrates in many bioassay formats, the advantages are compounded when the beads are magnetic. Magnetic beads, aside from having the large surface-to-volume ratio and amplified interaction of the surface with passing fluids, can be magnetically controlled independent of normal fluid flow. This increases the relative bead motion with respect to the surrounding fluid medium and enhances sample pre-concentration on the magnetic bead surface.[86] For fluid manipulation of beads, the magnetic force must be greater than the hydrodynamic drag force acting on the particles. For this research, the use of an external permanent magnet was sufficient to meet the above conditions. In general, magnetic beads can have a single magnetic core (usually in the case of nanoparticles) or a core composed of multiple magnetically interacting nanoparticles encapsulated in a non-magnetic matrix. Commercially available magnetic beads, used in the research discussed in this dissertation, are provided with various surface modifications and chemistries, high iron content, and narrow size distribution. These particles are superparamagnetic, meaning they exhibit magnetic properties when in the presence of a magnetic field, but have no residual magnetism once the magnetic field is removed, rendering them easily recoverable in solution. They additionally boast high magnetic mobility and low sedimentation rates. Figure 3.7 illustrates the spherical shape and low sedimentation rate of the commercial products used in the research discussed in the following chapters. Magnetic beads have been employed for cell separation, immunoassays, DNA hybridization studies and drug delivery.

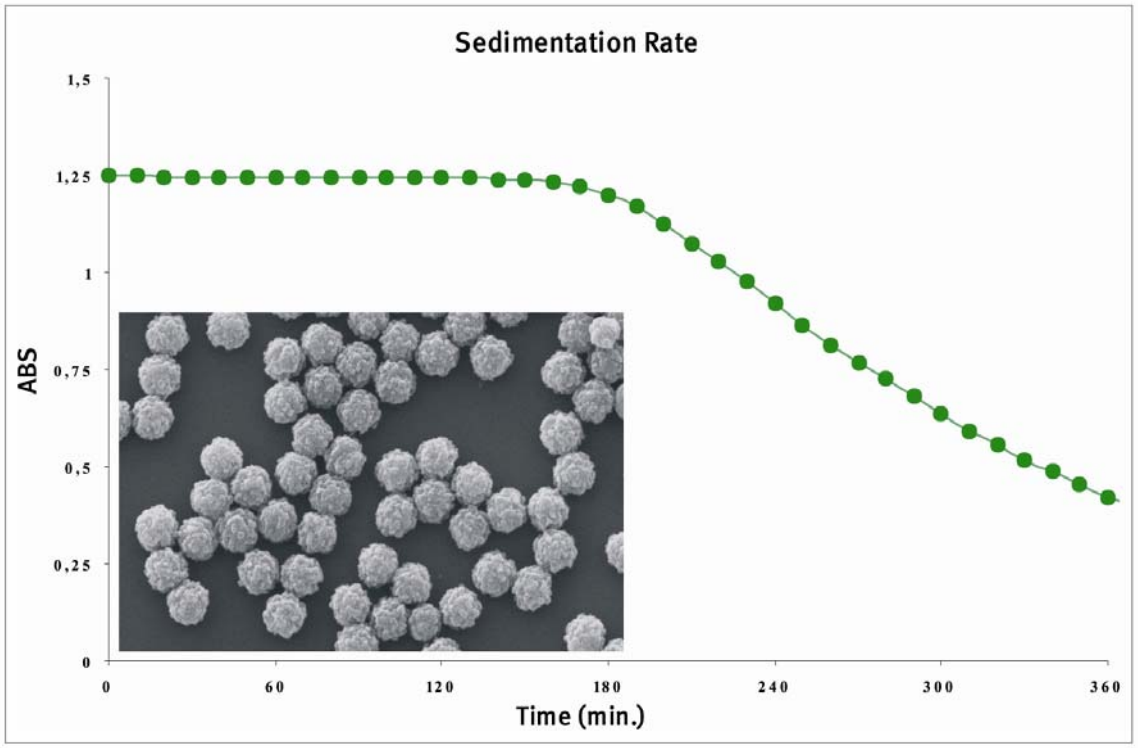

Figure 3.7 Illustration of slow sedimentation rate and excellent size distribution for 1 μm Dynal magnetic beads. Photo Courtesy of Dynal Bead Based Separations (Invitrogen Group)

MATEFFs Design Rationale

Both homogenous and heterogeneous assay formats have benefits and drawbacks. Selective sequestration of analyte on a solid surface, as with heterogeneous assays, has advantages, but requires wash steps. The measurement of signal without need for wash steps, as in a homogeneous assay, is attractive but normally results in background interference. MATEFFs utilize magnetic beads as the solid phase for analyte sequestration, resulting in analyte concentration and subsequent delivery to a localized field created by TIR for detection. This eliminates both the need for multiple wash steps and background interference from bulk matrix components. The magnetic beads are easily dispersed and recovered in solution, making it possible to not only regenerate the EW sensing surface between measurements by simply removing the magnet that retains the magnetic bead plug, but to fully interact with the sample solution without relying on diffusion to a single spot on a planar surface. This novel technique that cleverly integrates, for the first time, concepts that have been researched and implemented for decades is described and optimized in the following chapters.

CHAPTER 4.
MAGNETICALLY ASSISTED TRANSPORT EVANESCENT FIELD FLUOROIMMUNOASSAYS

Introduction

The immunoassay, a diverse suite of techniques combining chemistry and immunology whereby an antibody is used in the determination of sample composition, is a biomedical tool commonly used in toxicology, drug analysis and immunoscreening procedures.[87] Antibodies boast strong binding interactions and unique specificity with their target antigen, making possible measurements of very low antigen concentration even in complex matrices.[33] The inherent sensitivity of fluorescence spectroscopy combined with the existence of a wide range of commercial antibodies and labels renders fluoroimmunoassays (FIAs) an attractive method of analysis. The two principle quantitative protocols for FIAs are heterogeneous assay, requiring a separation step to remove bound target analyte from a sample mixture, and homogeneous assay, whereby the target analyte is directly detected within the mixture.[65] Homogeneous assays are attractive due to the preemption of many laborious and time consuming steps necessitated by the heterogeneous assay. However, homogeneous assays suffer from limited sensitivity and interference from fluorescent impurities present in the matrix, not to mention the fact that many homogeneous assays actually require the addition of several reagents before detection.[65]

Conventional immunoassays, performed in microtiter plates, consume large amounts of expensive reagents and can take as long as a few days for target molecules to diffuse

through solution and completely react with immobilized probes.[88] Microfluidic separation and fluid handling systems have garnered much attention in the past decade as a portable, small footprint means of carrying out chemical and biological processes on a manageable, solvent- and sample-conserving platform.[89] It is logical, then, that the immunoassay format could benefit from these miniaturized systems. In fact, homogeneous and heterogeneous immunoassays have been performed in capillaries and microfluidic devices.[66, 67, 90-92] For heterogeneous assay application, antibodies and antigens were immobilized on microchips with multiple operations performed (loading, washing and labeling) before detection.[66, 67, 92] In the case of homogenous assays, some sort of separation and detection step must follow antigen-antibody complexation in solution. Two groups have reported electrophoretic separation of reaction products from a competitive homogeneous assay.[90, 91] However, separation can be difficult in systems with small differences between free and complexed antigen or antibodies, limiting widespread application of this technique.

Magnetic microspheres (μspheres) have found utility as solid phases for biomolecule immobilization. In general, μspheres have several advantages when used as the solid support in immunoassays, including a large specific surface for binding, mobility of the solid phase, and an attendant enhancement in interaction of the phase surface with passing fluids. When the μspheres are magnetic, there are still more advantages. Magnetic manipulation of μspheres independent of fluidic flow makes possible the delivery of immobilized analytes, be they proteins or small molecules, to a specific zone. These μspheres are practical, well tested, and readily commercially available with

modifications that allow attachment of antibodies or other specific recognition groups, thereby allowing analyte-specific sequestration within a complex matrix. Finally, magnetic μspheres are amenable to miniaturization and multiplexing using different capture probes. In recent work, magnetic μspheres containing an immobilized antibody were held stationary in a fused-silica capillary by an external magnet and used to capture an antigen in solution, which was subsequently rinsed from the μspheres for downstream detection.[93] Additionally, a clever heterogeneous sandwich immunoassay was performed in a simple microchannel using a stationary plug of magnetic μspheres as the solid phase with antigen capture by one immobilized antibody and detection performed by imaging fluorescence resulting from a second fluorescent antibody.[94] Very recent work by Petkus et al. uses magnetic bead rotation and lock in amplification to demonstrate that overall assay sensitivity can be enhanced by eliminating the wash step, especially when dealing with hapten derived monoclonal antibodies.[95] These techniques demonstrate the utility and reward of incorporating magnetic bead solid supports into microfluidic devices. Nevertheless, there are some aspects of the microimmunoassay that can be optimized before realization of the full potential of this method. For instance, the precise control and formation of a small magnetic bead plug in a microchannel is not trivial. Inconsistencies in bead plug packing density or length could greatly affect fluid dynamics, flow rates, reaction rates, bead plug stability and reproducibility. Furthermore, multiple labeling and wash steps required with the heterogeneous assay format, in general, introduce the potential for non-specific adsorption anomalies, complicate sample handling and increase time consumption. The current work seeks to reconcile the

advantages of solid support sample concentration with the need to eliminate complicated separation steps by, for the first time, combining selective magnetic transport of analyte to a highly localized evanescent electromagnetic field.

The work presented in this chapter serves as a proof of concept and details the development and preliminary optimization of a novel technique, immunological Magnetically-Assisted Transport Evanescent Field Fluoro-assays (MATEFFs), which combines the advantages of both the homogenous and heterogeneous assay while eliminating some of the drawbacks.[96, 97] MATEFFs realize selective sequestration of target analyte on magnetically controlled beads, affording the heterogeneous assay benefit of low detection limits, while still allowing the delivery of the target from within the bulk mixture to a localized evanescent field sensing surface. Evanescent field techniques make use of the property of total internal reflectance at an optical interface, in this current illustration of MATEFFs defined as the interface between the prism and sample. Total internal reflection (TIR) occurs when light traveling from a higher refractive index medium into a lower refractive index medium strikes the interface at an angle larger than the critical angle. The light is totally reflected, except for an electromagnetic (evanescent) wave (EW) that is generated at the reflecting surface and penetrates a fraction of a wavelength into the lower refractive index medium. The EW intensity decreases exponentially with increasing distance from the interface.

MATEFFs employ magnetic μspheres as solid supports for a representative sandwich fluoroimmunoassay as well as a medium for transport of this assay to the evanescent sensing surface. Direct detection of bound analyte within the sample mixture is effected by driving the μspheres to the prism surface, and thus into the evanescent wave (EW),

using an external magnet. Thanks to the diminutive evanescent field depth, d (~200 nm), the magnetically delivered analytes can be detected with fewer complications arising from non-optically homogeneous biological matrices. This means a lower background (i.e., a higher signal to noise ratio) due to the confinement of the exciting wave to the prism surface that will contain a monolayer or more of labeled μspheres for TIR fluorescence (TIRF). The term monolayer is used in discussion of the magnetic particle assemblies on the prism surface in this chapter, although the particles are separated by some distance due to inter-structure repulsion. This term is used to differentiate between a primarily single bead layer and formation of multiple layers or clusters of magnetic beads on the surface. When referring to a close packed traditional monolayer assembly in later discussion, the term *traditional monolayer* is employed. Because only a monolayer of μspheres is required for optimum technique performance, the need for and requisite control of very small well-defined bead beds is circumvented and the magnetic transport of solid phase reagents is greatly simplified when it entails only the driving of beads to contact an impenetrable optical interface. What's more, paramagnetic μspheres are easily dispersed and recovered in a solution, allowing facile regeneration of the localized evanescent sensing surface. This technique eliminates wash steps without compromising sensitivity, all the while minimizing interference from fluorescing species present in the bulk sample matrix thanks to a surface-localized evanescent field. MATEFFs has been optimized by assessing the impact of background interferents (fluorescein), an optically dense matrix (milk), incident angle, magnetic field direction, laser power density via focusing and laser power adjustments, and bead concentration. Utilizing a model sandwich assay system (biotinylated anti-IgG; rabbit IgG; anti-IgG-R-

phycoerythrin), the analytical figures of merit for the technique are evaluated and reported.

Experimental

Reagents

Sodium dihydrogen phosphate, disodium hydrogen phosphate, Tween 20, bovine serum albumin (BSA), fluorescein isothiocyanate (FITC), biotin (5-fluorescein), biotinylated anti-rabbit IgG capture antibody, rabbit IgG, and anti-rabbit IgG-R-phycoerythrin (RPE) were purchased from Sigma-Aldrich (St. Louis, MO) and used as obtained. FITC and RPE were used in this work as labels because they can be spectrally distinguished reasonably well and are readily available. Sodium chloride (NaCl) was obtained from Mallinckrodt, Inc. (Phillipsburg, NJ) and used as received. Dynabeads® MyOne™ Streptavidin C1 superparamagnetic μspheres (1 μm diameter) were purchased from Dynal Biotech (Brown Deer, WI) and diluted using phosphate buffered saline (PBS) prepared according to Dynal Biotech recommendations. All buffers and solutions were prepared in deionized, distilled water from a Barnstead 1800 (18 MΩ resistivity).

Apparatus Design

A schematic representation of the MATEFFs instrumental setup is depicted in Figure 4.1. The 488-nm beam from an argon-ion laser (Uniphase Model 2201, San Jose, CA) was directed through a laser line filter (Edmund Optics, Barrington, NJ) and pinhole using first surface mirrors (Edmund Optics, Barrington, NJ). The beam was then focused using a plano-convex lens (Edmund Optics, Barrington, NJ) with either a 125-mm or 175-mm focal length and sent to a beam steering mirror directly mounted

on a rotary stage for controlling the incident angle of the laser beam on the TIR prism. To ensure the same spot on the prism surface was illuminated with changing angles, the vertical position of the rotary stage was controlled via a single axis translational stage. The TIR prism was an inverted right angle BK7 prism (Edmund Optics, Barrington, NJ) with n=1.52, surface flatness of $\lambda/4$, and surface quality 40-20. By milling flat the angle opposite the hypotenuse face of the prism, the prism could be placed flush with the surface of a delrin holder fabricated in-house. The holder contained a sliding block, which housed a pressure-formed neodymium bar magnet rated at a 10.7 lb. lift (McMaster-Carr, Atlanta, GA). The block was used to slide the magnet beneath the prism, as well as remove it when necessary.

A sample compartment was formed from a polydimethylsiloxane (PDMS, Sylgard 184, Dow-Corning, Midland, MI) reservoir, bored using a modified 1.5 mm syringe, placed directly on the prism surface and enclosed with a glass cover slip. Fluorescence was collected through a bi-convex F1 lens, passed through a razor-edge 514 nm Raman filter (Semrock, Rochester, NY), and focused onto a Hamamatsu HC120 photomultiplier tube-based photosensor module (PMT) (Hamamatsu, Bridgewater, NJ) using another bi-convex F1 lens. The fluorescence was additionally filtered before reaching the PMT using a narrow bandpass interference filter centered at 580 nm (Edmund Optics, Barrington, NJ) for RPE and 532 nm (Melles Griot, Rochester, NY) for fluorescein. The output voltage from the PMT was converted at 1Hz by a PMD-1208LS data acquisition board with TracerDaq® software (Measurement Computing, Middleboro, MA). The optical photographs shown in Figure 4.1 demonstrate delivery of the magnetic μspheres to the prism surface, but are not indicative of optimized surface coverage.

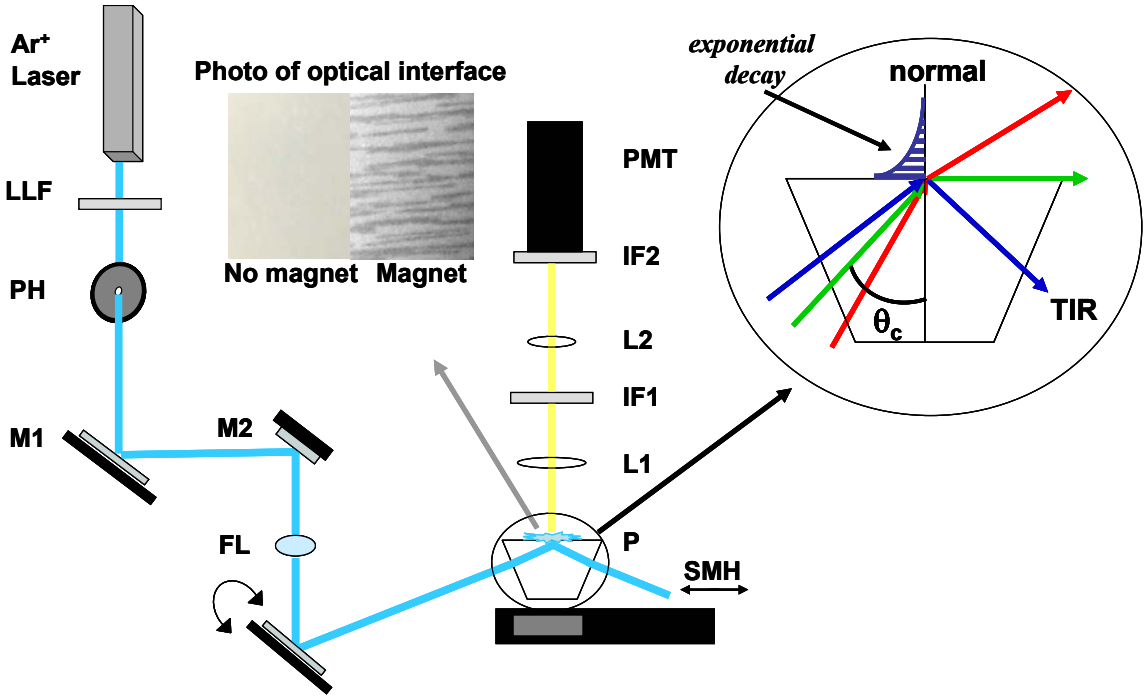

Figure 4.1 Schematic of MATEFFs Apparatus. LLF, laser line filter; PH, pinhole; M, mirrors; P, prism; L, lens; IF, interference filter; FL, focusing lens; PMT, photomultiplier tube; SMH, sliding magnet holder. Optical photos (200 µm x 200 µm) illustrate surface sequestration of beads. Inset illustrates the bending of light at the interface between prism and solution and the exponential decay of the evanescent wave. Refraction (red arrow) occurs at angles smaller than the critical angle, at the critical angle (green arrow) the light is refracted at 90° along the interface, and total internal reflection (blue arrow) occurs at angles larger than the critical angle.

Labeling of μspheres: In order to perform the optimization tests, Dynal Biotech Dynabeads MyOne Streptavidin C1 μspheres were fully functionalized, using a sandwich assay format, with biotinylated anti-rabbit IgG as the capture antibody; rabbit-IgG as the antigen; and anti-rabbit IgG RPE as the reporter antibody. The μspheres were first washed with PBS and diluted to 1 mg/mL. A 400 μL aliquot of μspheres was then removed, separated using an external magnet, resuspended in 400 μL of biotinylated anti-rabbit IgG (0.05 mg/mL) and allowed to incubate for one hour with gentle rotation. These μspheres were considered fully biotinylated. The μspheres were then separated, washed two times with PBS, one time with 0.01% Tween 20 in PBS, resuspended in 400 μL of rabbit-IgG (0.5 mg/mL) and again allowed to incubate for one hour with gentle rotation. These fully antigen labeled μspheres were again separated, washed as described previously and resuspended in 400 μL of anti-rabbit IgG RPE (0.1 mg/mL). Lastly, the μspheres were separated, washed and resuspended in 400 μL of PBS. This fully labeled μsphere solution was used for all optimization experiments, with 0.6 μL aliquots used to fill the PDMS reservoir for each individual experiment.

The labeling steps for calibration curve experiments were the same as described above, except for the concentration of rabbit IgG antigen. After fully biotinylating the μspheres, they were divided into 50 μL aliquots and labeled using rabbit IgG standards ranging in concentration from 20 to 200,000 μg/L, followed by full labeling as previously described. For multi-analyte experiments, the DynaBead μspheres were directly labeled with biotin-5-fluorescein (6000 pmol) by incubating for one hour with gentle rotation.

Results and Discussion

In this work, functionalized magnetic μspheres are driven into contact with the surface of a prism, where an evanescent wave has been generated via total internal reflection, using a strong external magnet on the underside of the prism. To our knowledge, this represents the first attempt to use magnetic transport of a fluoroimmunoassay to a localized field for EW excitation. Consequently, experimental conditions for the MATEFFs technique require optimization.

Evanescent wave penetration depths are dependent upon the wavelength of the laser, the incident angle, and the refractive indices of the liquid and solid. At the critical angle, light traveling from the high refractive index medium (prism) to the low refractive index medium (solution) will be refracted at 90° along the interface. At any angle larger than the critical angle, the light is totally internally reflected except for the EW generated at the prism surface. The penetration depth of the EW increases as the incident angle approaches the critical angle as given below

$$d = \frac{\lambda}{4\pi\sqrt{n_1^2 \sin^2\theta - n_2^2}} \tag{4-1}$$

where λ is the laser wavelength, θ is the incident angle, and n_1 and n_2 are the refractive indices of the prism and solution, respectively.

In this work, penetration depth is changed by incrementally varying the angle on the mirror steering the incident beam. Initially, the formation of the EW was confirmed by magnetically transporting RPE functionalized μspheres to the prism surface and scanning through incident angles using the beam-steering mirror until a marked increase in fluorescence signal resulted from refraction of the laser light into the bulk solution. The

merit of MATEFFs as a method of delivery to a localized field in the presence of a complex matrix was then established by preparing the RPE functionalized μsphere solution in a background matrix containing 1 μM fluorescein as a model interferent. Figure 4.2 compares the emission of RPE and fluorescein (emission bandpass filters centered at 580 nm [10 nm FWHM; 67% transmission] and 532 nm [10 nm FWHM; 45% transmission], respectively) as a magnet is used to deliver the μspheres to the EW. Because the broad fluorescence emission of fluorescein overlaps with that of RPE, corrections were made to the 580 nm emission data in order to eliminate the signal contribution from fluorescein, which was determined to be 13% of the fluorescein emission at 532 nm. In addition, a small amount of autofluorescence from the μspheres themselves is present at 532 nm and that emission is corrected by subtracting the value of autofluorescence determined from the solution of RPE alone. Starting at an incident angle of ~63° and approaching the critical angle (~61°, CA in the figure) the RPE fluorescence intensity increases as more molecules are excited by the deeper penetrating EW. The change in fluorescence emission as the incident angle is approached follows the shape of the calculated curve for the change in EW penetration depth with incident angle change as expected (Figure 4.2 inset). Once the incident angle falls below the critical angle, refraction of the laser beam into the bulk solution causes the fluorescence intensity of both RPE and fluorescein to dramatically increase (grey and black bars off scale in Figure 4.2) due to excitation of fluorophore in the bulk solution. This experiment was repeated and similar angle-fluorescence trends were observed. The signal resulting from excitation of μsphere immobilized RPE is significantly diminished at the optimum

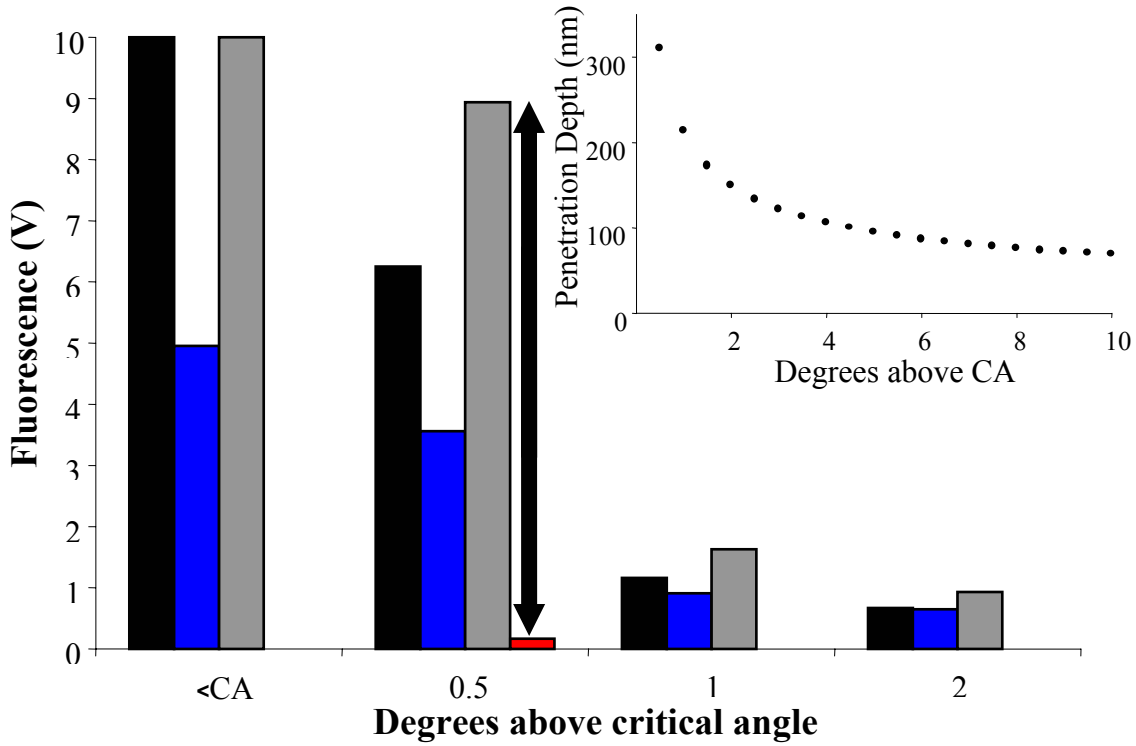

Figure 4.2 Comparison of fluorescence emission from fully functionalized RPE μspheres in a 1 μM fluorescein solution in the presence and absence of an external magnet field at different incident angles. RPE μsphere emission with magnet (grey bars); RPE μsphere emission without magnet (red bar); 1 μM fluorescein emission without magnetically delivered μspheres (black bars); 1 μM fluorescein emission with magnetically delivered μspheres (blue bars). The arrow demonstrates the difference between signals when the magnetically labeled beads are delivered to the localized field with an external magnet as compared to no magnetic delivery. The insert demonstrates the change in penetration depth with incident angle calculated from Equation 4-1

incident angle upon removal of the external magnet (~1/90th the signal with magnetic delivery; red bar) due to transport of the beads away from the interface and out of the most intense portion of the EW. In addition, fluorescein emission is reduced upon magnetic delivery of the μspheres to the evanescent field due to displacement of matrix volume by the μspheres.

These results serve as a preliminary demonstration of the ability of MATEFFs to reduce complications arising from spectral matrix interferences. All further experiments were performed at an incident angle ~0.5º above the critical angle. To further illustrate the MATEFFs advantage when dealing with an optically dense medium, milk was used as an opaque matrix (Figure 4.3). The detection of fully RPE functionalized magnetic μspheres was realized using the MATEFFs technique in two different milk matrices and compared to fluorescence detection of rhodamine 6G in the same matrices using a simulated homogeneous assay. The signal from R6G in 1:1 milk:PBS matrix using the simulated homogeneous assay was less than 8% of the signal from R6G in PBS alone. Conversely, using the MATEFFs method, the fluorescence signal from immobilized RPE in the same milk matrix was nearly 65% that of the signal from RPE in PBS alone Optically dense matrices in conventional immunoassays create problems by significatntly reducing response intensity, thereby necessitating multiple wash steps to get rid of interfering effects. In MATEFFs, there is only moderate reduction in response intensity in the presence of a very optically dense matrix (1:1 milk:PBS), due to passage of the emission through approximately 1.5 mm of matrix (see Figure 4.1), and the analyte of interest can be detected in the presence of fluorescent interferents because of selective target delivery to the highly localized evanescent field without call for multiple wash

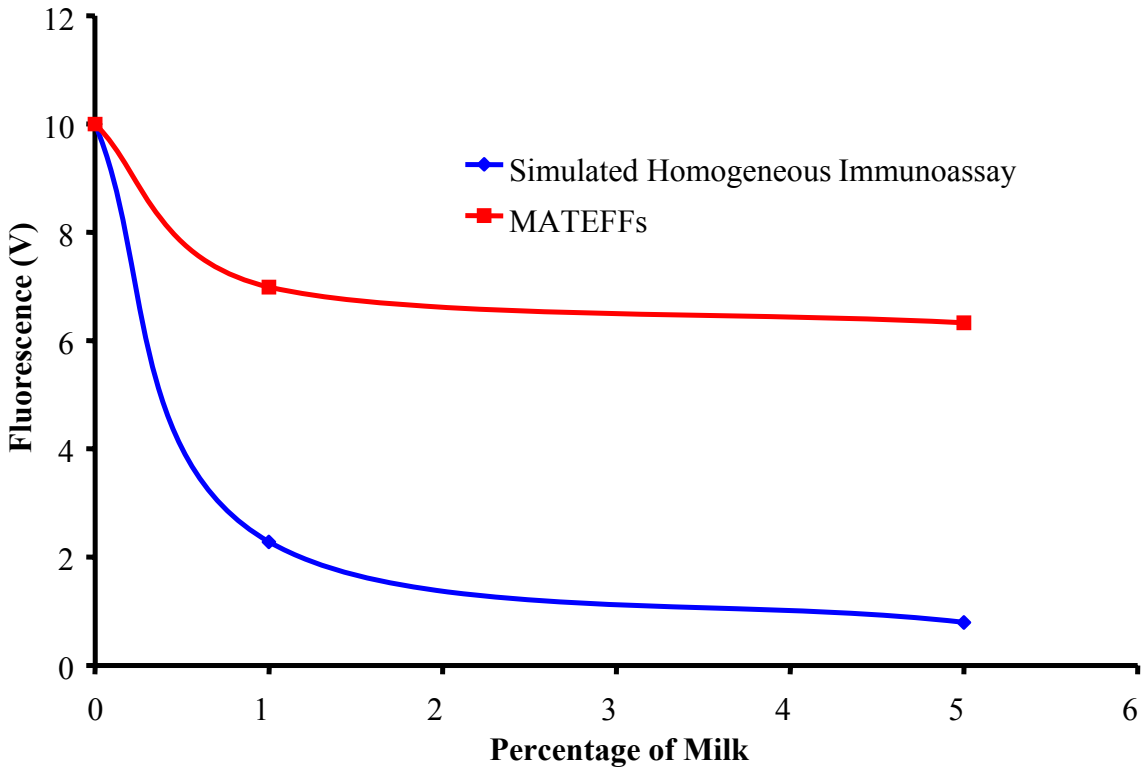

Figure 4.3 Matrix interference experiment comparing MATEFFs technique to a simulated homogeneous assay using milk as an optically dense matrix.

steps.

It is important that μsphere coverage on the prism surface be maximized, as relevant analyte is transported to the EW by the μspheres. Superparamagnetic particles, when placed in a magnetic field, will acquire a magnetic moment and interact by way of magnetic dipole forces.[86] Because of these dipole forces, the particles will begin to cluster into large, column-like structures often called supraparticle structures (SPS), which align in the direction of the magnetic field. For this reason, the effect of magnetic field direction on the resulting fluorescence signal from the model sandwich assay system was probed. Micrographs taken in the lab (Figure 4.4) reveal that perpendicular magnetic fields, created by a bar magnet with field lines approximately perpendicular to the prism surface, cause the SPS to align vertically and grow larger in the vertical direction with increasing bead concentration. In contrast, a magnetic field created by a bar magnet with field lines approximately parallel to the prism surface leads to SPS that form horizontally along the prism surface. These micrographs are not indicative of optimized prism surface coverage, as they only serve to make a distinction between the parallel and perpendicular magnetic fields. As evidenced in Figure 4.4, a magnetic field that is parallel to the surface of the prism yields a greater fluorescent signal at every incident angle tested in comparison to a magnetic field perpendicular to the prism surface. Although the parallel magnet orientation proved to be important in maximizing fluorescent signal, presumably due to an increase in the amount of functionalized μspheres in contact with the prism surface with a parallel magnetic field, perfect parallel field alignment was not critical as slight tilting of the bar magnet to manipulate SPS surface placement exhibited no improvement in observed signal.

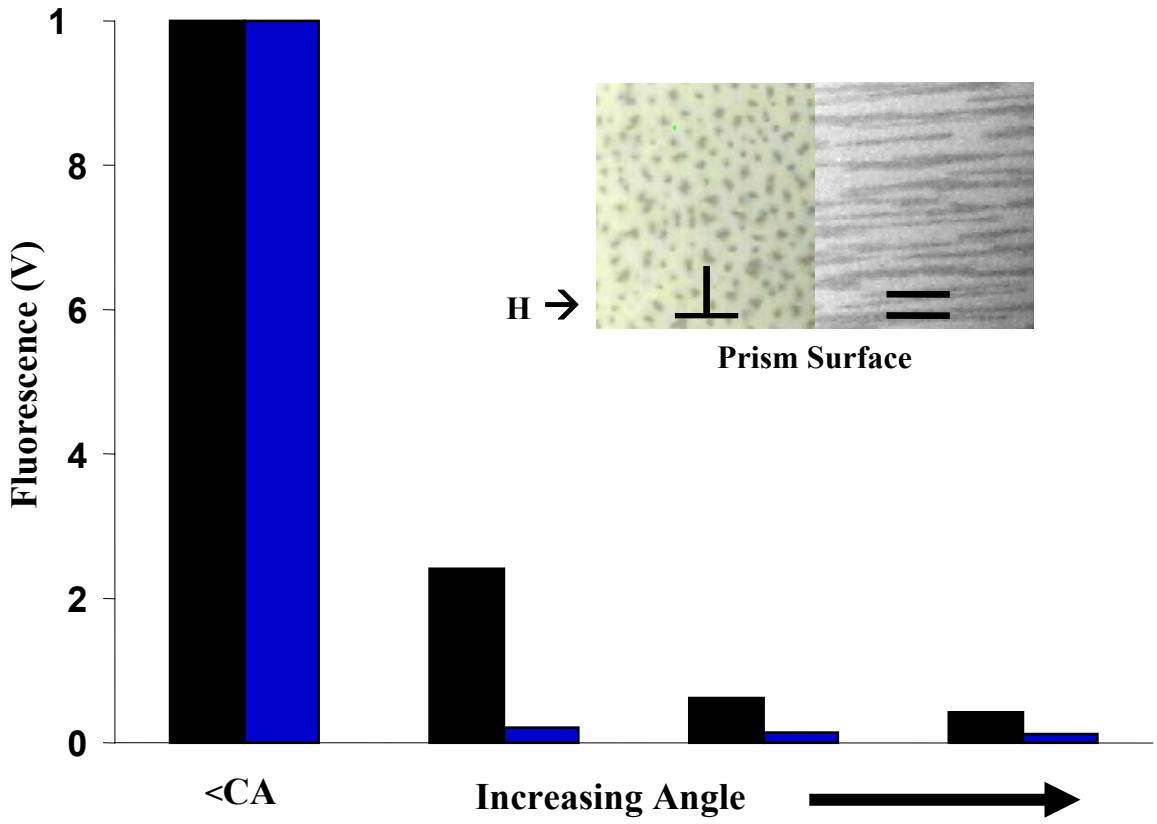

Figure 4.4 The orientation of the magnetic field with respect to the prism surface (parallel (black bars) or perpendicular (blue bars)) has a marked effect on fluorescent signal. Once past the critical angle, fluorescence signal from both magnetic fields is off scale due to refraction of the laser light into the bulk solution. Optical photos (200μm x 200μm) illustrate the direction of supraparticle structure growth.

The effect of increasing laser power on the ability of the EW to excite bead-bound fluorophores was also investigated. The goal is to evanescently excite the maximum number of fluorophores while avoiding any deleterious effects, such as photobleaching, bond degradation, or thermally induced migration away from the EW. In addition to varying power over the range available with our laser, we used two lenses with different focal lengths; 125 mm that produced a smaller focused diameter of ~77 μm and 175 mm that produced a larger focused diameter of ~108 μm.[98] The plots shown in Figure 4.5 demonstrate an expected behavior. Signals increase rapidly with increasing power at low powers but show evidence of the aforementioned deleterious effects at higher powers as seen by leveling-off of the plots. The longer focal length lens probes roughly a factor of two greater surface area than the short focal length lens. The bottom two data points for each of the two lenses (each curve) happen to be at equivalent power densities incident on the prism surface (~ 30 W/cm^2) and show almost a factor of two greater signal for the long focal length lens, correlating well with greater probed surface area. Although the larger probe area is desirable in terms of raw signal, it does require larger confinement vessels or channels and more beads.

As a final optimization study, different concentrations of functionalized μspheres were utilized in an effort to achieve the most uniform surface coverage. When using one micron diameter μspheres, the evanescent wave (~200 nm) cannot fully probe the entire μsphere, thereby necessitating only a monolayer of beads on the prism surface. Although it is important to maximize surface coverage, any excess bead formation (multilayers or would not be excited by the EW and would serve only to interfere with signal collection.

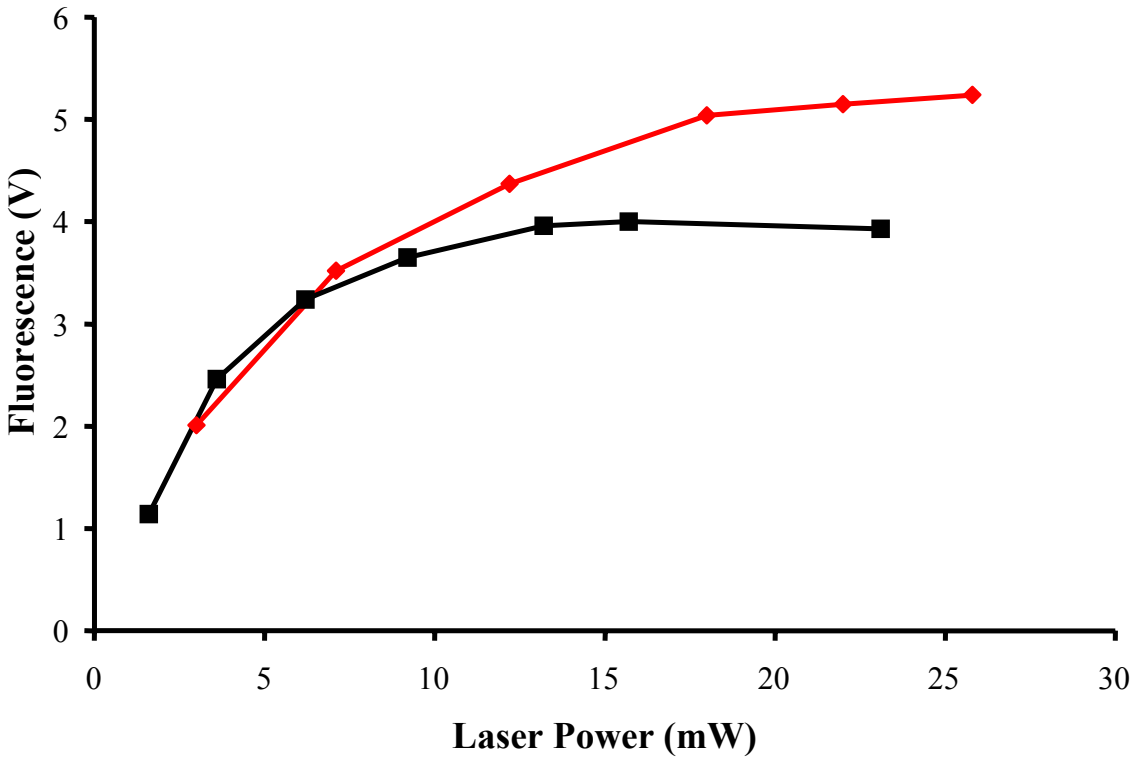

Figure 4.5 Assessment of the relationship between laser power and fluorescence signal using two lenses with different focal length. The larger focal length 175 mm lens (red diamonds) probes a greater surface area than the 125 mm lens (black squares).

clustering) on the prism surface may hinder TIRF signal collection, as these multilayers This is evidenced in Table 4.1, which displays fluorescence signals measured and relative standard deviation (RSD) values calculated (n = 4) for six concentrations of functionalized magnetic μspheres. As μsphere concentration increases, the fluorescence signal increases and then begins to decrease at the highest measured concentration. Additionally, the RSD values decrease and again increase with the concentration of μspheres. A μsphere concentration of 0.6 μg was selected for use in construction of the calibration curve due to the desire to conserve sample while maintaining acceptable signal and RSD values.

The linear dynamic range and detection limits of this immunoassay technique were evaluated by constructing a calibration curve (Fig 4.6). Standard solutions of rabbit IgG ranging in concentration from 20-20,000 ng/mL were tested using the MATEFFs technique. A quite respectable linear dynamic range ($y_{(V)} = 0.0007x_{(ng/mL)} + 0.111$) of nearly three orders of magnitude is established (R^2=0.991) with a detection limit of 42 ng/mL (~280 pM) for this particular assay. Error bars for the calibration curve were assigned based on the RSD values defined in Table 4.1 for 0.6 μg bead concentration.

Table 4.1 RSD values (n=4) and fluorescence signals for 6 μsphere concentrations.

Bead Concentration (μg)	**Fluorescence Signal (V)**	**RSD Value (%)**
0.15	1.32	7.8
0.30	1.98	6.8
0.45	2.06	3.1
0.60	2.70	5.0
0.75	3.76	7.9
0.90	3.34	7.6

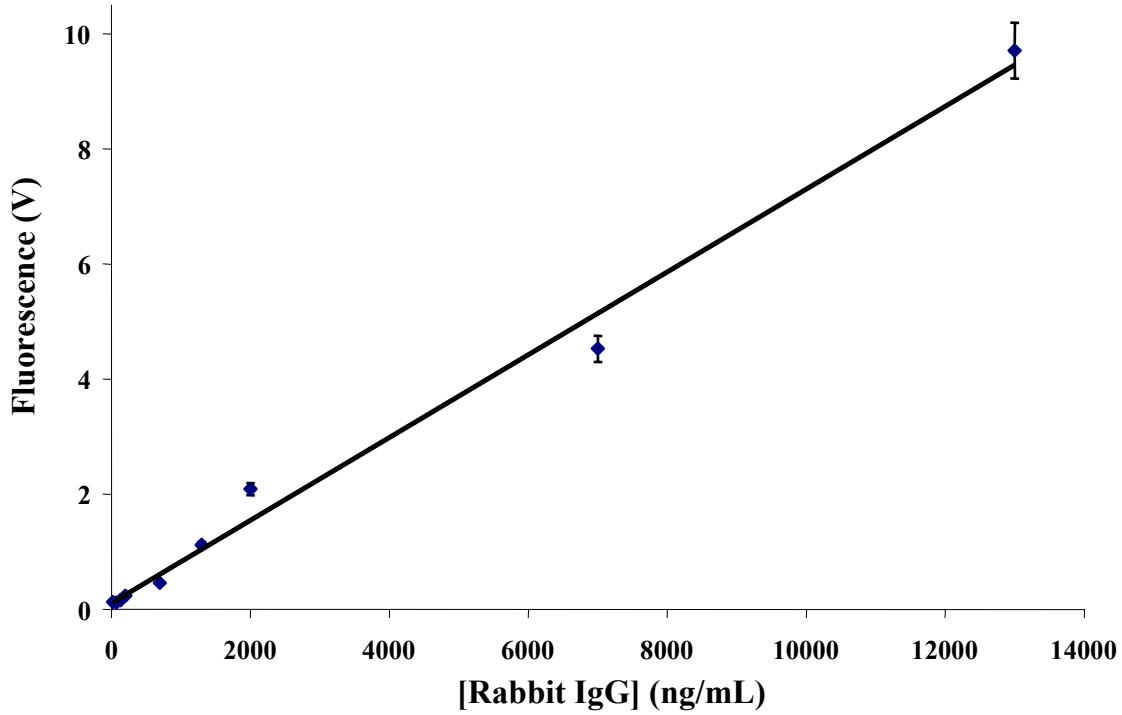

Figure 4.6 Calibration Curve for Rabbit IgG with R^2=0.991 and detection limit of 42 ng/mL.

In order to demonstrate the compatibility of MATEFFs with multi-analyte systems, μspheres fully labeled with RPE and fluorescein were employed. Simultaneous detection was achieved by using the two narrow band interference filters, centered at 532 nm for fluorescein (Melles Griot, Rochester, NY) and 580 nm for RPE (Edmund Optics, Barrington, NJ), interchangeably. As mentioned in the discussion for Figure 4.2, corrections were made to the data to adjust for autofluorescence from the μspheres themselves at 532 nm, as well as the overlap of fluorescein emission with that of RPE at 580 nm. Comparison of fluorescence emission from solutions of RPE labeled beads, fluorescein labeled beads and mixtures of the two at different ratios were measured using the MATEFFs technique (Figure 4.7). There is a clear trend shown between the fluorescence emission from the two analytes and the changing ratios of the mixtures. Though not quantitated, this illustrates that the MATEFFS technique is amenable to measurement of multiple analytes in one sample mixture by employing spectrally distinct fluorophores and interchanging emission filters.

Conventional heterogeneous immunoassays performed in microtiter wells are diffusion limited, as the antigen/antibody must migrate to the surface of the well to interact with an immobilized antigen/antibody, resulting in reaction solid surface area to solution volume ratios (S/V) on the order of 10 cm^{-1}. A recent report cleverly incorporated polystyrene bead solid supports into a glass microchannel using a capture dam and reported a S/V of 480 cm^{-1}.[99] This improvement in S/V essentially meant a larger reaction field and the reaction rate was made 90 times faster compared to a similar conventional microtiter plate immunoassay due to a decrease in diffusional distances between antibody and immobilized antigen. The work of Hayes et al. took this concept

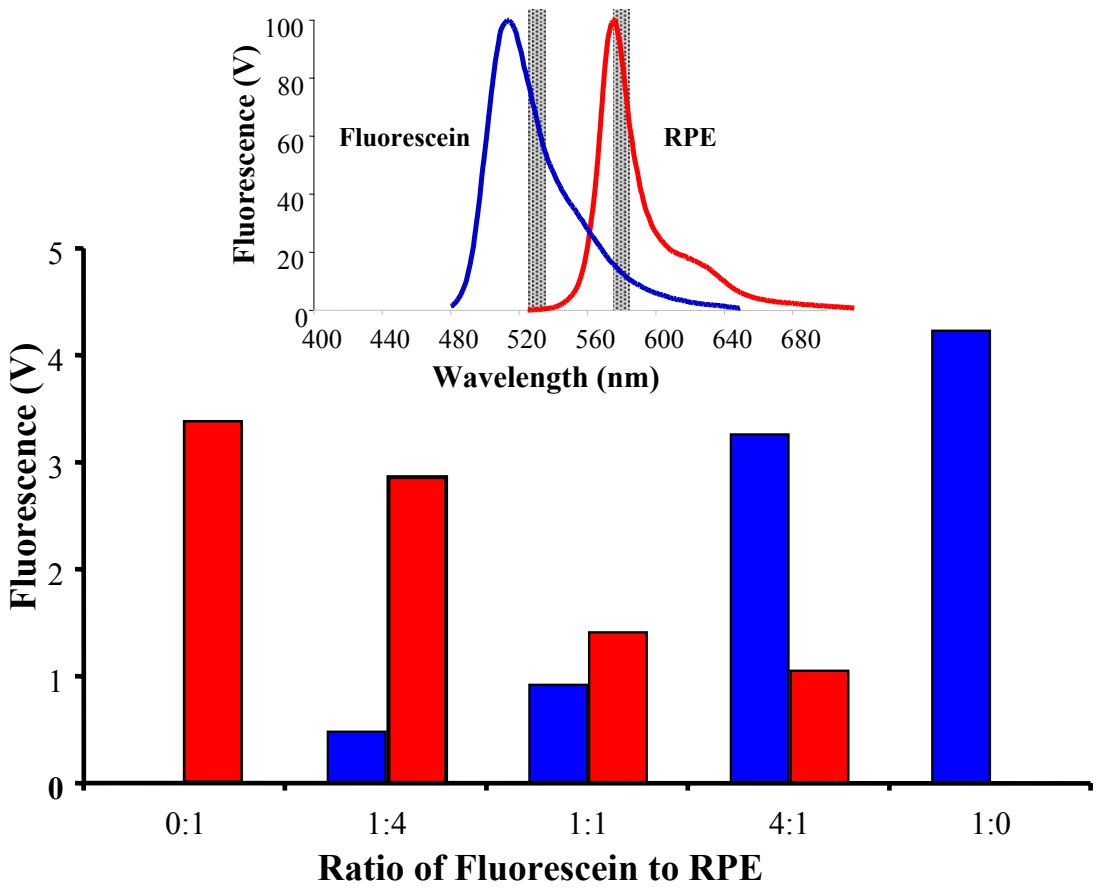

Figure 4.7 Multi-analye experimental data. RPE emission is monitored via a 580 nm bandpass filter (red bars) and fluorescein emission is monitored via a 532 nm bandpass filter (blue bars). The inset illustrates emission for each fluorophore collected by their respective bandpass filter (greyed areas on emission spectra).

even further by using an orthogonal magnetic field to hold stationary a plug of magnetic beads in a microchannel. This flow based microimmunoassay resulted in a S/V of 1.3 x 10^4 cm^{-1} within the detection volume, defined by the specific area quantitated within a fluorescence micrograph.[94] Within the current detection volume for MATEFFs, the evanescent wave volume, the S/V is 4.0 x 10^4 cm^{-1}. However, MATEFFs is not a classical heterogeneous immunoassay. A unique advantage of the MATEFFs technique is that μsphere labeling occurs in free solution without any type of μsphere sequestration (weirs, membranes, applied magnetic fields, etc) followed by delivery of the labeled μspheres from within the bulk solution to a localized evanescent sensing surface for detection. MATEFFs are not volume limited because the μspheres are able to fully interact with the analyte-containing sample before delivery to the detection zone for EW probing. Since it is only necessary to deliver a monolayer of μspheres to the evanescent sensing surface, the concentration of magnetic μspheres employed is adjusted accordingly and the entire μsphere constituent is interrogated via the EW. By concentrating the μsphere volume at the sensing surface, much free solution (or matrix) volume is displaced. This fact, combined with the localized EW, serves to reduce background interference from the bulk medium. It is, therefore, important to illuminate the largest possible μsphere surface area, in order to boost analyte density in the EW, while limiting the free solution volume within the EW interrogated region. It is clear from calculation (Table 4.2) that, for a given area of EW illumination, matching EW penetration depth to the diameter of the μsphere creates an ideal situation whereby μsphere surface area interrogated by the EW is maximized and free solution volume is minimized. For ease of comparison, the calculations from Table 4.2 were based on the

Table 4.2 Calculations for Optimized Analyte Density. Optimization of analyte density within EW assuming a traditional monolayer μsphere surface coverage within a 10 μm X 10 μm square illuminated by the given evanescent wave depth. In order to perform the calculations for this data, equations for the surface area and volume of a spherical cap were used to approximate bead surface area and volume. Additionally, the EW volume was calculated assuming a square with dimensions stated above.

	Evanescent Wave Depth (*d*)			
	100 nm		200 nm	
Bead Size (nm)	**Surface Area Probed (μm^2)**	**Free Solution Volume (%)**	**Surface Area Probed (μm^2)**	**Free Solution Volume (%)**
100	314	48	314	74
500	63	73	127	54
1,000	31	85	63	73

assumption of traditional close packed monolayer coverage for each bead size on the prism surface. It should be noted that as the bead density increases the interfacial optical properties of the system may also change. The high specific interface of the MATEFFs technique directly relates to the minimization of interference from complicated, non-optically homogeneous matrices. The amount of matrix present in the detection volume, free solution volume, decreases as the specific interface is increased. By optimizing conditions, as shown in Table 4.2, the specific interface could be increased to 4.0×10^5 cm^{-1} while lowering detection limits and minimizing reagent consumption.

The following chapter will discuss ongoing MATEFFs studies taking advantage of a microfluidic device for multiplexing and passive sample delivery to a localized evanescent sensing surface. Planar waveguide technology is explored for efficient surface-confined excitation of magnetically delivered analyte within the evanescent field created by waveguide light propagation.

CHAPTER 5.
MULTIPLEXED, WAVEGUIDE APPROACH TO MAGNETICALLY ASSISTED TRANSPORT EVANESCENT FIELD FLUORO-ASSAYS

Introduction

Bioaffinity systems, encompassing such techniques as immunoassay and oligonucleotide hybridization, are routinely used in clinical, environmental and genetic analyses.[60, 87, 100, 101] It is important, when dealing with these systems, that sample and time are conserved while preserving sensitivity and specificity. Moreover, simultaneous parallel analysis of several analytes or samples is desirable. Addressing these needs, microfluidic separation and fluid handling systems have garnered much attention in the past decade as a portable, small footprint means of carrying out chemical and biological processes on a manageable, solvent- and sample-conserving platform.[89] The current work integrates microfluidic and planar waveguide technology for simultaneous investigation of multiple bioaffinity systems using judicious sequestration of target analyte on magnetically controlled beads, thereby facilitating delivery of the target from within a bulk mixture to a localized evanescent field sensing surface inside a microfluidic platform. To our knowledge, this represents the seminal report of selective magnetic transport of analyte to a localized evanescent field present on the surface of a simple and versatile integrated microfluidic/waveguide device.

Magnetic microspheres (μspheres) have found utility as solid phases for biomolecule immobilization. In general, μspheres possess a large specific surface for

binding, mobility of the solid phase, and an attendant enhancement in interaction of the phase surface with passing fluids. Furthermore, magnetic μspheres permit manipulation independent of fluidic flow, making possible the delivery of immobilized analytes, be they proteins or small molecules, to a specific zone. Magnetic μspheres are amenable to miniaturization and multiplexing using different capture probes. This work expands upon the recently developed magnetically-assisted transport evanescent field fluoro-assay (MATEFFs), a novel technique combining the advantages of both the homogenous and heterogeneous assay while eliminating some of the drawbacks, as discussed in the previous chapter.[102] MATEFFs sought to reconcile the advantages of solid support sample concentration with the need to eliminate complicated separation steps by, for the first time, combining selective magnetic transport of analyte to a highly localized evanescent electromagnetic field. In this work, the electromagnetic field is created using a planar waveguide to direct excitation light.

Planar waveguide technology makes use of the process of total internal reflectance at an optical interface. The concept of TIR, having previously been discussed, basically entails the total reflection of light at an interface under ideal conditons except for an exponentially decaying, localized evanescent field. The evanescent field, in the present work, is created at the surface of a standard microscope slide used as a type of bulk, planar waveguide with propagation of incident light by way of multiple internal reflections. The implementation of a microscope slide is attractive due to the low cost and ease of waveguide development, as compared to other planar waveguide systems.[80] The process of waveguide excitation was achieved using a

cylindrical lens to focus collimated laser light on the edge of the waveguide, providing a uniform evanescent sensing surface after a couple of non-collimated reflections, as previously described.[82] The cylindrical lens results in divergence only in the direction of beam propagation, enhancing uniformity while maintaining good photon density.

The two dimensional microscope slide structure allows for construction of multichannel microfluidic architecture on the waveguide surface. A PDMS microfluidic device, conformally sealed to the slide surface, makes possible simultaneous interrogation of six analyte samples in separate channels. Labeled magnetic beads are passively pumped, using a previously published method, through microfluidic channels and sequestered within the evanescent wave at the microscope slide surface using an external magnet.[103] The passive pumping method utilizes the surface energy of a droplet placed in the microchannel reservoir to pump liquid through the channel. The only equipment required for this pumping method is a pipette, making it simple, effectual and semi-autonomous. A controlled quantity of magnetic beads can be efficiently pumped through each microchannel and delivered to the waveguide surface using an appropriately placed external magnet. Thanks to the diminutive evanescent field depth, the magnetically delivered analytes can be detected with fewer complications arising from nonoptically homogeneous biological matrices. Facile regeneration of the evanescent sensing surface is possible, as a result of the ease with which paramagnetic beads are dispersed and recovered in a solution, by simply removing the external magnet. The current technique was optimized using a sandwich immunoassay for IgG to determine appropriate experimental conditions.

Analytical figures of merit are reported for this technique using IgG and IL-4 sandwich immunoassays. Additionally, the potential applicability of this technique to a DNA hybridization study is explored.

Experimental

Reagents

Sodium dihydrogen phosphate, disodium hydrogen phosphate, Tris-HCl, EDTA, ethidium bromide, Tween 20, bovine serum albumin (BSA), fluorescein, biotinylated anti-rabbit IgG capture antibody, rabbit IgG, and anti-rabbit IgG-R-phycoerythrin (RPE) were purchased from Sigma-Aldrich (St. Louis, MO) and used as obtained. Biotin anti-human interleukin-4 (IL-4), recombinant human IL-4, and phycoerythrin (PE) anti-human IL-4 were purchased from Ebiosciences (San Diego, CA) and used as received. All custom DNA primers (including a biotinylated 100mer strand, the 100mer complement, and a 100mer non-complement) were purchased in lyophilized form from Invitrogen Corporation (Carlsbad, CA) and reconstituted according to Invitrogen recommendations. Sodium chloride (NaCl) was obtained from Mallinckrodt, Inc. (Phillipsburg, NJ) and used as received. Dynabeads® MyOne™ Streptavidin C1 superparamagnetic μspheres (1 μm diameter) were purchased from Dynal Biotech (Brown Deer, WI) and diluted using phosphate buffered saline (PBS) prepared according to Dynal Biotech recommendations. All buffers and solutions were prepared in deionized, distilled water from a Barnstead 1800 purification system (18 MΩ resistivity).

Apparatus Design

A schematic of the instrumental setup is depicted in Figure 5.1. For immunoassay work, the 488-nm beam from an argon-ion laser (Uniphase Model 2201, San Jose, CA) was directed through a laser line filter (Edmund Optics, Barrington, NJ) and pinhole using first surface mirrors (Edmund Optics, Barrington, NJ). The beam was then sent to a beam steering mirror directly mounted on a rotary stage for controlling the incident angle of the laser beam on the microscope slide (waveguide). To ensure the same spot on the waveguide was illuminated with changing angles, the vertical position of the rotary stage was controlled via a single axis translational stage. The incident beam was passed through a cylindrical lens (Edmund Optics, Barrington, NJ) before reaching the waveguide edge. The waveguide was positioned using a delrin holder fabricated in-house. The holder contained a sliding block, which housed a pressure-formed neodymium bar magnet rated at 10.7 lb lift (McMaster-Carr, Atlanta, GA). The block was used to slide the magnet beneath the waveguide and remove it when necessary. Additionally, the holder included a side mounted, motorized translational stage with an attached cage system housing all collection optics. Fluorescence was collected through a biconvex F1 lens, passed through a razor edge 514 nm Raman filter (Semrock, Rochester, NY), and focused onto a Hamamatsu HC120 photomultiplier tube (PMT) (Hamamatsu, Bridgewater, NJ) using another biconvex F1 lens. Fluorescence was additionally filtered before reaching the PMT

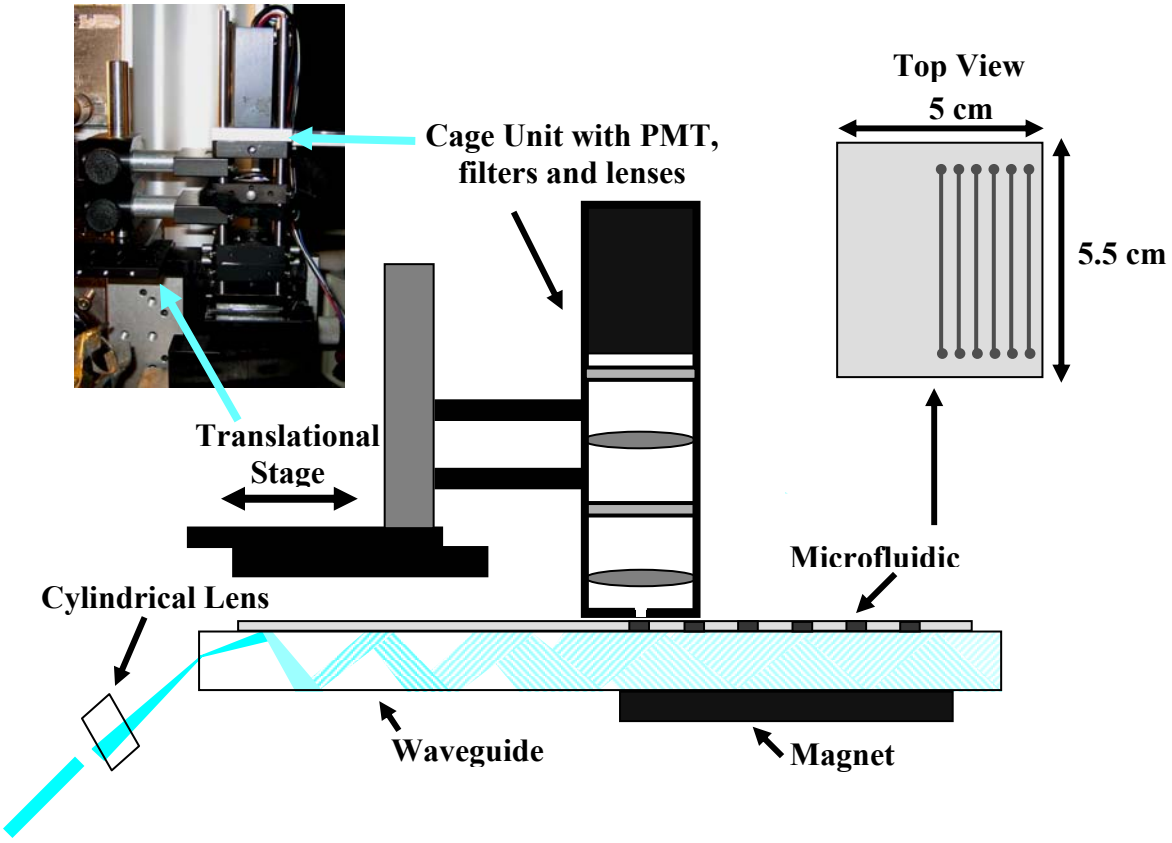

Figure 5.1 Schematic of experimental apparatus. The cage unit is translated via motorized translational stage while the waveguide, PDMS microfluidic and magnet remain fixed.

using a longpass filter with cut-off position at 610 nm (Edmund Optics, Barrington, NJ) for RPE detection and a narrow bandpass interference filter centered at 532 nm (Melles Griot, Rochester, NY) for detection of fluorescein. DNA hybridization studies employed virtually the same optical set-up with the exception of the use of a portable 50 mW, 532 nm laser for ethidium bromide excitation (OnPoint Lasers, Minneapolis, MN). Output voltage from the PMT was converted at 1 Hz by a PMD-1208LS data acquisition board with TracerDaq software (Measurement Computing, Middleboro, MA). The entire cage system could be scanned a total of 12 mm at up to 425 μm/sec across the surface of the waveguide and could, thus, interrogate six microfluidic channels.

The six channel microfluidic platform was fabricated from PDMS (Sylgard 184, Dow-Corning, Midland, MI) using a previously published procedure with the exception of the use of a transparency in place of an aluminum photomask.[104] The six channels were approximately 450 μm wide, 200 μm deep, and 4.5 cm long. A passive solution pumping method was employed for filling that simply involved adjusting the fluid levels at the channel terminating reservoirs.[103] The magnet was positioned at the approximate channel midpoint.

Labeling of μspheres.

IgG. In order to perform the optimization tests, Dynal Biotech Dynabeads MyOne Streptavidin C1 μspheres were fully functionalized, using a sandwich assay format, with biotinylated anti-rabbit IgG as the capture antibody; rabbit-IgG as the antigen; and anti-rabbit IgG RPE as the reporter antibody. The μspheres were first washed with PBS and

diluted to 1 mg/mL. A 400 µL aliquot of µspheres was then removed, separated using an external magnet, resuspended in 400 µL of biotinylated anti-rabbit IgG (0.05 mg/mL) and allowed to incubate for one hour with gentle rotation. These µspheres were considered fully biotinylated. The µspheres were then separated, washed two times with PBS, one time with 0.01% Tween 20 in PBS, resuspended in 400 µL of rabbit-IgG (0.5 mg/mL) and again allowed to incubate for one hour with gentle rotation. These fully antigen labeled µspheres were again separated, washed as described previously and resuspended in 400 µL of anti-rabbit IgG RPE (0.05 mg/mL). Lastly, the µspheres were separated, washed and resuspended in 400 µL of PBS. This fully labeled µsphere solution was used for all optimization experiments. Labeling steps for generation of a calibration curve were basically the same as described above, except for the concentration of rabbit IgG antigen. After dividing into 50 µL aliquots, rabbit IgG standards ranging in concentration from 20 to 200,000 ng/mL were used, followed by full labeling with the reporter antibody.

IL-4. For IL-4 studies, 500 µL of pre-washed Dynal µspheres (1 mg/mL) were separated using an external magnet, washed and resuspended for a 30 minute incubation with rotation in 500 µL of biotin anti-human interleukin-4 (0.05 mg/mL). These beads were then washed as previously described and resuspended in the same volume. Aliquots were removed (50 µL) and diluted to 100 µL for incubation with appropriate concentrations of interleukin-4 antigen followed by labeling with phycoerythrin anti-human IL-4 (.025 mg/mL).

DNA. Following the protocol from Dynal Biotech for biotinylated oligonucleotide labeling, the µspheres were first washed and resuspended in a 2x Binding & Washing

(B&W) buffer at a concentration of 1 mg/mL. To this solution was added an equal volume of TE buffer containing 50 pmol of biotinylated DNA. This mixture was incubated with rotation for 15 minutes followed by three wash steps with 1x B&W. The μspheres are then resuspended in 100 μL of either complement or non-complement DNA (50 pmol) and incubated for 15 minutes, followed by wash steps. The dsDNA complex was then resuspended in 5 μM ethidium bromide for subsequent fluorescence detection.

Results and Discussion

In order to fully exploit the advantages of our previously reported MATEFFs technique, this work integrates planar waveguide and microfluidic technology. This is, to our knowledge, the first report detailing magnetic transport of a bioaffinity system to a localized evanescent field created on a waveguide surface using microfluidic sample delivery. The application of microfluidics to the field of heterogeneous immunoassay is attractive due to consequent improvement in assay kinetics, reagent and time consumption, waste production and the possibilities for automation.[105, 106] Evanescent wave detection has long been used in immunoassay research. Some work in the area of bioaffinity reaction monitoring using both microfluidics and evanescent wave detection has been reported, but requires immobilization procedures for the capture element on the transducer surface and employs complicated fluidic systems.[80, 107] In the present work, experimental conditions were first optimized using a model sandwich immunoassay system for IgG.

The occurrence of total internal reflection (TIR), confining excitation light traveling through the waveguide, depends upon laser wavelength, incident angle, and refractive indices of the waveguide and surrounding medium. It is important to establish a set of conditions that maximizes depth of EW penetration into the sample channels, and thus evanescent field strength, when using the EW to probe molecules at the interface. In this work, penetration depth is changed by incrementally varying the angle on the mirror steering the incident beam. Evanescent wave formation was initially confirmed by magnetically transporting RPE functionalized μspheres to the waveguide surface and scanning through incident angles using the beam-steering mirror. Figure 5.2 illustrates the change in fluorescence emission from the magnetically delivered RPE labeled beads with change in incident angle (approaching the critical angle). The fluorescence signal increases in all six microfluidic channels until an incident angle of ~71º is reached. The signal then begins to decrease, presumably due to inefficient coupling of light into the waveguide once conditions for TIR are no longer satisfied. PDMS ($n \cong 1.47$) was the waveguide surrounding medium, as the microfluidic platform was constructed from PDMS, and the critical angle for PDMS:glass was calculated to be ~75º. However, the optimal angle needed to be determined experimentally as the use of the cylindrical lens causes a distribution of angles impinging on the interface. Additonally, the refractive index for PDMS could vary depending on the curing temperature employed during the fabrication process. Additional experiments were performed for optimization of laser power and bead plug concentration. It was determined that the optimal concentration of beads used in formation of a plug was 0.5 μg and a plot of fluorescence emission versus

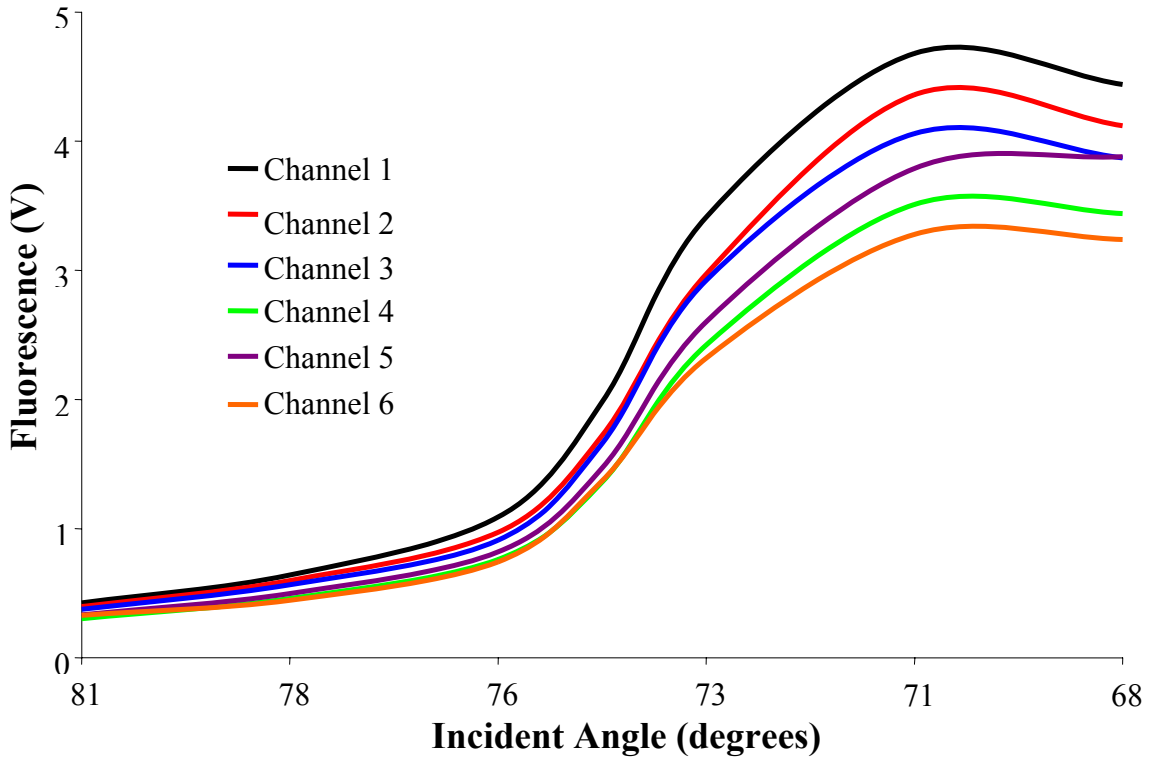

Figure 5.2 Fluorescence emission from RPE labelled magnetic μspheres in each of six microfluidic channels with change in incident angle (approaching critical angle). Channel 1 is the first channel interrogated in the direction of waveguide excitation.

laser power linearly increased from 1.5 to 12 mW (data not shown). Further experiments were performed using a 0.5 µg bead plug and ~10mW laser power

A benefit of evanescent wave detection is the localization of the electromagnetic field to the waveguide surface. In this case, the analytes are delivered to this surface and, even in the presence of background interferents, can be detected without call for multiple wash steps. This fact is evidenced in Figure 5.3, where a 1 µM solution of fluorescein was used as model interferent. Figure 5.3A measures the signal at 532 nm, which originates primarily from background fluorescein (blue bars). When magnetic beads are added to the fluorescein solution and a field transported plug is formed, the fluorescein signal sharply decreases due to the displacement of matrix volume in the evanescent field by the µspheres (black bars). Additionally, Figure 5.3B depicts the signal measured by the longpass filter with a cut-off position at 610 nm, which results from bead immobilized RPE (red bars). This signal in the presence of 1 µM fluorescein is only slightly decreased, presumably due to absorbance of some evanescent radiation by fluorescein present at the waveguide surface (black bars). Therefore, fluorescence measurements for the analyte of interest can be accomplished in the presence of background matrix, and bead delivery actually aids in matrix displacement from the EW.

As laser light travels through the waveguide, it naturally decays as a result of waveguide losses, such as absorbance or scattering. This is evidenced in Figure 5.2 by the fact that the signal decreases as the EW propagates longitudinally from channel 1 to 6. In order to correct for the natural abatement of signal across the waveguide, an

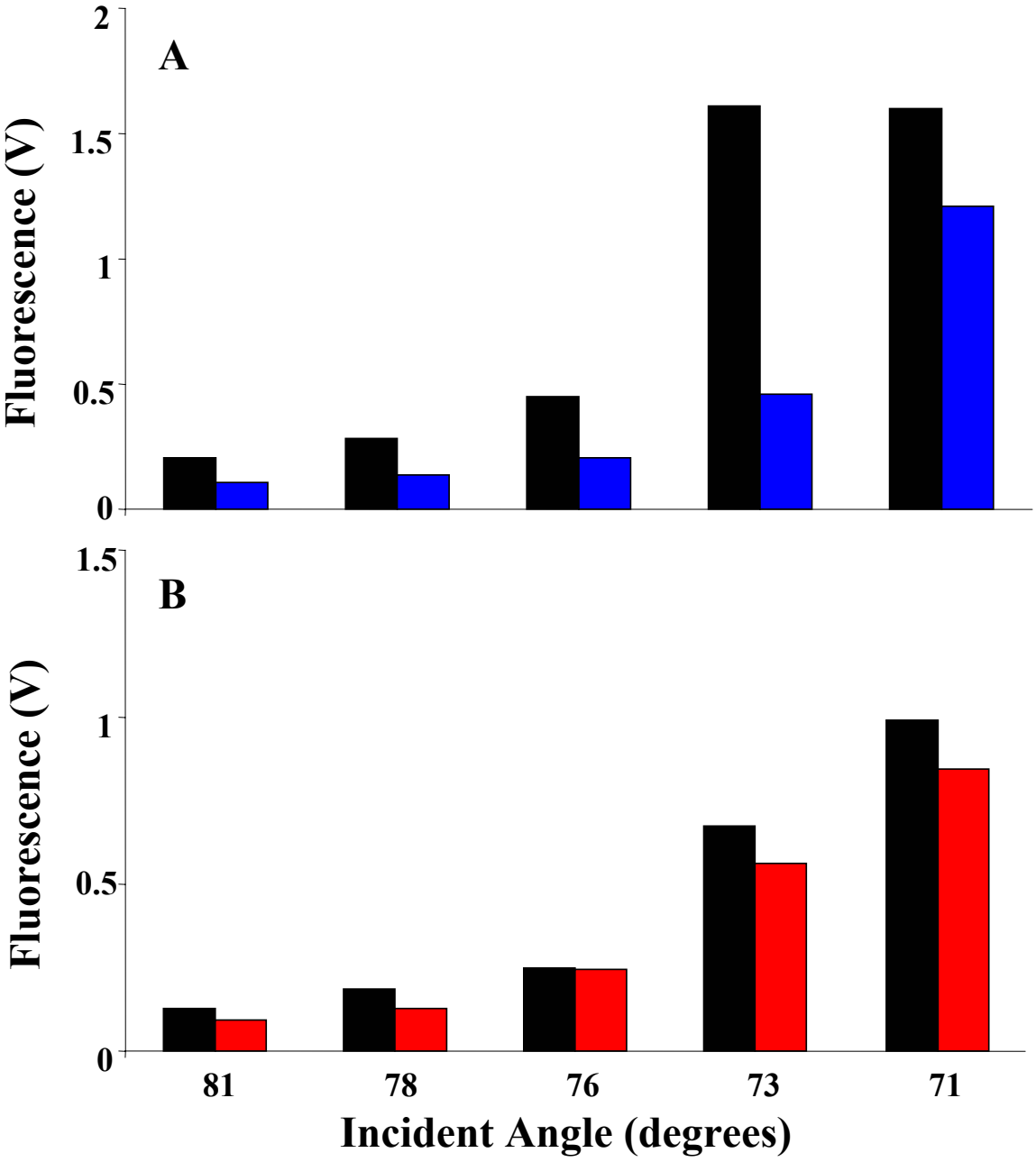

Figure 5.3 Determination of matrix interference effects using RPE labelled magnetic beads with 1 μM fluorescein as background matrix. A) Fluorescence emission of fluorescein measured at 532 nm with (black bars) and without (blue bars) magnetic beads. B) Fluorescence emission of RPE measured at 580 nm with (black bars) and without (red bars) fluorescein.

experiment was performed whereby change in signal from a 1 μM fluorescein solution was measured across the six channels and used to normalize data. The normalization plot (Figure 5.4) exhibited a ~6% decrease/channel in signal from channel 1 to 6.

The linear dynamic range and detection limits of this immunoassay technique were evaluated by constructing a calibration curve for detection of rabbit IgG. Standard solutions of rabbit IgG ranging in concentration from 20 to 20,000 ng/mL were tested. As shown in Figure 5.5, a quite respectable linear dynamic range (y(V) = 0.0005x (mg/mL) + 1.156) of nearly 3 orders of magnitude is established (R^2=0.997) with a limit of detection of ~120 ng/mL (800 pM).

To demonstrate selectivity, a sandwich immunoassay for the detection of interleukin-4 (IL-4), a cytokine which promotes proliferation and differentiation of B cells, was employed. IL-4 was detected with an RSD of 5% at four different concentrations. IgG was used as a model cross reactant to test specificity of the IL-4 sandwich immunoassay. The fluorescence emission for 700 ng/mL IgG was less than 2% that of an equivalent concentration of IL-4 (Figure 5.6). Additionally, using the four measured concentrations of IL-4 to generate a best fit line, a detection limit of 10 ng/mL was established (R^2=0.999).

In order for miniaturized assay systems to compete with accepted macroscopic techniques in terms of sensitivity, the detectable signal must be maximized along with minimization of background. Since, in sandwich immunoassays, only those analyte molecules bound to capture antibody will generate a signal upon binding of the reporter antibody, it is important to maximize binding. Although always governed by

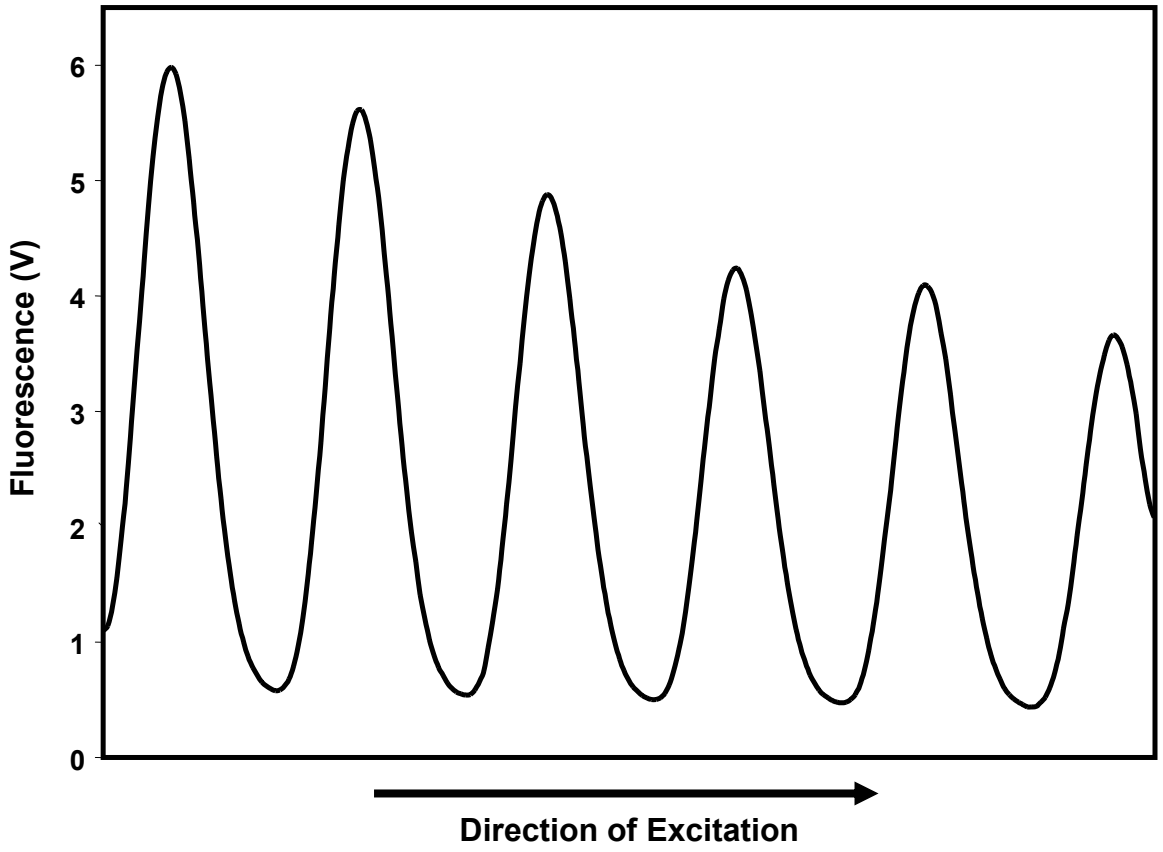

Figure 5.4 Normalization plot illustrating decrease in emission from the six channels as light propagates longitudinally across the waveguide

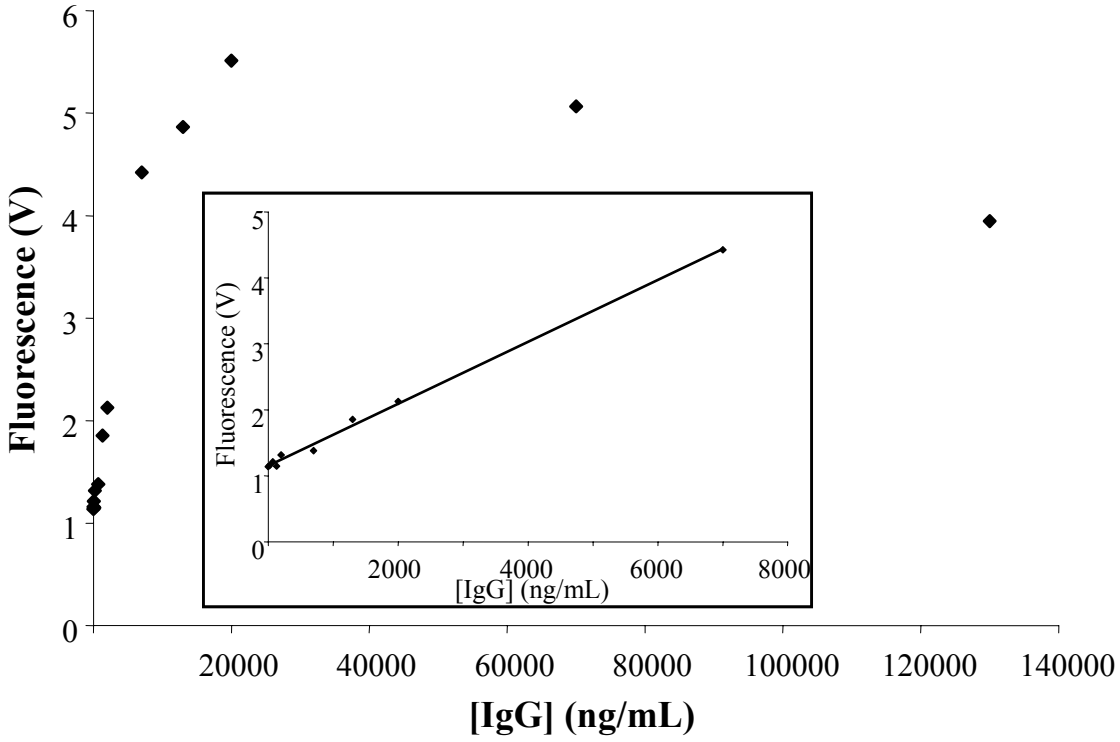

Figure 5.5 Calibration curve using a sandwich immunoassay for detection of IgG. The graph is linear over nearly three orders of magnitude with a detection limit of ~120 ng/mL.

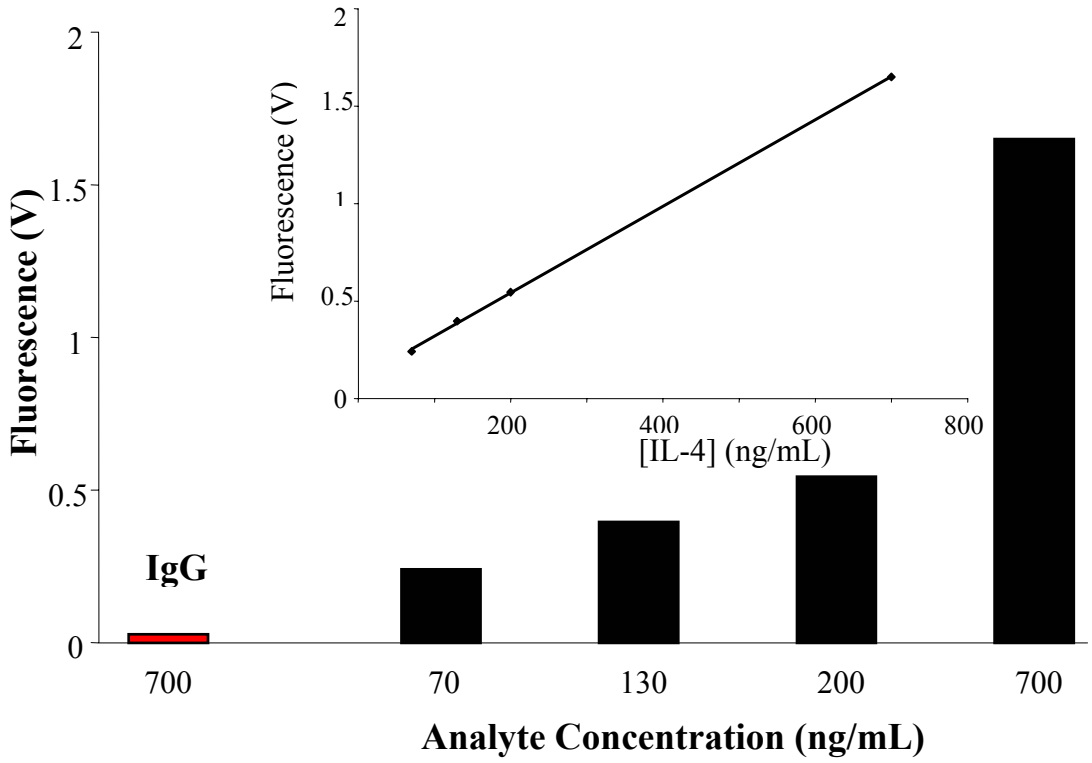

Figure 5.6 Calibration data for interleukin-4 . Four different concentrations of IL-4 were measured and are shown. The inset illustrates the best fit line for these four measurements. Using this data, an RSD of 5% was calculated with a detection limit for IL-4 of 10 ng/mL. Additionally, the signal from IgG as a model cross reactant was measured.

the affinity binding equilibrium, sandwich immunoassays have been classified as either "ambient analyte" or "mass-sensing" assays based upon how analyte concentration in solution is changed upon binding to capture antibody.[72] For an ambient analyte assay, a small amount (e.g., <1.5%) of the total analyte concentration is bound to capture antibody, whereas a mass sensing assay could result in near complete depletion of antigen from a sample solution (~ 100% bound). This means that for a given concentration of analyte solution, the measured signal from an ambient analye assay will not change with changes in assay volume. Conversely, a mass sensing assay will yield a signal proportional to the actual amount (mass) of analyte present in solution.[108]

It follows, then, that analyte harvesting by a mass sensing assay would decrease detection limits by permitting detection of practically all analyte molecules present in a given sample. The ability of a given assay to exhibit mass sensing characteristics is attributed to a capture antibody concentration greater than $0.01/K_a$ (where K_a is the affinity constant) and/or high K_a values. If higher affinity antibodies are not available, then the density of capture antibody in a given area must be increased in order to improve sensitivity. This is a difficult task, since high density arrays normally require sophisticated and expensive printing processes. However, using the technique described herein, we illustrate mass sensing behavior that also has the inherent advantage of efficient magnetic bead mixing with the sample. Furthermore, the "concentrated" bound analyte can then be delivered to a localized field for detection in a miniaturized volume. To demonstrate the ability of the technique to perform mass sensing, a sample of IL-4 at a concentration of 700 ng/mL was divided

into four aliquots, with three of the aliquots diluted to concentrations of 350, 233, and 140 ng/mL by incrementally increasing the sample volume. The actual analyte mass stayed the same in all samples, although the concentration decreased. Each analyte sample was then used to label the magnetic beads and fluorescence emission was measured as previously described. The fluorescence measurements from each of these samples resulted in an RSD of only 12% (data not shown). This is significant because it demonstrates that changes in the effective concentration of the analyte solution (up to a 5x dilution) did not result in a proportional decrease in signal. This is because the signal reflected the amount of analyte present, or actual mass of analyte. Based on these results, this method appears to operate as a mass sensing assay with actual harvesting of all analyte present in the sample. The incubation times for all samples were the same, although the solution volumes were different. The RSD value may have been lowered by increasing incubation time for larger volume samples to ensure complete mixing. Consequently, the actual concentration detection limits stated for the IL-4 assay could be made significantly lower by increasing sample volume. It is especially significant that the magnetic beads act as analyte harvesters as they are the ultimate means of analyte delivery to the localized detection zone and, moreover, decrease background interference due to the matrix volume displacement upon magnetic delivery.

As a final example of versatility, the technique was applied to detection of DNA hybridization via fluorescence emission from ethidium bromide intercalator. While, in genetic studies, it is currently important to apply high density oligonucleotide arrays to gene expression monitoring, there is also a need for methods to rapidly

analyze samples based on a specific question related to such issues as disease diagnosis and susceptibility, or drug discovery.[107-109] The work reported herein is a preliminary step seeking to demonstrate the potential of this method in such specific analysis. A single stranded DNA 100mer was immobilized on the magnetic bead, followed by incubation with either a complementary or non-complementary strand in the presence of ethidium bromide (EB). EB, upon intercalation into the DNA double helix, undergoes a fluorescence enhancement. Therefore, successful DNA hybridization should be detectable via measurable increase in EB fluorescence emission as compared to EB background from running buffer.[110] Figure 5.7 depicts the results for the comparison of DNA with complement compared to non-complement hybridization in the presence of EB running buffer. The signal from complement hybridization was nearly 300% greater than that for non-complement after EB background subtraction. This suggests that the technique could find application in genetic analyses. The system described herein is non-ideal due to possible electrostatic interaction of EB with ssDNA and regions of homo-duplex formation in the ssDNA 100mer sequences. Addressing these issues, with the use of a better intercalator that is more specific for dsDNA and/or shorter DNA sequences, could improve discrimination between complement and non-complement. Additionally, conditions such as temperature, salt concentration, and ssDNa binding density could be investigated and optimized. Upon completion of these steps, the presence of a specific disease-related sequence upon hybridization to its complement or the interaction of a drug with a hybridized DNA-EB complex could be detected

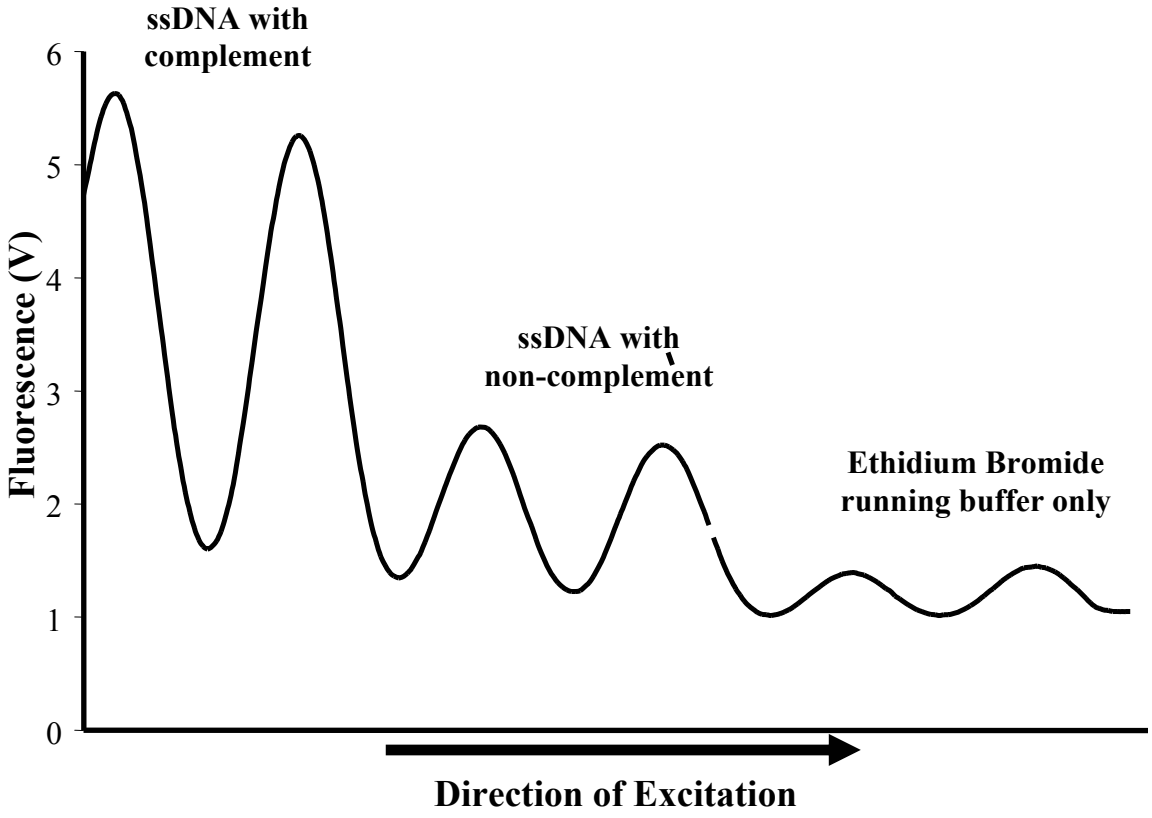

Figure 5.7 Comparison of fluorescence emission for complement vs. non-complement DNA hybridization in the presence of 5 μM ethidium bromide running buffer.

via changes in EB fluorescence using this simple lab-on-a-chip platform without need for pre-labeling steps or expensive instrumentation and complicated data analysis required for the use of current DNA microarrays.

Conclusions and Future Work

This work represents the integration of microfluidic and planar waveguide technology for simultaneous investigation of multiple bioaffinity systems. A simple PDMS microfluidic platform is employed for delivery of magnetic bead containing solution using a passive pumping technique which circumvents the need for sophisticated and expensive external equipment. Furthermore, the waveguide is a basic microscope slide which provides a planar surface for microfluidic attachement and efficiently propagates the EW uniformly across six channels. The use of magnetic beads as a mechanism of analyte delivery to the localized evanescent field on the waveguide surface eliminates the need for multiple wash steps and simultaneously minimizes interference from fluorescing species in the sample matrix via displacement of matrix volume. The ease of magnetic bead dispersement in solution upon removal of the external magnet facilitates regeneration of the evanescent sensing surface. In essence, this novel bioassay method has the advantages of the homogeneous assay, in that measurements can be made in the presence of the sample matrix, and the heterogeneous assay, in that the analyte is concentrated on the surface of a solid and mobile substrate. However, unlike regular heterogeneous assays, assay kinetics resemble liquid phase due to the enhancement of interaction between magnetic beads and the analyte-containing sample.

Future work could take advantage of the mass sensing characteristics of this system to substantially lower detection limits for the bioaffinity systems described herein. The use of integrated optical waveguides (IOWs) in the place of the bulk, planar waveguide used in the current work, though complicated in terms of fabrication, could reduce detection limits up to two orders of magnitude.[80] With IOWs, the waveguide thickness is comparable to the wavelength of propagating light and it is possible to achieve 10^4 reflections/cm. However, coupling light into these devices is quite difficult, normally requiring prisms or gratings. Furthermore, using magnetic beads that more closely approximate the dimensions of the EW depth could lower detection limits by maximizing the probed surface area and minimizing matrix volume in the EW. More sophisticated PDMS architectures could also be utilized for analysis of maximal numbers of samples.

List of References

(1) Issaq, H. J. *Electrophoresis* **2000**, *21*, 1921-1939.

(2) Kemp, G. *Biotechnology and Applied Biochemistry* **1998**, *27*, 9-17.

(3) Heiger, D. *High performance capillary electrophoresis: An introduction*; Agilent Technologies, 2000.

(4) Marina, M. L.; Torre, M. *Talanta* **1994**, *41*, 1411-1433.

(5) Wallingford, R. A., Ewing, A.G., Ed. *Advances in Chromatography*; Marcel Dekker, Inc.: New York, 1989.

(6) Jorgenson, J. W.; Lukacs, K. D. *Science* **1983**, *222*, 266-272.

(7) Jorgenson, J. W.; Lukacs, K. D. *Analytical Chemistry* **1981**, *53*, 1298-1302.

(8) Landers, J. P., Ed. *Handbook of Capillary Electrophoresis*, 2nd ed.; CRC Press: New York, 1997.

(9) Anon *Chromatographia* **2001**, *54*, S15-S23.

(10) Tagliaro, F.; Manetto, G.; Crivellente, F.; Smith, F. P. *Forensic Science International* **1998**, *92*, 75-88.

(11) Watzig, H.; Gunter, S. *Clin Chem Lab Med* **2003**, *41*, 724-738.

(12) Khaledi, M. G., Ed. *High Performance Capillary Electrophoresis*; John Wiley & Sons, Inc.: New York, 1998.

(13) Kuhn, R., Hoffstetter-Kuhn, S. *Capillary Electrophoresis: Principles and Practice*; Springer-Verlag: Berlin, 1993.

(14) Ghosal, S. *Annu. Rev. Fluid Mech.* **2006**, *38*, 309-338.

(15) Weinberger, R. *Practical Capillary Electrophoresis*, 2nd ed.; Academic Press: San Diego, 2000.

(16) Kuhr, W. G. *Analytical Chemistry* **1990**, *62*, 403R-414R.

(17) Mathies, R. A., Peck, K. *Anal. Chem.* **1990**, *62*, 1786-1791.

(18) Camilleri, P., Ed. *Capillary Electrophoresis: Theory and Practice*, 2nd ed.; CRC Press: New York, 1998.

(19) Murphy, R. M. *Anal. Biotech.* **1997**, *8*, 25-30.

(20) Zarrin, F., Risfelt, J.A., Dovichi, N.J. *Anal. Chem.* **1987**, *59*, 850-854.

(21) Zarrin, F., Dovichi, N.J. *Anal. Chem.* **1985**, *57*, 1826-1829.

(22) Rezenom, Y. H.; Wellman, A. D.; Tilstra, L.; Medley, C. D.; Gilman, S. D. **in preparation.**

(23) Rosenzweig, Z., Yeung, E.S. *Anal. Chem.* **1994**, *66*, 1771-1776.

(24) Altria, K. D. *J. Chrom. A* **1999**, *856*, 443-463.

(25) Kasicka, V. *Electrophoresis* **2006**, *27*, 142-175.

(26) Smith, A. J. *Methods in Mol. Biol.* **2002**, *211*, 91-98.

(27) Grossman, P. D.; Colburn, J. C.; Lauer, H. H.; Nielsen, R. G.; Riggin, R. M.; Sittampalam, G. S.; Rickard, E. C. *Analytical Chemistry* **1989**, *61*, 1186-1194.

(28) Offord, R. E. *Nature* **1966**, *211*, 591-593.

(29) Cifuentes, A.; Rodriguez, M. A.; Garcia-Montelongo, F. J. *Journal of Chromatography, A* **1996**, *742*, 257-266.

(30) Kheterpal, I., Williams, A., Murphy, C., Bledsoe, B., Wetzel, R. *Biochem.* **2001**, *40*, 11757-11767.

(31) Lashuel, H., A., Hartley, D.M., Petre, B.M., Wall, J.S., Simon, M.N., Walz, T., Lansbury, P.T., Jr. *J. Mol. Biol.* **2003**, *332*, 795-808.

(32) Kayed, R.; Head, E.; Thompson, J. L.; McIntire, T. M.; Milton, S. C.; Cotman, C. W.; Glabe, C. G. *Science (Washington, DC, United States)* **2003**, *300*, 486-489.

(33) Nistor, C.; Emneus, J. In *Biosensors and Modern Biospecific Analytical Techniques*; Gorton, L., Ed.; Elsevier, 2005; Vol. XLIV, pp 490.

(34) Varesio, E., Rudaz, S., Krause, K., Veuthey, J. *J Chromatogr A* **2002**, *974*, 135-142.

(35) Sweeney, P. J.; Darker, J. G.; Neville, W. A.; Humphries, J.; Camilleri, P. *Analytical Biochemistry* **1993**, *212*, 179-184.

(36) Sabella, S., et al. *Electrophoresis* **2004**, *25*, 3186-3194.

(37) Stoppini, M., Andreola, A., Foresti, G., Bellotti, V. *Pharm. Res.* **2004**, *50*, 419-431.

(38) Lansbury, P. T., Jr. *Proc. Nat. Acad. Sci.* **1999**, *96*, 3342-3344.

(39) Forloni, G.; Terreni, L.; Bertani, I.; Fogliarino, S.; Invernizzi, R.; Assini, A.; Ribizzi, G.; Negro, A.; Calabrese, E.; Volonte, M. A.; Mariani, C.; Franceschi, M.; Tabaton, M.; Bertoli, A. *Neurobiology of Aging* **2002**, *23*, 957-976.

(40) Rochet, J.-C.; Lansbury, P. T., Jr. *Current Opinion in Structural Biology* **2000**, *10*, 60-68.

(41) Kheterpal, I., Lashuel, H.A., Hartley, D.M., Walz, T., Lansbury, P.T., Jr., Wetzel, R. *Biochem.* **2003**, *42*, 14092-14098.

(42) Taylor, J. P.; Hardy, J.; Fischbeck, K. H. *Science (Washington, DC, United States)* **2002**, *296*, 1991-1995.

(43) Lashuel H., A., Hartley D.M., Petre B.M., Walz, T., Lansbury P.T., Jr. *Nature* **2002**, *418*, 291.

(44) Williams, A. D.; Sega, M.; Chen, M.; Kheterpal, I.; Geva, M.; Berthelier, V.; Kaleta, D. T.; Cook, K. D.; Wetzel, R. *Proc. Nat. Acad. Sci.* **2005**, *102*, 7115-7120.

(45) Levine, H. *Methods Enzymol.* **1999**, *309*, 274-284.

(46) Yokoyama, K.; Welchons, D. R. *Nanotechnology* **2007**, *18*, 105101.

(47) Johansson, A. S.; Berglind-Dehlin, F.; Karlsson, G.; Edwards, K.; Gellerfors, P.; Lannfelt, L. *FEBS Journal* **2006**, *273*, 2618-2630.

(48) Walsh, D. M., Hartley, D.M., Dusumoto, Y., Fezoui, Y., Condron, M.M., Lomakin, A., Benedek, G.B., Selkoe, D.J., Teplow, D.B. *J Biol Chem* **1999**, *274*, 25945-25952.

(49) Nilsberth, C.; Westlind-Danielsson, A.; Eckman, C. B.; Condron, M. M.; Axelman, K.; Forsell, C.; Stenh, C.; Luthman, J.; Teplow, D. B.; Younkin, S. G.; Naeslund, J.; Lannfelt, L. *Nature Neuroscience* **2001**, *4*, 887-893.

(50) Moses, J. P.; Wellman, A. D.; Kheterpal, I.; Wetzel, R.; Gilman, S. D. **in preparation**.

(51) Landsteiner, K. *Zbl Bakteriol Parasitol* **1899**, *25*, 546-549.

(52) Yalow, R. S.; Berson, S. A. *J. Clin. Invest.* **1960**, *39*, 1157-1175.

(53) Wild, D., Ed. *The Immunoassay Handbook*, Third ed.; Elsevier: Amsterdam, 2005.

(54) Hayden, M. S.; Gilliland, L. K.; Ledbetter, J. A. *Current Opinion in Immunology* **1997**, *9*, 201-212.

(55) Law, B., Ed. *Immunoassay: A Practical Guide*; Taylor & Francis: London, 1996.

(56) Boder, E. T.; Midelfort, K. S.; Wittrup, K. D. *Proc. Nat. Acad. Sci.* **2000**, *97*, 10701-10705.

(57) Lipman, N. S.; Jackson, L. R.; Trudel, L. J.; Weis-Garcia, F. *ILAR Journal* **2005**, *46*, 258-268.

(58) Diamandis, E. P.; Christopoulos, T. K., Eds. *Immunoassay*; Academic Press: San Diego, 1996.

(59) Kohler, G.; Milstein, C. *Nature* **1975**, *256*, 495-497.

(60) Knopp, D. *Anal. Bioanal. Chem.* **2006**, *385*, 425-427.

(61) Englebienne, P. *Immune and Receptor Assays in Theory and Practice*; CRC Press: Boca Raton, 2000.

(62) Ekins, R. P. *J. Chem. Ed.* **1999**, *76*, 769-780.

(63) Dandliker, W. B.; Schapiro, H. C.; Meduski, J. W. *Immunochemistry* **1964**, *1*, 165-191.

(64) Ullman, E. F.; Schwarzberg, M.; Rubenstein, K. E. *J. Biol. Chem.* **1978**, *251*, 4172-4178.

(65) Zuk, R.; Rowley, G.; Fullman, E. *Clin. Chem.* **1979**, *25*, 1554-1560.

(66) Dodge, A.; Fluri, K.; Verpoorte, E.; de Rooij, N. F. *Anal. Chem.* **2001**, *73*, 3400-3409.

(67) Gao, Y.; Lin, F. Y. H.; Hu, G.; Sherman, P. M.; Li, D. *Analytica Chim. Acta.* **2005**, *543*, 109-116.

(68) Nakamura, R. M.; Kasahara, Y.; Rechnitz, G. A., Eds. *Immunochemical Assays and Biosensor Technology for the 1990s*; American Society for Microbiology: Washington, D.C., 1992.

(69) Gosling, J. P. *Clin. Chem.* **1990**, *36*, 1408-1427.

(70) Chan, W.; Maxwell, D.; Gao, X.; Bailey, R.; Han, M.; Nie, S. *Current Opinion in Biotech.* **2002**, *13*, 40-46.

(71) Hemmila, I. *Applications of Fluorescence in Immunoassays*; Wiley: New York, 1991.

(72) Saviranta, P.; Okon, R.; Brinker, A.; Warashina, M.; Eppinger, J.; Geierstanger, B. *Clin. Chem.* **2004**, *50*, 1907-1920.

(73) Kusnezow, W.; Syagailo, Y. V.; Goychuk, I.; Hoheisel, J. D.; Wild, D. G. *Expert Rev. Mol. Diagn.* **2006**, *6*, 111-124.

(74) "evanescent." Dictionary, M.-W. O. 2007. www.webster.com (March 9, 2007).

(75) He, Y.; Li, H. W.; Yeung, E. S. *J. Phys. Chem. B* **2005**, *109*, 8820-8832.

(76) Axelrod, D.; Burghardt, T. P.; Thompson, N. L. *Ann. Rev. Biophys. Bioeng.* **1984**, *13*, 247.

(77) Robertson, S. K.; Uhrick, A. F.; Bike, S. G. *J. Colloid Interface Sci.* **1998**, *202*, 208.

(78) Axelrod, D. *Methods Enzymol.* **2003**, *361*, 1.

(79) Sarkar, A.; Robertson, R. B.; Fernandez, J. M. *Proc. Nat. Acad. Sci.* **2004**, *101*, 12882.

(80) Lehr, H. P.; Reimann, M.; Brandenburg, A.; Sulz, G.; Klapproth, H. *Anal. Chem.* **2003**, *75*, 2412-2420.

(81) Plowman, T. E.; Durstchi, J. D.; Wang, H. K.; Christensen, D. A.; Herron, J. N.; Reichert, W. M. *Anal. Chem.* **1999**, *71*, 4344-4352.

(82) Feldstein, M. J.; Golden, J. P.; Rowe, C. A.; MacCraith, B. D.; Ligler, F. S. *J. Biomed. Microdevices* **1999**, *1*, 139-153.

(83) Bradshaw, J. T.; Mendes, S. B.; Saavedra, S. S. *Anal. Chem.* **2005**, 29A.

(84) Plowman, T. E.; Saavedra, S. S.; Reichert, W. M. *Biomaterials* **1998**, *19*, 341-355.

(85) Taitt, C. R.; Anderson, G. P.; Ligler, F. S. *Biosens. & Bioelec.* **2005**, *20*, 2470-2487.

(86) Gijs, M. A. M. *Microfluid Nanofluid* **2004**, *1*, 22-40.

(87) Hage, D. *Anal. Chem.* **1999**, *71*, 294R-304R.

(88) Diamandis, E. P.; Christopoulos, T. K. *Immunoassay*; Academic Press: San Diego, 1996.

(89) Dolnik, V.; Liu, S.; Jovanovich, S. *Electrophoresis* **2000**, *21*, 41-54.

(90) Chiem, N.; Harrison, D. J. *Anal. Chem.* **1997**, *69*, 373-378.

(91) Koutney, L. B.; Schmalzing, D.; Taylor, T. A.; Fuchs, M. *Anal. Chem.* **1996**, *68*, 18-22.

(92) Linder, V.; Verpoorte, E.; N.F., d. R.; Sigrist, H.; Thormann, W. *Electrophoresis* **2002**, *23*, 740-749.

(93) Rashkovetsky, L. G.; Lyubarskaya, Y. V.; Foret, F.; Hughes, D. E.; Karger, B. L. *J. Chrom. A* **1997**, *781(1-2)*, 197-204.

(94) Hayes, M. A.; Polson, N. A.; Phayre, A. N.; Garcia, A. A. *Anal. Chem.* **2001**, *73*, 5896-5902.

(95) Petkus, M.; Mclaughlin, M.; Vuppu, A.; Rios, L.; Garcia, A. A.; Hayes, M. A. *Anal. Chem.* **2006**, *78*, 1405-1411.

(96) Tromberg, B. J.; Sepaniak, M. J.; Vo-Dinh, T.; Griffin, G. D. *Anal. Chem.* **1987**, *59*, 1226-1230.

(97) Alarie, J. P.; Sepaniak, M. J.; Vo-Dinh, T. *Analytica Chim. Acta.* **1990**, *229*, 169-176.

(98) Melles, G. *The Practical Application of Light*, 2005.

(99) Sato, K.; Tokeshi, M.; Odake, T.; Kimura, H.; Ooi, T.; Nakao, M.; Kitamori, T. *Anal. Chem.* **2000**, *72*, 1144-1147.

(100) Klotz, A.; Brecht, A.; Barzen, C.; Gauglitz, G.; Harris, R. D.; Quigley, G. R.; Wilkinson, J. S.; Abuknesha, R. A. *Sens. Actuat. B* **1998**, *51*, 181-187.

(101) Drmanac, R.; Drmanac, S.; Strezoska, Z.; Paunesku, T.; Labat, I.; Zeremski, M.; Snoddy, J.; Funkhouser, W. K.; Koop, B.; Hood, L.; Crkvenjakov, R. *Science* **1993**, *260*, 1649-1652.

(102) Wellman, A. D.; Sepaniak, M. J. *Anal. Chem.* **2006**, *78*, 4450-4456.

(103) Walker, G. M.; Beebe, D. J. *Lab Chip* **2002**, *2*, 131-134.

(104) Connatser, R. M.; Riddle, L. A.; Sepaniak, M. J. *J. Sep. Sci.* **2004**, *27*, 1545-1550.

(105) Hosokawa, K.; Omata, M.; Sato, K.; Maeda, M. *Lab Chip* **2006**, *6*, 236-241.

(106) Lin, F. Y. H.; Sabri, M.; Erickson, D.; Alirezaie, J.; Li, D.; Sherman, P. M. *Analyst* **2004**, *129*, 823-828.

(107) Schuderer, J.; Akkoyun, A.; Brandenburg, A.; Bilitewski, U.; Wagner, E. *Anal. Chem.* **2000**, *72*, 3942-3948.

(108) Yamugachi, Y.; Ogura, K.; Yamashita, K.; Miyazaki, M.; Nakamura, H.; Maeda, H. *Talanta* **2006**, *68*, 700-707.

(109) Wang, X.; Krull, U. *J. Materials Chem.* **2005**, *15*, 2801-2809.

(110) Alonso, A.; Almendral, M.; Curto, Y.; Criado, J.; Rodriguez, E.; Manzano, J. *Anal. Biochem.* **2006**, *355*, 157-164.

Vita

Amber was raised in Dickenson County, VA, where she attended Ervinton Elementary and High School. After graduating as valedictorian of her senior class in 1997, she attended The University of Virginia's College at Wise in Wise, VA, on a full-paid scholarship. She graduated in 2001 with a Bachelor of Science degree in Chemistry, Magna Cum Laude, before continuing her education at The University of Tennessee Knoxville as a Ziegler Buehler Fellow in The Department of Chemistry. For the first three years of her graduate career, she was advised by Dr. S. Douglass Gilman. She finished her graduate career under the direction of Dr. Michael J. Sepaniak. In May 2007, she will graduate with a Ph.D. in Analytical Chemistry. She accepted a position as a Scientist in the Technical Services Division of Chattem, Inc. in Chattanooga, TN.